ABSTRACT

Title of Document: OPTICAL KERR EFFECT SPECTROSCOPY OF SIMPLE LIQUIDS

Qin Zhong, Doctor of Philosophy, 2009

Directed By: Professor John T. Fourkas, Department of Chemistry and Biochemistry

Optical Kerr effect (OKE) spectroscopy has become a prominent nonlinear optical technique for studying liquids, which allows for the direct, time-resolved probing of collective orientational diffusion as well as Raman-active intermolecular and intramolecular modes.

The temperature-dependent orientational dynamics of 1, *n*-dicyano *n*-alkane liquids ranging from dicyanomethane to 1,8-dicyanooctane has been investigated by ultrafast OKE spectroscopy. The dependence of the reorientational times on temperature and viscosity is consistent with the molecules adopting a largely extended structure in the liquid state, with a preference for gauche conformations at the methylenes bonded to the cyanide groups. The data are also suggestive of temperature-dependent, collective structural rearrangements in these liquids.

Ultrafast OKE spectroscopy has also been used to study the intermolecular dynamics of aromatic liquids. A model that links the differences in the OKE spectra to corresponding differences in the local ordering of the liquids has been proposed

previously based on the temperature-dependent OKE study of five aromatic liquids. The spectra of some other aromatic liquids such as pyridine, pyridine-d5, 2,4,6-trifluoropyridine and 1,3,5-tris(trifluoromethyl) benzene has been obtained to test this model, and the relative importance of molecular shape and electrostatic forces in determining the form of the OKE reduced spectral density for such liquids has been realized. It has recently been shown that liquid tetrahydrofuran (THF) has an unusual structure that features voids of significant dimension. Such voids should affect other observable properties of this liquid. Temperature-dependent, optical Kerr effect spectra for THF and a number of related liquids (furan, cyclopentane, tetrahydropyran, cyclohexane, diethyl ether, hexamethylphosphoramide and *n*-pentane) has been obtained to test whether the shape of the spectra can be used to reveal the presence of sizeable voids in liquids. Liquid under tension is another interesting system to study: A method based on Berthelot tube technique has been developed to hold benzene and acetonitrile under tension successfully.

A new scheme for measuring different tensor elements of the OKE response is developed. A dual-ring, polarization dependent Sagnac interferometer is used to create two co-propagating probe pulses that arrive at the sample at different times but that reach the detector simultaneously and collinearly. The tensor element of the response that is measured is determined by the polarization of the pump pulse. By controlling the relative timing of the probe pulses it is also possible to perform optical subtraction of two different tensor elements of the response at two different times, a strategy that can be used to enhance or suppress particular contributions to the OKE response.

OPTICAL KERR EFFECT SPECTROSCOPY OF SIMPLE LIQUIDS

By

Qin Zhong

Thesis submitted to the Faculty of the Graduate School of the
University of Maryland, College Park, in partial fulfillment
of the requirements for the degree of
Doctor of Philosophy
2009

Advisory Committee:
Professor John T. Fourkas, Chair
Professor Amy S. Mullin
Professor Thomas E. Murphy
Professor John D. Weeks
Professor Robert A. Walker

Acknowledgements

It is a pleasure to thank the many people who made this thesis possible.

It is difficult to overstate my gratitude to my Ph.D. supervisor - Dr. John T. Fourkas, who was the main creator of the great ideas and techniques of this thesis. Throughout my whole graduate period, he provided tons of great ideas, advanced device, sufficient funding, and even nice colleagues. He was always patient and encouraging when I was in trouble during experiments. He tought me how to work independently, but at any time, his useful advice was always available to me. I should say I have lived a very happy life during my five years in Fourkas group and I feel so lucky to work for such a nice and polite person.

I am grateful to my committee members – Dr. Amy S. Mullin, Dr. Thomas E. Murphy, Dr. John D. Weeks and Dr. Robert A. Walker. For their kind assistance with helpful discussions, giving wise advice, refining my thesis and helping with postdoc applications, and so on.

I would like to express my warmest thanks to all my presnt and former colleagues in Fourkas group:

Dr. Xiang Zhu, former colleague of our OKE project. He taught me everything about OKE experiment and also gave me a lot of helps in everyday life such as taught me how to drive; Dr. Feng (Terry) Ding, current colleague of SFG project, we experienced together all the ups and downs when setting up the SFG spectrometer, her good knowledge, huge work experience and patience were necessary for finishing this project, and it's a great experience to work with her; Dr Christopher N. LaFratta, he has been very kind to me and especially very patient in teaching me. I learned a

lot of knowledge from him not only about science but also about American culture. He was also the leader of our BBQ group and coach of our Wiffle ball team; Dr. Erez Gershgoren, he passed his great passion in science to everyone in the group and he gave me a lot of supports in OKE project including helpful disccusions and writing powerful Labview programs for data analysis; Dr. George Kumi, he worked together with me on holding liquids under tension and his cautious attitude on research sets good example for me; Dr. Rafael R. Gattass, he taught me how to repair laser, helped us write Labview programs, and also brought a lot of laugh and fun to tour lab; Linjie Li, current colleague, my best friend and also my five-year long roommate, we get through many difficulties together from Boston to College Park, thank him for all the support, comraderie, entertainment… Thanks also go to Xiaoxiao He and Katherine Manfred for their diligent work, making our project advancing faster; all other present and former colleagues of Fourkas group, for their assistance and providing an excellent working atmosphere: Mike Stocker, Kathleen Monaco, Hana Hwang, Sanghee Nah, Pearl Horng, Yunbo Shi, Soner Erduran, Meghan Driscoll, Sijia Qin, Floyd Bates, Juliet Znovena, Daniel Lim and Amity Ziegler.

I would like to thank the many other people in the department: Dr. Liwei Yuan and Dr. Qingnan Liu for helpful disccusion about research; Dr. Yuanhua Wang, Dr. Jing Zhang, Huan Wang and Yang Zhao for their helps on organic chemistry knowledge; Dr. Wei Zhang for help on sealing glass cell; Dr. Suleyman Can and Michael Brindza for collaborations on SFG experiment; Dr. Wendy Heiserman for teaching me how to use the contact angle goniometer; Dr. Yiu-Fai Lam for NMR training; people at Physics and IPST machine shop and Robert Letiecq at Coherent.

Lastly, I sincerely thank my family – my parents and my sister for their encouragements and supports through all these years. Special thanks to my wife Jiao for her great support, understanding and love.

Most of the work presented in this thesis was supported by funds from the National Science Foundation.

Table of Contents

List of Tables

List of Figures

List of Abbreviations

a.u.	Arbitrary Unit
ARKS	Antiresonant Ring Kerr Spectrometer
cm^{-1}	Wavenumber
cP	Centipoise
DC	Direct Current
DID	Dipole/Induced Dipole
DSE	Debye-Stokes-Einstein
E_A	Activation Energy
fs	Femtosecond
FW	Formula Weight
HFB	Hexafluorobenzene
HMPA	Hexamethylphosphoramide
HWP	Half-wave Plate
II	Interaction-Induced
k_B	Boltzmann Constant
K	Kelvin
KDP	Potassium Dihydrogen Phosphate
LO	Local Oscillator
NFM	Nonafluoromesitylene
OHD	Optical Heterodyne Detected
OKE	Optical Kerr Effect
p	Dipole Moment
ps	Picosecond
PBC	Polarizing Beam Cube
QWP	Qarter-wave Plate
RSD	Reduced Spectral Density
TFB	1,3,5-trifluorobenzene
TFP	2,4,6-trifluoropyridine

THF	Tetrahydrofuran
THP	Tetrahydropyran
TMP	2,4,6-trimethylpyridine
V_m	Molar Volume
η	Viscosity
τ	Decay Time Constant
ρ	Density

Chapter 1: Introduction

1.1 Introduction and Motivation

Being able to understand complex systems, ranging from liquids to biological tissues, on a microscopic level is increasingly important to research in chemistry, physics, biology, and other physical and natural sciences. Many experimental methods have been developed for studying complex systems, among which one powerful category is ultrafast spectroscopy. Popular ultrafast spectroscopy techniques include time-resolved fluorescence spectroscopy[1,2], pump/probe spectroscopy[3,4], transient grating spectroscopy[5,6], and photon echo spectroscopy[7,8].

Pump/probe spectroscopy is the simplest format of nonlinear ultrafast spectroscopy. The basic idea of this technique is that one ultrafast pulse (the pump) is used to affect a system of interest and a second pulse (the probe), which arrives at a variable delay time, is used to probe how the system has been altered by the pump pulse. The pump-induced change in the sample can be absorption, stimulated emission, refractive index, reflectivity, or some combination of all of four; the probe pulse will record the time dependence of these changes. Within the realm of pump/probe spectroscopy, optical Kerr effect (OKE) spectroscopy[9-12] is one of the longest established methods of capturing the ultrafast dynamics of liquids.

Since its first demonstration in 1969,[13] optical Kerr effect (OKE) spectroscopy has become a widely used technique for studying ultrafast dynamics in transparent fluids. There are several reasons accounting for its popularity. First, the implementation of

the experiment is simple. Second, by the implement of optical heterodyne detection (OHD) detection[14], the experiment provides data of extremely high signal-to-noise ratio, permitting detailed analysis. Third, OKE spectroscopy allows for the direct, time-resolved probing of collective orientational diffusion as well as of the dynamics of Raman-active intramolecular and intermolecular modes. The orientational diffusion dynamics can be analyzed in the time domain; Due to the pioneering work of McMorrow and Lotshaw,[15] we can also transform time-domain OKE data into Bose-Einstein-corrected, low-frequency Raman spectra. Upon removal of the contribution of orientational diffusion, the low-frequency portion of the "reduced spectral density" (RSD) contains information about intermolecular dynamics. As such, this technique has provided numerous insights into the microscopic behavior of fluids such as simple liquids. Examples of more complex systems that have been studied include liquid crystals,[16-18] supercooled liquids,[19-22] ionic liquids,[23-28] confined liquids,[29-31] and liquids inside of polymer networks.[32-36]

Our research is focused on simple liquids and we have completed a number of OKE studies of orientational dynamics of bulk liquids in the past decades, including rod-like molecules such as acetonitrile and 2-butyne[37,38] and disk-like molecules such as benzene[39]. Recently OKE studies on temperature-dependent orientational dynamics in *n*-alkyl cyanides (n=1 to 11)[40] showed that these molecules adopt extended configurations and reorient as rigid rods. Even more interestingly, the liquid molecules with shorter alkyl chains undergo an apparent ordering transition as they are cooled. We know of no other liquids in which such a phenomenon has been observed above the melting point. This behavior is also reminiscent of transitions that

occur in rotator phases of alkanes and *n*-alkyl alcohols below their melting points. Whether or not our observations are indicative of an actual phase transition is an open question that merits further investigation. For comparison, we also studied the reorientational dynamics of 1, *n*-dicyano *n*-alkanes, and similar conclusions have been discovered.

While the orientational dynamics of these simple molecules have been studied in detail and the interpretation has been understood well, the same can not be said for the intermolecular dynamics, in part due to the featureless reduced spectral density (RSD). We have recently shown[41], for a series of aromatic liquids for which local structural information is available, that there is a direct correlation between local structure and the shape of the RSD. Ryu and Stratt[42] have suggested that the form of the OKE RSD can, in part, be a manifestation of molecular shape, especially insofar as the structure of liquids is dominated by effective repulsive interactions. Here we have finished further OKE experiments on more aromatic liquids, and the relative importance of molecular shape and electrostatic forces in determining the form of the OKE reduced spectral density (RSD) for such liquids has been realized[43].

OKE spectroscopy has also proven to be a powerful means of studying the influence of different media on liquid dynamics. Nanoscopic confinement (i.e., confinement on distance scales up to a few times larger than the dimensions of a single molecule) can have a profound influence on the structure and dynamics of liquids.[44-48] The orientational dynamics of liquids confined in nanoporous sol-gel glasses have been studied in detail over the past few years using OKE spectroscopy.[29,30,37,38,49-55] OKE spectroscopy allows us to measure the collective

orientational correlation function of confined liquids on time scales ranging from femtoseconds to hundreds of picoseconds, thus providing a powerful means of obtaining quantitative microscopic information on the dynamics and dynamic populations of nanoconfined liquids.

We also have great interests in studying liquids under extreme conditions. Stretched liquids (i.e. liquids under tension) are one of such interesting systems. The density of a liquid under tension will be smaller than under normal conditions, which will decrease intermolecular interactions; thus attractive, rather than repulsive forces will be the dominant intermolecular interactions. We therefore expect that the microscopic structure and dynamics of liquids will be changed under tension, and these changes should be measurable by examining the intermolecular dynamics with OKE spectroscopy.

The Berthelot tube technique[56] has been the most popular method to stretch water to negative pressures. In this method (Figure 1.1), a vessel is filled with liquid water at high temperature and positive pressure, then is sealed and cooled down at constant volume. The liquid sample follows an isochore and is brought to negative pressure.

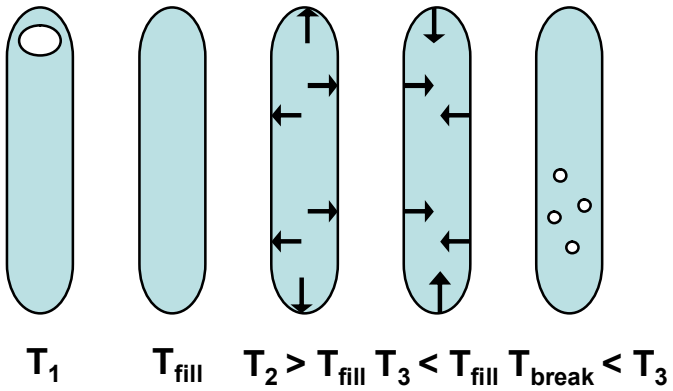

Figure 1.1 The Berthelot method schematically illustrated.

(First, one fills a capillary tube with pure and degassed liquid, cools the sample and holds it under modest vacuum, then flame-seal the cell under vacuum, after the sample melts, the tube contains the liquid plus a bubble (tube 1); Heating the tube to T_{fill} (filling temperature) until the liquid just occupy the whole volume (tube 2); Keep heating the tube to T_2, the liquid will keep expanding and therefore will be under positive pressure (tube 3); Then cool the liquid to T_3 (supposed to be lower than T_{fill}), the liquid would contract, but it would be hold to the wall by surface adhesive forces (tube 4), then liquid would be under negative pressure at T_3; Keep cooling the liquid to T_{break}, nucleation of vapor phase will happen, some bubbles come out, liquid is not under negative pressure any more (tube 5).)

Water was the first liquid to have been studied to any significant extent under extreme tension.[57-64] Water is in many ways an ideal liquid for such studies, in that it has an extremely high tensile strength for a liquid due to the high degree of hydrogen bonding. However, heterogeneous nucleation generally prevents water from being stretched to its intrinsic tensile strength. Furthermore, water is not readily amenable to study with OKE spectroscopy due to its extremely low polarizability anisotropy. The same holds true for other hydrogen-bonded liquids that would have high tensile strengths. As a result, little spectroscopic work has been done on liquids under negative pressure.

The results of our recent experiments suggest that aromatic liquids are excellent candidates for initial experiments on liquids under tension. Simple aromatic liquids

such as benzene have medium to high surface tensions for organic liquids,[65] and yet they also have small contact angles on silica. The small contact angles indicate a large enough affinity for glass that it should be possible to achieve large tensions in silica cells. The fact that the contact angle on silica is so small despite these liquids having healthy surface tensions is also an indication that these liquids are likely to have relatively large tensile strengths even though they are nondipolar. We believe that OKE experiments on aromatic liquids should yield clear signatures of the effects of negative pressure, due both to the strength of the OKE signal and the high sensitivity of the OKE spectrum to local structures in these liquids.

The synthesis of nonlinear optical techniques with microscopy over the past decade and a half has proven revolutionary for imaging. Nonlinear optical techniques such as multiphoton absorption,[66,67] second-[68,69] and third-[70-72] harmonic generation, and coherent anti-Stokes Raman scattering[73-77] (CARS) are all being used to great advantage in microscopy. Due to their nonlinear intensity dependence, all of these techniques offer exceptional three-dimensional spatial resolution while generally not affecting the sample being studied anywhere except in the focal region. These techniques also offer many different options for generating contrast; multiphoton absorption is usually used with fluorescent labels, second- and third-harmonic generation are sensitive to interfaces, and CARS probes Raman-active vibrations.

Given the simplicity of the OKE technique,[9,11] the nonlinear dependence of the signal and its potential to generate different types of contrast, OKE spectroscopy promises to be as powerful a technique for microscopy as any of the other techniques discussed above, especially for monitoring some important biological process taking

place on ultrafast time scale less than 100 ps. There has been one report about the use of OKE spectroscopy in microscopy[78] in which the mobility of water molecules in cellular domains was investigated.

A new scheme for measuring different tensor elements of the optical Kerr effect response was developed in our lab[79]. A dual-ring, polarization dependent Sagnac interferometer is used to create two copropagating probe pulses that arrived at the sample at different times but that reached the detector simultaneously and collinearly. The tensor element of the response that is measured is determined by the polarization of the pump pulse. By controlling the relative timing of the probe pulses it is also possible to perform optical subtraction of two different tensor elements of the response at two different times, a strategy that can be used to enhance or suppress particular contributions to the OKE response. We call this technique antiresonant ring Kerr spectroscopy (ARKS). Next we need to incorporate microscope objectives rather than lenses into this ARKS setup to use spectroscopy for microscopy. We can also incorporate a sample-scanning nanostage into the setup for performing imaging experiments in the future.

1.2 History

In 1875, John Kerr discovered the effect that now bears his name. In the Kerr effect, a DC electric field applied to a transparent, isotropic medium induces birefringence. From a molecular standpoint, the electric field interacts with molecular dipole moments, leading to a degree of net alignment in the liquid. So long as the molecules

are optically anisotropic, this alignment will lead to the medium having different indices of refraction parallel to and perpendicular to the electric field.

In 1964, Mayer and Gires[80] showed theoretically that a laser field could be strong enough to induce birefringence in a liquid, in what has become known as the optical Kerr effect. The OKE was first demonstrated experimentally in 1969 by Duguay and Hansen, who used pulses of a few picoseconds in duration to study the orientational dynamics of CS_2 and nitrobenzene.[13] In 1975, Ippen and Shank[81] demonstrated how to incorporate optical heterodyne detection in OKE spectroscopy, allowing for the direct probing of the nonlinear response of the liquid, rather than its magnitude squared. Heterodyne detection also amplifies the OKE signal considerably.

Another major milestone in the evolution of OKE spectroscopy was the development of the Fourier-transform deconvolution technique by McMorrow and Lotshaw.[15] In Fourier-transform deconvolution, heterodyne-detected OKE data are combined with a second-harmonic-generation autocorrelation to calculate the OKE spectral density, which is formally equivalent to the Bose-Einstein corrected Raman spectral density. This procedure compensates for the effects of the finite bandwidth of the laser pulses used, producing spectral densities that should not depend upon the instrument used to obtain the data.

The past two decades have seen many other important advances in OKE spectroscopy. For instance, a number of different techniques have been developed that allow multiple elements of the OKE response tensor to be investigated,[79,82-87] revealing important microscopic details of the liquid dynamics and allowing specific contributions to the signal to be isolated. Multiple-beam techniques involving

diffractive optics have proven to be powerful and robust methods for collecting data for different elements of the response tensor.[84,87]

1.3 Theory of the Optical Kerr Effect

1.3.1 Origin of the Optical Kerr Effect (OKE)

When a transparent liquid composed of anisotropically polarizable molecules is exposed to an intense ultrafast laser pulse (the "pump"), a dipole moment is induced along the axis of maximum polarizability of each molecule. The induced dipole moment interacts with the instantaneous electric field of the laser pulse, providing an impulsive torque that drives the axis of maximum polarizability of the molecules toward alignment with the polarization of the pump pulse. Since it is the polarizability of the molecules in a liquid that determines its index of refraction, the pump pulse creates a slight birefringence in the liquid. The induced birefringence can be monitored by a low-intensity "probe" pulse. The time dependence of the birefringence reveals information about microscopic dynamics.

There are two obvious effects caused by the intense pump pulse.[9] First, it will lead to the distortion of the electron cloud of the atoms and molecules and induce a strong and instantaneous electronic contribution to the OKE signal. It will also modify the random orientational distribution of the molecules, causing a partial alignment of the molecules in the direction of the electric field. This slightly uneven distribution is one important source for the transient birefringence. The spontaneous rotational diffusion of the molecules brings the system back to an isotropic equilibrium situation in a time

that is characteristic of rotational diffusion. We can measure this relaxation time directly by measuring the intensity change of the transmitted probe as a function of the delay time between the pump and probe pulses. We call this time the orientational correlation time. These two effects can just give us a simple physical picture of the transient OKE. If we focus on a short time range (typically 1-2 ps), some other processes have to be taken into account. Processes originating from intermolecular interactions may also produce a transient anisotropy, resulting in additional contributions to OKE signal. These motions include frustrated oscillatory motions (librations), density fluctuations and the collisions between molecules. In addition, if ultrafast pulses(with fs pulse width) are used, some intramolecular Raman-active low-frequency modes will also be coherently excited and this will also contribute to the OKE signal. The pump pulse serves as a "starting gun" for molecular dynamics, and plenty of information can be contained in the OKE signal. By analyzing the OKE signal, it is possible for us to extract useful information about the dynamics of many liquids we are interested in at a microscopic level.

1.3.2 Experimental Geometry and Heterodyne Detected Signal

The most common implementation of the optical Kerr effect is in a polarization spectroscopy geometry (Figure 1.2). Excitation is accomplished with a pump pulse polarized at 45°. The probe pulse, which has a variable time delay t relative to the pump pulse, is polarized vertically. After the sample, the probe pulse enters an "analyzer" polarizer that is set to pass horizontally polarized light. If the refractive index of the sample is isotropic, no light is transmitted by the analyzer polarizer.

However, any birefringence induced by the pump pulse leads to depolarization of the probe pulse, allowing a signal to pass through the analyzer. This leakage is related linearly to the degree of birefringence in the sample, and so by scanning the delay between the two pulses the time-dependent birefringence can be measured.

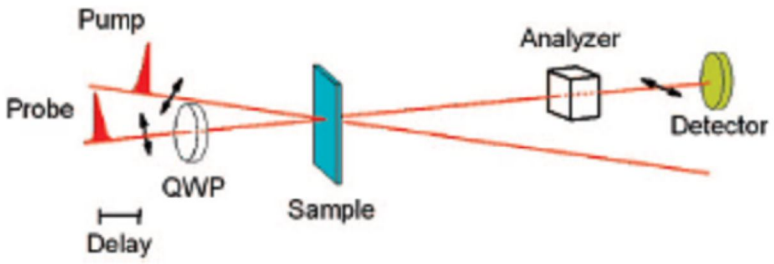

Figure 1.2 Schematic layout for a polarization spectroscopy implementation of the optical Kerr effect.

The polarization spectroscopy configuration is sensitive to the difference between two elements of the third order response, $R^{(3)}_{xxxx}(t)$ and $R^{(3)}_{xxyy}(t)$. (In frequency domain, these response functions correspond to the third order susceptibility tensor elements: $\chi^{(3)}_{xxxx}(-\omega_{signal};\omega_{pump},-\omega_{pump},\omega_{probe})$ and $\chi^{(3)}_{xxyy}(-\omega_{signal};\omega_{pump},-\omega_{pump},\omega_{probe})$; The subscripts correspond to the polarizations of signal, probe, pump and pump respectively.) In an isotropic medium, this difference is proportional to $R^{(3)}_{xyxy}(t)$ (or $\chi^{(3)}_{xyxy}(-\omega_{signal};\omega_{pump},-\omega_{pump},\omega_{probe})$),[88] which is known as the depolarized response. Because it is the intensity that is detected in this experimental configuration, the signal is proportional to the magnitude squared of the depolarized response; this situation is known as homodyne detection of the signal. By scanning *t*, the time dependence of the depolarized Kerr signal can be determined.

The phase of the third-order polarization of the OKE signal is determined purely by the phase of the probe field. Referenced to the phase of the probe field, the signal field generated by the polarization can be written as：

$$E_s = (\mathrm{Re}\, E_s + i\, \mathrm{Im}\, E_s) e^{-i\omega t} \qquad \text{(Eq. 1.1)}$$

where $\mathrm{Re}\, E_s$ and $\mathrm{Im}\, E_s$ correspond respectively to the absorption and index of refraction portions of the response and ω is the carrier frequency.

By placing a quarter-wave plate (QWP) after the first polarizer in the probe path but before the sample, optical heterodyne detection can be implemented. The QWP is aligned such that one of its axes is along the polarization of the probe beam. The input polarizer is then rotated by a slight amount (a few degrees at most), allowing some light to pass through the analyzer polarizer. This leakage is 90° out of phase with the rest of the probe beam, and acts as a local oscillator that mixes in phase with the OKE signal field.

$$E_{LO} = E_{probe} e^{-i\omega t} e^{i\pi/2} \qquad \text{(Eq. 1.2)}$$

The total electric field that passes through the analyzer is then $E_{\mathrm{LO}} + E_{\mathrm{OKE}(t)}$:

$$(\mathrm{Re}\, E_s + i\, \mathrm{Im}\, E_s) e^{-i\omega t} + E_{probe} e^{-i\omega t} e^{i\pi/2} \qquad \text{(Eq. 1.3)}$$

The intensity detected is the magnitude squared of this field, $I_{\mathrm{LO}} + 2E_{\mathrm{LO}}E_{\mathrm{OKE}(t)} + I_{\mathrm{OKE}(t)}$.

$$\begin{aligned} I &= \left|E_s + E_{LO}\right|^2 = \left|(\mathrm{Re}\, E_s + i\, \mathrm{Im}\, E_s) e^{-i\omega t} + E_{probe} e^{-i\omega t} e^{i\pi/2}\right|^2 \\ &= \left|e^{-i\omega t}\right|^2 \left|\mathrm{Re}\, E_s + i(\mathrm{Im}\, E_s + E_{probe})\right|^2 = E_{probe}^2 + \left[(\mathrm{Re}\, E_s)^2 + (\mathrm{Im}\, E_s)^2\right] + 2E_{probe}\, \mathrm{Im}\, E_s \\ &= I_{LO} + I_s + 2E_{probe}\, \mathrm{Im}\, E_s \end{aligned}$$

(Eq. 1.4)

The intensity of the local oscillator is the largest term in this equation but does not depend on the delay time t and so is a constant; it can also be removed by lock-in detection if the pump beam is chopped. The homodyne OKE intensity, $I_{S(t)}$, is the smallest term in the equation, and is generally dwarfed by the cross-term. Thus, via this crossterm, the local oscillator both amplifies the signal and makes it linear in the signal field, and thereby linear in the depolarized response. If the input polarizer is rotated by the same amount but in the opposite direction, then the local oscillator field is given by:

$$E_{LO} = E_{probe} e^{-i\omega t} e^{-i\pi/2} \qquad \text{(Eq. 1.5)}$$

which results in a detected intensity of $I_{\mathrm{LO}} - 2E_{\mathrm{LO}}E_{\mathrm{OKE}(t)} + I_{\mathrm{OKE}(t)}$.

$$I = I_{LO} + I_s - 2E_{probe}\,\mathrm{Im}\,E_s \qquad \text{(Eq. 1.6)}$$

and the sign of the cross-term in the intensity changes sign. By subtracting data collected at opposite heterodyne angles, any homodyne contribution to the signal can therefore be removed completely.

The first few picoseconds of a representative heterodyne detected OKE decay, in this case for 2, 4, 6-trifluoropyridine at 306 K, are shown in Figure 1.3. This decay shows all of the features seen in typical time-domain OKE data.

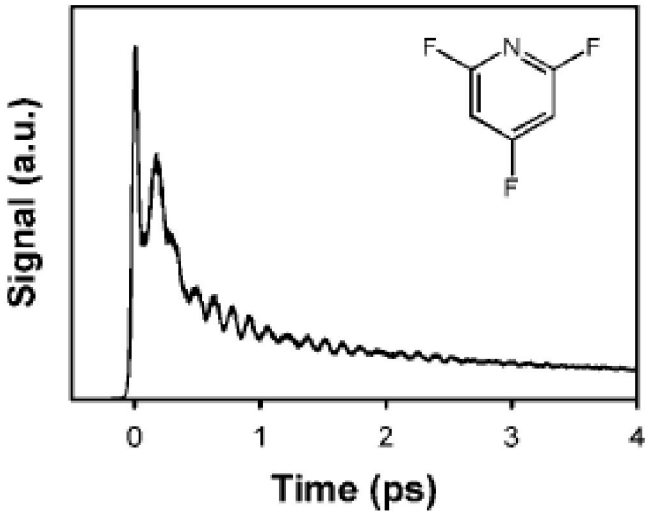

Figure 1.3 A typical OKE decay, in this case for 2,4,6-trifluoropyridine at 306 K. The sharp feature at zero delay time is the electronic response. The oscillations arise from Raman-active intramolecular vibrational modes. Coherently excited intermolecular modes contribute significantly to the decay for more than a picosecond, and orientational diffusion dominates at longer times.

For a typical time-resolved OKE signal, five contributions can be distinguished:

(1) A fast purely electronic contribution, due to the molecular hyperpolarizability, gives an instantaneous response;

(2) An intermolecular contribution is from the librational motion of the molecules in the cages of the first neighbor molecules. The librational decay is fast (typically up to a few picoseconds) due to the inhomogeneous dephasing in the liquid environment;

(3) An intramolecular vibrational "Raman" contribution decays with the dephasing time of the molecular vibrations (typically up to a few picoseconds);

(4) A term originating from the intermolecular interactions is correlated to the density fluctuations and hence to the collision-induced anisotropy of the molecular polarizability. Its relaxation is governed by the lifetime of the local structure in the liquids, again a few picoseconds;

(5) There is also a reorientational contribution, whose time scale can span a wide range of values, from a few picoseconds to several nanoseconds, depending on the molecular size and the viscosity, we call this contribution orientational diffusion.

The OKE response is proportional to the negative time derivative of the collective orientational correlation function, $C_{coll}(t)$.[89] The derivative nature of the response implies that slower processes necessarily give weaker signals. However, in many cases, the OKE response can be integrated to determine $C_{coll}(t)$ directly.[40,54] Proper integration requires the accurate determination of the constant of integration, which is possible so long as the long-time form of $C_{coll}(t)$ is known. For simple liquids, the long-time form of $C_{coll}(t)$ is generally exponential,[90] and so integration is a straightforward process. A semilogarithmic plot of the OKE decay from Figure 1.3 and the corresponding $C_{coll}(t)$ are shown in Figure 1.4. Integration not only increases the contribution of the slowly decaying portion of the dynamics but also helps to remove high-frequency noise. In addition, the delay time at which low-frequency noise begins to affect the reliability of the OKE data is readily apparent from integrated decays, and the data can be truncated before this point for fitting purposes.

From the fitting procedure above, the collective orientational correlation time can be obtained quite accurately. The orientational correlation time of a solute in a simple solvent is given by Debye-Stokes-Einstein (DSE) Equation[91]:

$$\tau = \frac{4\pi r_h^3 \eta}{3k_B T} \qquad \text{(Eq. 1.7)}$$

where η is the solvent viscosity, r_h is the solute hydrodynamic radius, T is the temperature, k_B is Boltzmann's constant. The reorientational correlation time can be measured at different temperatures for the liquid sample. After measurement of the viscosity, information on hydrodynamic volume can be obtained by plotting τ vs. η / T. By analyzing the the orientational correlation time and the hydrodynamic volume, information about dynamics of orientational diffusion will be gained.

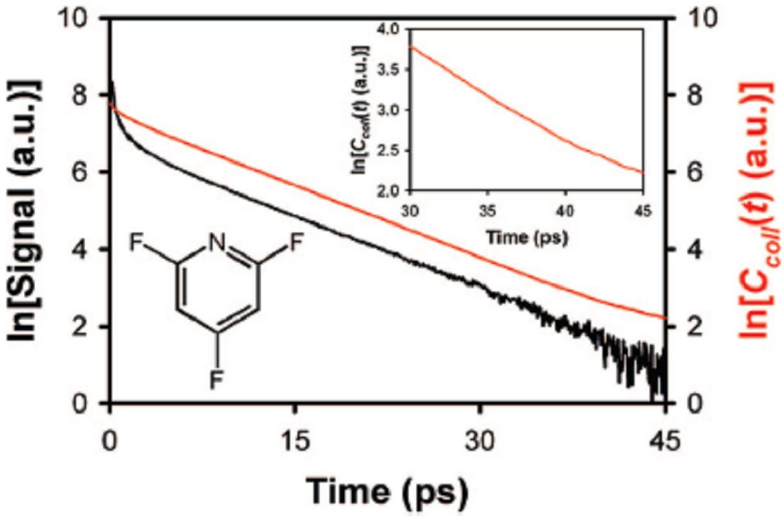

Figure 1.4 Comparison of the OKE decay (black) and $C_{\mathrm{coll}}(t)$ ($0.86\exp(-t/8.1)+0.14\exp(-t/1.8)$) derived by integrating the OKE decay (red) for 2,4,6-trifluoropyridine at 306 K. From the magnified portion of $C_{\mathrm{coll}}(t)$ shown in the inset, it is apparent that the integrated data begin to exhibit low-frequency noise and deviation from linearity at a time of about 35 ps. This is the cutoff time that was chosen in fitting the correlation function.

Because OKE spectroscopy is sensitive to the collective orientational correlation function, orientational decay times measured with this technique may differ from those measured by techniques that are sensitive to the single-molecule orientational correlation function, such as Raman spectroscopy and NMR. The collective orientational correlation time, τ_{coll}, is related to the single-molecule orientational correlation time, τ_{sm}, via[92]

$$\tau_{coll} = \frac{g_2}{j_2}\tau_{sm} \qquad \text{(Eq. 1.8)}$$

here, g_2 is the static pair orientational correlation parameter and j_2 is the dynamic pair orientational correlation parameter. The value of g_2 depends upon the degree of parallel ordering in a liquid, and takes on a value of unity when there is no net ordering. It is generally assumed that j_2 is unity in simple liquids. Thus, comparison of OKE orientational relaxation times with single-molecule relaxation times can give us estimation for g_2 value and yield microscopic structural information about a liquid.

1.3.3 Fourier-Transform Deconvolution

Fourier-transform deconvolution makes it possible to remove the effects of a laser pulse of finite duration from the OKE data, allowing for the accurate determination of Bose-Einstein corrected spectral densities.[15] The heterodyne-detected OKE signal $S(t)$ is given by

$$S \propto \left[I_{pump} \otimes I_{probe} \right] \otimes R^{(3)}_{xyxy} \qquad \text{(Eq. 1.9)}$$

where $\otimes$ denotes a convolution. The quantity in square brackets is the instrument response, which can be written as

$$G^{(2)}(t) = \int_{-\infty}^{+\infty} I_{pump}(t')I_{probe}(t-t')dt' \qquad \text{(Eq. 1.10)}$$

So long as the pulses used are transform limited, $G^{(2)}(t)$ is exactly the quantity measured by taking a second-harmonic-generation cross-correlation between the pump and the probe. Thus, $G^{(2)}(t)$ can be determined readily with a simple measurement.

According to the convolution theorem,[93] the Fourier transform of the convolution of two functions is equal to the product of the Fourier transforms of each function. Thus, we can write $\mathbb{F}\left[G^{(2)}(t) \otimes R^{(3)}_{xyxy}(t)\right] = \mathbb{F}\left[G^{(2)}(t)\right] \times \mathbb{F}\left[R^{(3)}_{xyxy}(t)\right]$, which implies that by dividing the Fourier transform of $S(t)$ by the Fourier transform of $G^{(2)}(t)$ we can determine the Fourier transform of $R^{(3)}_{xyxy}(t)$. The electronic response is a delta function centered at zero time, and therefore, its Fourier transform is a real constant. The nuclear response is zero before zero delay time, and therefore its Fourier transform is imaginary. This imaginary portion of the Fourier transform is called the spectral density. In Figure 1.5, we show the spectral density that corresponds to the OKE decay from Figure 1.3 as well as the deconvolved nuclear response function obtained by inverse Fourier transformation of the spectral density.

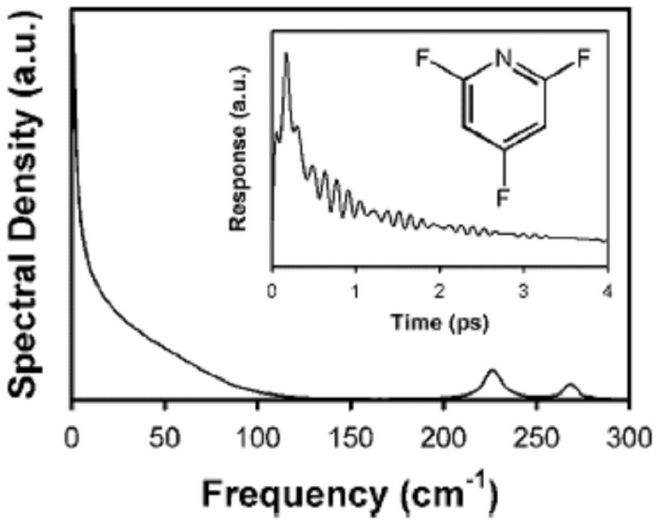

Figure 1.5 Spectral density for 2,4,6-trifluoropyridine at 306 K. The peaks near 230 and 270 cm^{-1} arise from intramolecular vibrations. Shown in the inset is the deconvolved nuclear response function for this liquid. Note that the electronic response is no longer present after deconvolution.

It is common practice to remove the diffusive orientational portion of the spectral density to obtain what is known as the reduced spectral density (RSD). A function of the form

$$\exp(-t/\tau_{OKE})\left[1-\exp(-t/\tau_{rise}\right] \qquad \text{(Eq. 1.11)}$$

is subtracted from the nuclear response function, which is then Fourier transformed to obtain the RSD. The rise time τ_{rise} is generally assumed to be 200 fs or less, and its value does not have a substantial effect on the shape of the RSD. The RSD corresponding to the OKE decay in Figure 1.3 is shown in Figure 1.6, along with the nuclear response function from which the contribution of orientational diffusion has

been removed. This is an example of a "triangular" RSD. Note that, if we neglect the oscillatory contributions from intramolecular vibrations, the response function with orientational diffusion removed still appears to decay exponentially. We will discuss the origin of this additional exponential decay below.

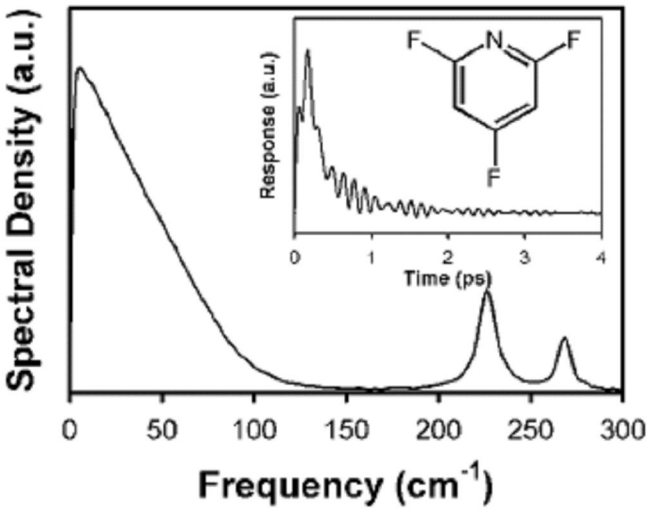

Figure 1.6 Reduced spectral density for 2,4,6-trifluoropyridine at 306 K. This is an example of a "triangular" RSD typical of fluorinated aromatics. Shown in the inset is the nuclear response function without the contribution from orientational diffusion. Once the contribution from intermolecular modes has decayed completely, any remaining contributions from intramolecular modes oscillate about zero.

1.3.4 Microscopic Origin of the Intermolecular Portion of the OKE Signal

The long-time portion of a typical OKE decay arises from orientational diffusion, and any high-frequency oscillations arise from intramolecular Raman modes. The source of the remainder of the signal, which is related to intermolecular motions, is

somewhat more complicated. As is the case for the intramolecular modes, any intermolecular mode that contributes to the OKE signal must be Raman active and must have a depolarized component.

The simplest mechanism through which intermolecular modes can contribute to the OKE signal is through librations. A libration is a rocking motion of a molecule that arises from the hindrance of rotational motion imposed by the surrounding cage of nearest neighbors. So long as the molecule has a polarizability anisotropy, such motion can lead to depolarized Raman scattering. [94] Although librations may involve complex motions of multiple molecules, librational scattering can be described in terms of motions of the polarizability tensors of individual molecules, and so is considered to be a molecular effect.

Liquids whose molecules have isotropic polarizabilities, such as CCl_4, can still exhibit substantial OKE signals.[95] The mechanism for this phenomenon is called interaction-induced (II) scattering, which arises from dipole/induced dipole (DID) effects.[94] A molecule in a liquid experiences not only an applied optical field but also the dipoles that the field induces in neighboring molecules. The strength of this DID effect on a given molecule depends strongly on the distance of its nearest neighbor or neighbors and their positioning relative to the molecule of interest and on the direction of the applied electric field. As the molecules move in their local potentials, the strength and directionality of the DID interactions is modulated, leading to II scattering. Both hindered translations and hindered rotations can contribute to II scattering. There can also be a cross-term between the contributions of librational scattering and II scattering.

To interpret RSDs, it is desirable to be able to understand the relative contributions of molecular and II scattering in the signal. Simulations are a powerful tool for attacking this problem, but a consensus has not been reached on this issue. Simulations that use a point anisotropic polarizability model or a point atomic polarizability model in which sites on the same molecule do not interact tend to give roughly equal importance to molecular and II scattering.[42,96]

Using CS_2 as a model system, detailed molecular dynamics simulations and instantaneous normal mode theory have been used to analyze the contributions to the OKE signal.[97,98] A point atomic polarizability model was used in which different polarizability sites on the same molecule are allowed to interact. While this type of model has some difficulties, we believe that it also more accurately represents the polarizability of real molecules, for which a close approach at one site can have a significant effect on the polarizability of the entire molecule. These studies indicated that, in both normal[97] and supercooled[98] CS_2, depolarized scattering is largely dominated by molecular effects, with II effects playing a relatively minor role. The same holds true in simulations in which the polarizability of CS_2 is made considerably larger, considerably smaller, or anisotropic (by giving the two sulfur atoms different atomic polarizabilities).[97] These results suggest that, for the majority of liquids in which the molecules have anisotropic polarizabilities, the OKE signal will arise predominantly from molecular effects. For supercooled CS_2, it was further found that even the isotropic spectrum, which arises solely from II effects, has a large component due to orientational motions.[98]

1.4 Outline of the Thesis

This thesis addresses a number of questions regarding the orientational diffusion and intermolecular dynamics of simple liquids. Questions addressed include what kind of microscopic structural information (conformation, local structure and molecular association) can we extract from the orientational diffusion data? How do intermolecular interactions affect the microscopic structure of liquids? What is the origin for the intermediate response, which appears in the OKE decay for all simple liquids? What is the dominant motion in determining the depolarized intermolecular dynamics, libration, translation or others? Which is the dominant factor in determining the shape of Reduced Spectral Density (RSD): molecular shape, local structure or distribution of polarizability? Is the breadth of the Reduced Spectral Density (RSD) dependent on moment of inertia of liquid molecules or not? What is the temperature dependence of depolarized intermolecular dynamics? Besides the depolarized response, how can we measure the other OKE responses such as isotropic response? Is it possible to develop an OKE microscopy technique? All these questions will be addressed in the following chapters and they are organized as follows:

- Chapter 2. We describe the setup for the optical-heterodyne-detected optical Kerr effect (OKE) spectrometer, and also the method to obtain the Reduced Spectral Density (RSD) from time-domain OKE data;
- Chapter 3. The temperature dependent orientational dynamics of 1,*n*-dicyano *n*-alkane liquids ranging from dicyanomethane to 1,8-dicyanooctane are described. The dependence of the reorientational times on temperature and viscosity is

consistent with the molecules adopting a largely extended structure in the liquid state, with a preference for gauche conformations at the methylenes bonded to the cyanide groups. The data are also suggestive of temperature-dependent, collective structural rearrangements in these liquids.

- Chapter 4. I describe a detailed, temperature-dependent, OKE study of pyridine, pyridine-d_5, 2,4,6-trifluoropyridine, 2,4,6-trimethylpyridine, and 1,3,5-tris(trifluoromethyl)benzene. By combining these data with those for other aromatic liquids that we have studied previously (Loughnane, B. J.; Scodinu, A.; Fourkas J. T. *J. Phys. Chem. B*, **2006**, *110*, 5708), we are able to assess the relative importance of molecular shape and electrostatic forces in determining the form of the OKE reduced spectral density for such liquids.
- Chapter 5. It has recently been shown [*J. Chem. Phys.* **2005**, *122*, 134506; *J. Am. Chem. Soc.* **2006**, *128*, 5119] that liquid tetrahydrofuran has an unusual structure that features voids of significant dimension. Such voids should affect other observable properties of this liquid. I present a temperature-dependent, OKE study of tetrahydrofuran and a number of related liquids (furan, cyclopentane, tetrahydropyran, cyclohexane, diethyl ether, and *n*-pentane) as well as hexamethylphosphoramide to test whether this technique can be used to reveal the presence of sizable voids in liquids.
- Chapter 6. Liquids under tension are an interesting system to study, in which the intermolecular interactions can be dominated by attractive forces, instead of repulsive forces. Based on a Berthelot tube technique, we develop a method to stretch liquids to negative pressure. We have been able to hold benzene and

acetonitrile samples under tension, and we expect OKE experiments should yield clear signatures of the effects of negative pressure of these liquids.

- Chapter 7 A new spectrometer for measuring different tensor elements of the OKE response has been developed. A dual-ring, polarization-dependent Sagnac interferometer was used to create two copropagating probe pulses that arrive at the sample at different times but that reach the detector simultaneously and collinearly. The tensor element of the response that is measured is determined by the polarization of the pump pulse. By controlling the relative timing of the probe pulses it is also possible to perform optical subtraction of two different tensor elements of the response at two different times, a strategy that can be used to generate contrast for microscopy.

1.5 References

(1) Valeur, B. *Molecular Fluorescence: Principles and Applications*. **2001**, Weinheim: Wiley-VCH.

(2) Lakowicz, J. R. *Principles of Fluorescence Spectroscopy*. 2 ed. **1999**, Berlin: Springer.

(3) Vanamerongen, H.; Vangrondelle, R. *Transient Absorption-Spectroscopy in Study of Processes and Dynamics in Biology*, in *Biochemical Spectroscopy*. **1995**, p. 201-226.

(4) Henriksen, N. E.; Engel, V. *Int. Rev. Phys. Chem.*, **2001**, 20, 93.

(5) Eichler, H. J.; Günter, P.; Pohl, D. W. *Laser-Induced Dynamic Gratings*. **1986**, New York: Springer-Verlag.

(6) Fourkas, J. T.; Fayer, M. D. *Acc. Chem. Res.*, **1992**, 25, 227.

(7) Kurnit, N. A.; Abella, I. D.; Hartmann, S. R., *Phys. Rev. Lett.* **1964**, 13, 567.

(8) de Boeij, W. P., Pshenichnikov, M. S. and Wiersma, D. A. *Annu. Rev. Phys. Chem.* **1998**, 49, 99.

(9) Righini, R. *Science* **1993**, 262, 1386.

(10) Kinoshita, S.; Kai, Y.; Ariyoshi, T.; Shimada, Y. *Int. J. Mod. Phys. B* **1996**, 10, 1229.

(11) Smith, N. A.; Meech, S. R. *Int. Rev. Phys. Chem.* **2002**, 21, 75.

(12) Fourkas, J. T., *Nonresonant Intermolecular Spectroscopy of Liquids*, in *Ultrafast Infrared and Raman Spectroscopy*, Fayer, M. D. Editor. **2001**, Marcel Dekker: New York. p. 473-512.

(13) Duguay, M. A.; Hansen, J. W. *Appl. Phys. Lett.* **1969**, 15, 192.

(14) McMorrow, D. *Opt. Comm.*, **1991,** 86, 236.

(15) McMorrow, D.; Lotshaw W. T. *J. Phys. Chem.*, **1991**, 95, 10395.

(16) Deeg, F. W.; Fayer, M. D. *J. Mol. Liq.* **1990**, 45, 19.

(17) Gottke, S. D.; Cang, H.; Bagchi, B.; Fayer, M. D. *J. Chem. Phys.* **2002**, 116, 6339.

(18) Hunt, N. T.; Meech, S. R. *J. Chem. Phys.* **2004**, 120, 10828.

(19) Torre, R.; Bartolini, P.; Pick, R. M. *Phys. Rev. E* **1998**, 57, 1912.

(20) Torre, R.; Bartolini, P.; Ricci, M.; Pick, R. M. *Europhys. Lett.* **2000**, 52, 324.

(21) Hinze, G.; Brace, D. D.; Gottke, S. D.; Fayer, M. D. *J. Chem. Phys.* **2000**, 113, 3723.

(22) Glorieux, C.; Nelson, K. A.; Hinze, G.; Fayer, M. D. *J. Chem. Phys.* **2002**, 116, 3384.

(23) Cang, H.; Li, J.; Fayer, M. D. *J. Chem. Phys.* **2003**, 119, 13017.

(24) Rajian, J. R.; Li, S. F.; Bartsch, R. A.; Quitevis, E. L. *Chem. Phys. Lett.* **2004**, 393, 372.

(25) Shirota, H.; Castner, E. W. *J. Phys. Chem. A* **2005**, 109, 9388.

(26) Li, J.; Wang, I.; Fruchey, K.; Fayer, M. D. *J. Phys. Chem. A* **2006**, 110, 10384.

(27) Xiao, D.; Rajian, J. R.; Li, S. F.; Bartsch, R. A.; Quitevis, E. L. *J. Phys. Chem. B* **2006**, 110, 16174.

(28) Shirota, H.; Wishart, J. F.; Castner, E. W. *J. Phys. Chem. B* **2007**, 111, 4819.

(29) Loughnane, B. J.; Farrer, R. A.; Scodinu, A.; Reilly, T.; Fourkas, J. T. *J. Phys. Chem. B* **2000**, 104, 5421.

(30) Farrer, R. A.; Fourkas, J. T. *Acc. Chem. Res.* **2003**, 36, 605.

(31) Portuondo-Campa, E.; Tortschanoff, A.; van Mourik, F.; Chergui, M. *Chem. Phys.* **2007**, 341, 11.

(32) Shirota, H.; Castner, E. W. *J. Chem. Phys.* **2006**, 125, 034904.

(33) Shirota, H. *J. Phys. Chem. B* **2005**, 109, 7053.

(34) Hunt, N. T.; Jaye, A. A.; Hellman, A.; Meech, S. R. *J. Phys. Chem. B* **2004**, 108, 100.

(35) Hunt, N. T.; Meech, S. R. *Chem. Phys. Lett.* **2004**, 400, 368.

(36) Heisler, I. A.; Correia, R. R. B.; Buckup, T.; Cunha, S. L. S.; da Silveira, N. P. *J. Chem. Phys.* **2005**, 123, 6.

(37) Loughnane B. J.; Farrer R. A.; Scodinu A.; Fourkas J. T. *J. Chem. Phys.* **1999**, 111, 5116.

(38) Scodinu A.; Farrer R. A.; Fourkas J. T. *J. Phys. Chem. B* **2002**, 106, 12863.

(39) Zhu X.; Farrer R. A.; Fourkas J. T. *J. Phys. Chem. B* **2005** 109, 12724.

(40) Zhu X.; Farrer R. A.; Zhong Q.; Fourkas J. T. *J. Phys. Cond. Matt.* **2005**, 17, 4105.

(41) Loughnane B. J.; Scodinu A.; Fourkas J. T. *J. Phys. Chem. B* **2006**, 110, 5708.

(42) Ryu, S.; Stratt, R. M. *J. Phys. Chem. B* **2004**, 108, 6782.

(43) Zhong, Q.; Fourkas, J. T. *J. Phys. Chem. B* **2008**, 112, 15342.

(44) Drake, J. M.; Klafter, J., Eds.; *Molecular Dynamics in Restricted Geometries*; Wiley: New York, **1989**.

(45) Drake, J. M.; Klafter, J.; Kopelman, R.; Awschalom, D.D., Eds.; *Dynamics in Small Confining Systems*; Materials Research Society: Pittsburgh, **1993**; Vol. 290, pp 377.

(46) Drake, J. M.; Klafter, J.; Kopelman, R.; Troian, S. M., Eds.;*Dynamics in Small Confining Systems II;* Materials Research Society: Pittsburgh, **1995**; Vol. 366, pp 466.

(47) Drake, J. M.; Klafter, J.; Kopelman, R., Eds. *Dynamics in Small Confining Systems III*;Materials Research Society: Pittsburgh, **1997**; Vol. 464, pp 388.

(48) Drake, J. M.; Grest, G. S.; Klafter, J.; Kopelman, R.,Eds.;*Dynamics in Small Confining Systems IV*; Materials Research Society: Warrendale, PA, **1999**; Vol. 543, pp 372.

(49) Farrer, R. A.; Loughnane, B. J.; Fourkas, J. T. *J. Phys. Chem. A* **1997**, 101, 4005.

(50) Loughnane, B. J.; Farrer, R. A.; Fourkas, J. T. *J. Phys. Chem. B* **1998**, 102, 5409.

(51) Loughnane, B. J.; Fourkas, J. T. *J. Phys. Chem. B* **1998**, 102, 10288.

(52) Loughnane, B. J.; Farrer, R. A.; Fourkas, J. T. Rotational Diffusion of Microconfined Liquids. In Dynamics in Small Confining Systems IV; Materials Research Society: Pittsburgh, **1999**; pp 33.

(53) Loughnane, B. J.; Scodinu, A.; Fourkas, J. T. *J. Phys. Chem. B* **1999**, 103, 6061.

(54) Loughnane, B. J.; Scodinu, A.; Fourkas, J. T. *Chem. Phys.* **2000**, 253, 323.

(55) Scodinu, A.; Fourkas, J. T. *J. Phys. Chem. B* **2002,** 106, 10292.

(56) Berthelot, M. *Ann. Chim. Phys.* **1850**, 30, 232.

(57) Trevena, D. H. *Contemp. Phys.* **1976**, 17, 109.

(58) Henderson, S. J.; Speedy, R. J. *J. Phys. E* **1980**, 13, 778.

(59) Green, J. L.; Durben, D. J.; Wokf, G. H.; Angell, C. A. *Science* **1990**, 249, 649.

(60) Zheng, Q.; Durben, D. J.; Wolf, G. H.; Angell, C. A. *Science* **1991**, 254, 829.

(61) Alvarenga, A. D.; Grimsditch, M.; Bodnar, R. J. *J. Chem. Phys.* **1993**, 98, 8392.

(62) Ruocco, G.; Sampoli, M.; Torcini, A.; Vallauri, R. *J. Chem. Phys.* **1993**, 99, 8095.

(63) Sciortino, F.; Essmann, U.; Stanley, E. H.; Hemmati, M.; Shao, J.; Wolf, G. H.; Angell, C. A. *Phys. Rev. E* **1995**, 52, 6481.

(64) Parker, M. E.; Heyes, D. M. *J. Chem. Phys.* **1998**, 108, 9039.

(65) Weast, R. C. *CRC Handbook of Chemistry and Physics* 66th edition (CRC Press, Boca Raton, **1985**).

(66) Denk, W.; Strickler, J. H.; Webb, W., *Science* **1990**, 248, 73.

(67) So, P. T. C.; Dong, C. Y.; Masters, B. R.; Berland, K. M. *Annu. Rev. Biomed. Eng.* **2000,** 2, 399.

(68) Moreaux, L.; Sandre, O.; Blanchard-Desce, M.; Mertz, J. *Opt. Lett.* **2000**, 25, 320.

(69) Kobayashi, M.; Fujita, K.; Kaneko, T.; Takamatsu, T.; Nakamura, O.; Kawata, S. *Opt. Lett.* **2002**, 27, 1324.

(70) Squier, J. A.; Muller, M.; Brakenhoff, G. J.; Wilson, K. R. *Opt. Expr.* **1998**, 3, 315.

(71) Millard, A. C.; Wiseman, P. W.; Fittinghoff, D. N.; Wilson, K. R.; Squier, J. A.; Muller, M. *Appl. Opt.* **1999**, 38, 7393.

(72) Millard, A. C.; Fittinghoff, D. N.; Wiseman, P. W.; Muller, M.; Brakenhoff, G. J.; Squier, J. A.; Wilson, K. R. *Biophys. J.* **2000**, 78, 800.

(73) Cheng, J. X.; Book, L. D.; Xie, X. S. *Opt. Lett.* **2001,** 26, 1341.

(74) Volkmer, A.; Cheng, J. X.; Xie, X. S. *Phys. Rev. Lett.* **2001,** 8702, 023901.

(75) Cheng, J. X.; Volkmer, A.; Book, L. D.; Xie, X. S. *J. Phys. Chem. B* **2001**, 105, 1277.

(76) Cheng, J. X.; Volkmer, A.; Xie, X. S. *J. Opt. Soc. Amer. B* **2002,** 19, 1363.

(77) Volkmer, A.; Book, L. D.; Xie, X. S. *Appl. Phys. Lett.* **2002,** 80, 1505.

(78) Potma, E. O.; de Boeij, W. P.; Wiersma, D. A. *Biophys. J.* **2001,** 80, 3019.

(79) Zhong, Q.; Zhu, X.; Fourkas, J. T. *Opt. Expr.* **2007**, 15, 6561

(80) Mayer, G.; Gires, F. *Compt. Rend.* **1964**, 258, 2039.

(81) Ippen, E. P.; Shank, C. V. *Appl. Phys. Lett.* **1975**, 26, 92.

(82) Cong, P. J.; Chang, Y. J.; Simon, J. D. *J. Phys. Chem.* **1996**, 100, 8613.

(83) Chang, Y. J.; Cong, P. J.; Simon, J. D. *J. Chem. Phys.* **1997**, 106, 8639.

(84) Hunt, N. T.; Jaye, A. A.; Meech, S. R. *Chem. Phys. Lett.* **2003**, 371, 304.

(85) Fecko, C. J.; Eaves, J. D.; Tokmakoff, A. *J. Chem. Phys.* **2002**, 117, 1139.

(86) Constantine, S.; Gardecki, J. A.; Zhou, Y.; Ziegler, L. D.; Ji, X. D.; Space, B. *J. Phys. Chem. A* **2001**, 105, 9851.

(87) Khalil, M.; Demirdoven, N.; Golonzka, O.; Fecko, C. J.; Tokmakoff, A. *J. Phys. Chem. A* **2000**, 104, 5711.

(88) Butcher, P. N.; Cotter, D. *The Elements of Nonlinear Optics*; Cambridge University Press: Cambridge, U.K., **1990**.

(89) Dhar, L.; Rogers, J. A.; Nelson, K. A. *Chem. Rev.* **1994**, 94, 157.

(90) Loughnane, B. J.; Scodinu, A.; Farrer, R. A.; Fourkas, J. T.; Mohanty, U. *J. Chem. Phys.* **1999**, 111, 2686.

(91) P. Debye, *Polar Molecules* Dover, New York, **1929**.

(92) Kivelson, D.; Madden, P. A. *Annu. Re*v. *Phys. Chem.* **1980**, 31, 523.

(93) Gradshteyn, I. S.; Ryzhik, I. M. *Tables of Integrals, Series, and Products*; Academic Press: San Diego, CA, **1980**.

(94) Murry, R. L.; Fourkas, J. T. *J. Chem. Phys.* **1997**, 107, 9726.

(95) Castner, E. W., Jr.; Chang, Y. J.; Melinger, J. S.; McMorrow, D. *J. Lumin.* **1994**, 60/61, 723.

(96) Ladanyi, B. M.; Klein, S. *J. Chem. Phys.* **1996**, 105, 1552.

(97) Murry, R. L.; Fourkas, J. T.; Keyes, T. *J. Chem. Phys.* **1998**, 109, 2814.

(98) Murry, R. L.; Fourkas, J. T.; Li, W.-X.; Keyes, T. *Phys. Rev. Lett.* **1999**, 83, 3550.

Chapter 2: Experimental Methods

2.1 Introduction

Optical Kerr effect spectroscopy is a pump/probe spectroscopy used to study refractive index changes[1-4]. The pump pulse induces a change in the refractive index; the probe pulse, which comes from the same laser as pump does and arrives at a variable delay time, is used to probe the change induced by pump.

There are many possible implementations of OKE spectroscopy, the most common of which is a polarization spectroscopy setup. The pump pulse is polarized at 45º and the probe at 90º. The probe passes through an analyzer polarizer set at 0º after the sample. Thus, unless the pump beam induces birefringence in the sample, no signal will be detected. This polarization spectroscopy setup therefore measures the anisotropic portion of the change in the refractive index.

The intensity of the OKE signal is relatively weak. However, the optical-heterodyne-detected (OHD) OKE method developed by McMorrow and Lotshaw[5,6] will introduce a local oscillator to enhance the OKE signal greatly. This can be simply done by using a quarter-wave plate.

2.2 Experimental setup

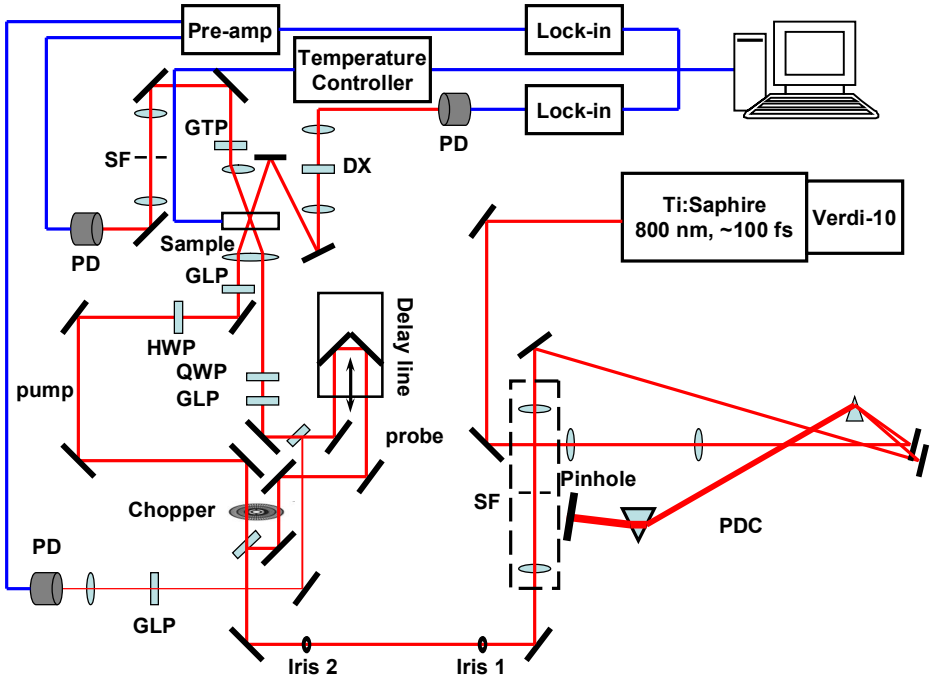

Fig. 2.1 Heterodyne-detected OKE setup. DX = doubling crystal, GLP = Glan laser polarizer, GTP = Glan-Thompson polarizer, HWP = half-wave plate, PD = photodiode, PDC = prism dispersion compensator, QWP = quarter-wave plate, SF =spatial filter.

Our experimental OKE setup (shown in Figure 2.1) is based upon the optical-heterodyne-detected OKE method developed by McMorrow and Lotshaw.[5,6] A modified commercial, mode-locked Ti:sapphire laser produces pulses with a center frequency near 800 nm at a repetition rate of 76 MHz. A pair of external LaFN28 prisms is used to compress the pulses and to compensate for dispersion caused by the optics in the experimental setup. The pulses that reach the sample are nearly

transform limited, and generally have duration of approximately 35 fs. After the prism dispersion compensator, the laser output is spatially filtered, and then is split into a strong pump beam and a weaker probe beam. The two beams are chopped at frequencies with a 7:5 ratio by the two rings of slots in the wheel of a mechanical chopper. The pump beam then passes through a half-wave plate and a Glan laser polarizer set to pass light polarized at 45° to the vertical, after which it is focused into the sample. The probe beam traverses an optical delay line with 0.1 μm resolution. It then passes through a Glan laser polarizer that is set to pass vertically polarized light, followed by a quarter-wave plate with its fast axis set to be along the vertical. The probe beam is then focused into the same spot in the sample as the pump beam. After the sample, the probe beam is recollimated by another lens and then it is incident on a Glan-Thompson polarizer that is set to pass horizontally polarized light. The leakage through the analyzer polarizer is spatially filtered and then is detected by a low-noise, amplified photodiode.

To implement optical heterodyne detection, the first polarizer in the path of the probe beam is rotated off of the vertical by a small amount (generally around 1°). This allows a small horizontally polarized component of the probe beam to pass along the slow axis of the quarter-wave plate, where its phase is retarded by 90°. This horizontal component passes through the analyzer polarizer, and thus can serve as a local oscillator that will amplify and linearize the OKE signal (which is also 90° out of phase with the probe beam). By collecting data at equivalent positive and negative heterodyne angles and subtracting one set from the other, the homodyne contribution to the signal can be removed, leaving the pure heterodyne component.

We have made several adaptations to the experimental setup to improve the signal-to-noise ratio. First, the pump beam is picked off after the sample and is frequency-doubled in a KDP crystal. The doubled light is detected with a photodiode and lock-in amplifier. Because second-harmonic generation has the same nonlinearity as the heterodyne-detected OKE signal, the doubled light can be used to normalize for any long-term intensity variations in the laser. Second, a small portion of the probe beam is picked off after the chopper and detected by a photodiode that is matched to the signal photodiode. The outputs of the signal and reference photodiodes are connected to the differential inputs of a low-noise preamplifier. With the pump beam blocked, the intensity of the reference beam is adjusted to zero the output of the preamplifier, thus removing the contribution of the local oscillator to the detected intensity. The pump beam is then unblocked, and the output of the preamplifier is sent to a lock-in amplifier that is referenced to the sum of the two chopping frequencies.

Autocorrelation scans are collected by replacing the sample with a KDP crystal. The doubled light created by the overlap of the pump and probe pulse is detected by a low-noise, amplified photodiode that is connected to a lock-in amplifier with its frequency set at the sum of the chopping frequencies of the pump and probe beams. Glass blanks are placed in front of the crystal to correct for the glass that is introduced by the sample cell and cryostat.

2.3 Data Acquisition

The data acquisition is completely computer controlled using programs written in LabView. The computer moves the delay line, reads and averages the values in the data buffers of each lock-in amplifier, and then saves the normalized signal for that

data point. No data are acquired unless the temperature of the sample is within 0.5 °C of the desired value. Between consecutive scans, the computer reverses the angle of the first polarizer in the probe path to switch the heterodyne angle. Data are generally acquired with short-step scans (0.67 fs) out to delays of several picoseconds, and then with long-step scans (33.3 fs or 66.7 fs) for longer delays.

Fig. 2.2 Data acquisition window Ⅰ: Getting GPIB addresses.

Here is the first window for the LabView program (Figure 2.2). For this step, one needs to input the GPIB addresses for all the instruments controlled by the program, the five instruments that are controlled are the delay line, the rotational stage for probe polarizer, the cryostat controller, and the two lock-in amplifiers. One lock-in collects OKE signal data from the preamplifier, while the other lock-in collects the doubled pump data from the photodiode. Each instrument has a unique address and

the LabView program uses the GPIB addresses to recognize and control the motions of individual instruments. The correct GPIB addresses of each instrument can be seen from the figure 2.2:

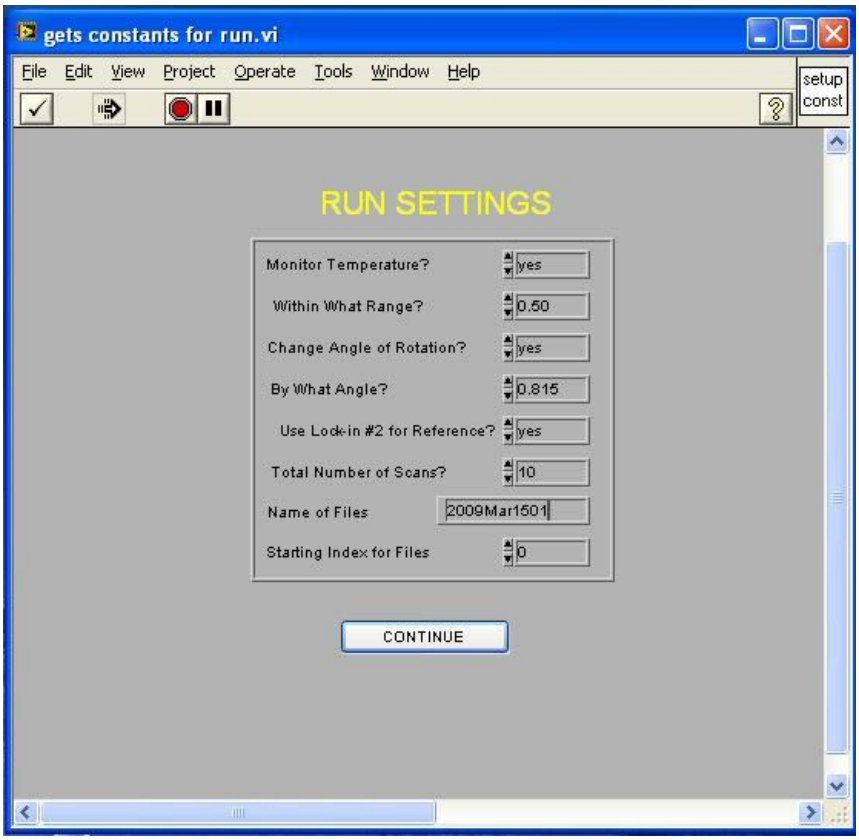

Fig. 2.3 Data acquisition window Ⅱ: Run settings.

After the user sets all the GPIB addresses correctly and presses the continue button, the next window (Figure 2.3) containing new parameters appears. This menu will let us set all options necessary for the experiment. The first setting asks if the user wish the temperature of sample to be monitored during the experiment, “Yes” or “No” depends on if you want to run the temperature dependent experiment or not. If you answer “Yes”, and define the range for the temperature, for example “0.5 K”, then if the real temperature of the sample falls out of the range, the program will suspend

operation until the temperature returns to the approved range. The “Change Angle of Rotation?” and “By What Angle?” queries concern the angle of the automatic rotation stage used to introduce the heterodyne portion of the probe beam. “Use Lock-in #2 for Reference” asks if the user want the collected OKE signal to be normalized by the intensity of double pump. The last three settings of the menu define the number and names of the scans to be collected. The first one is “Total Number of Scans?” in which the user enters the number of scans for this run and usually some even number between 10 and 20 is favored. The “Name of Files” are usually defined using the current date as the base name and plus a sequence number, for example, if the scan is the second run of March 15, 2009, then the name is defined as “2009Mar1501”. For “Starting Index for Files”, zero is usually used as the starting index, so if we use 10 as “Total Numbers of Scans”, then the names of data files collected by this run would be from “2009Mar15010” to “2009Mar15019”. Once all the parameters on this screen are satisfactory, the “continue” button is pressed.

Fig. 2.4 Data acquisition window ⅢⅣ: More run settings.

The next, also the last set of parameters is titled “More Run Settings” (Figure 2.4). This menu will define the components of each individual scan. The “starting” and “Ending Point” values will define the beginning and ending point on the delay line for each scan. The values are entered in tenths of a micron (the smallest step possible for the delay line). The “Step Size” value defines the distance the delay line travels between each successive point collected, “1” is used for short step size scans and “50” or “100” are often sued for long step size scans. The last two entries, “Time Constant” and “Time Constants to Read” are concerned with the signal-to-noise ratio of the data. As a lock-in amplifier collects data, it continuously computes an average of the data in the time range of the value of “Time Constant”, so the larger this value, the better the signal-to-noise ratio, but the longer time the total run takes. “100 ms” is usually used, which can give us not only a good signal-to-noise ratio for the data, but also a comfortable length of time for each scan. Finally, when user has entered all the necessary parameters for each scan, the “done” button can be pressed and the program starts collecting and saving data. At each scan, the program collects two sets of data: the OKE signal from lock-in amplifier #1 and the doubled pump signal from lock-in #2. Because each scan takes a significant amount of time to finish, the doubled pump is collected for the purpose of correcting the long-time fluctuations of laser intensity and normalizing the OKE signal. The normalization is simply done by dividing the detected OKE signal by the doubled pump. The pump beam is doubled so that it has the same nonlinearity to the intensity of laser as the OKE signal. The normalized OKE signal is also displayed on computer screen by ‘Total run program’

when collecting data (see Fig. 2.5). This is the basic procedure for collecting OKE data.

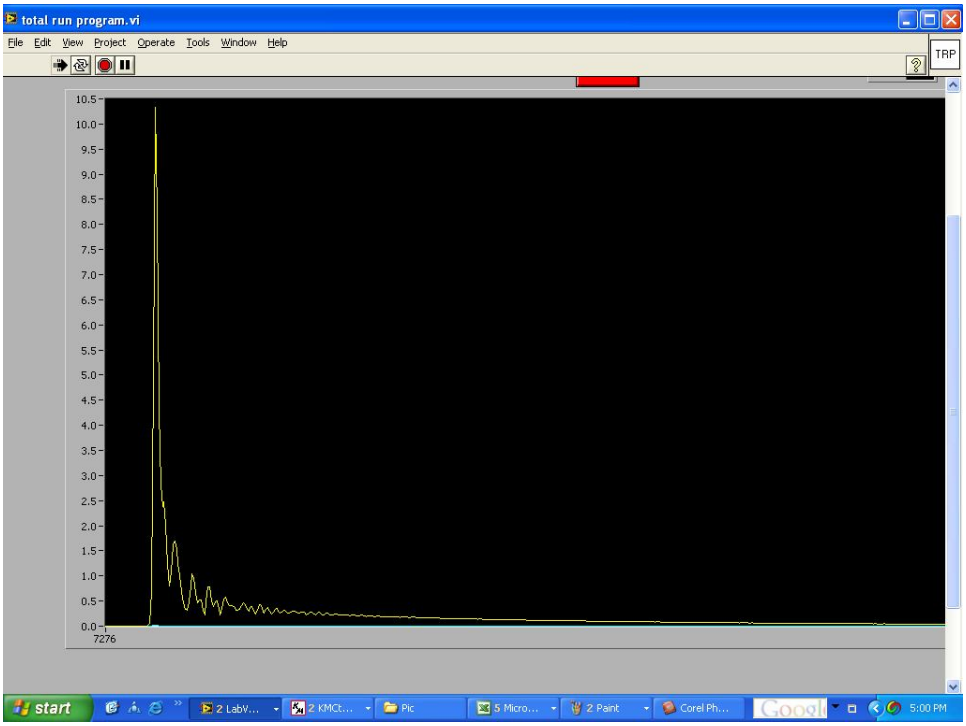

Fig. 2.5 Data acquisition window Ⅳ: Total run program.

2.4 Data Analysis

The analysis of the data can also be done by the program written in LabView. The basic analysis procedure can be described in this way:

First, we collect data for the whole decay by long step size. We know, the OKE signal is the negative time derivative of the collective orientational correlation function, $C_{coll}(\tau)$, where τ is the delay time between the pump and probe pulses, so $C_{coll}(\tau)$ can be computed by appropriate integration of the OKE decays. Then a nonlinear least-squares routine is used to fit $C_{coll}(\tau)$ to a biexponential decay starting

at delay times greater than 2 ps (usually longer for low temperature data). The two time constants, for the collective orientational correlation time and the intermediate response time, along with the corresponding amplitudes A_{or} and A_i can be determined. We thereby get the functional formula for the long-time tail of the OKE decay.

Second, OKE data are collected for the first 5 ps decay (including the contributions from intramolecular and intermolecular modes) with a short pulse width using a short step size. The determined long-time decay from $C_{coll}(\tau)$ is used to add the tail for the short step size data to extend the time range.

The third step is to apply the Fourier transform deconcolution procedure to the data from step 2, which helps to compensate for the effects of the finite duration of the laser pulse used. Once this step is finished, we can get the deconvolved response function. Then a function of the form

$$r(\tau) = Ae^{(-\tau/\tau_{or})}\left[1 - e^{(-\tau/\tau_r)}\right] \qquad \text{(Eq. 2.1)}$$

is subtracted from the response function to remove the contribution of orientational diffusion.

The final step is to get the RSD (Reduced Spectral Density). This can be done by Fourier transformation of the response function without the contribution from orientaional diffusion.

Following this procedure, we can get the collective orientational correlation time constants for orientational diffusion dynamics study, and also the reduced spectral density (RSD) for intermolecular dynamics study. This can be simply done with the

help of Labview program written for OKE data analysis, and please refer to ***Appendix A*** for the detail about how to use the program.

2.5 References

(1) Righini, R. *Science* **1993**, 262, 1386.

(2) Kinoshita, S.; Kai, Y.; Ariyoshi, T.; Shimada, Y. *Int. J. Mod. Phys. B* **1996**, 10, 1229.

(3) Fourkas, J. T. Nonresonant Intermolecular Spectroscopy of Liquids. In *Ultrafast Infrared and Raman Spectroscopy*; Fayer, M. D., Ed.; Marcel Dekker: New York, **2001**; Vol. 26; pp 473.

(4) Hunt, N. T.; Jaye, A. A.; Meech, S. R. *Phys. Chem. Chem. Phys.* **2007**, 9, 2167.

(5) McMorrow, D., *Opt. Comm.*, **1991,** 86, 236.

(6) McMorrow, D.; Lotshaw, W. T. *J. Phys. Chem.* **1991**, 95, 10395.

Chapter 3: Temperature-dependent Orientational Dynamics of 1,n-Dicyano n-Alkanes

3.1 Introduction

The dynamic behavior of a molecule in solution is highly sensitive to the details of its local environment. For example, the orientational diffusion rate of a solute molecule is sensitive to its conformation. In general, a solute molecule in an extended conformation must displace more solvent molecules in order to reorient than would the same solute molecule in a more compact conformation, and therefore the molecule in its extended conformation would be expected to have a lower rate of orientational diffusion. This behavior is embodied by the Debye-Stokes-Einstein (DSE) relation,[1,2] which in its simplest form is given by

$$\tau_{or,sm} \cong \frac{\eta V_H}{k_B T} \qquad \text{(Eq. 3.1)}$$

where $\tau_{or,sm}$ is the single-molecule orientational correlation time, η is the viscosity, V_H is the hydrodynamic volume for reorientation, k_B is Boltzmann's constant, and T is the temperature. A multiplicative term may also be included in this relation to account for the boundary conditions for reorientation.

The DSE relation was originally intended to apply to solute molecules that are considerably larger than the solvent molecules. However, experiments using techniques such as Raman spectroscopy, NMR spectroscopy, Rayleigh-wing spectroscopy, and optical Kerr effect[3-6] (OKE) spectroscopy indicate that in most

cases the DSE relation works quite well for neat, simple liquids as well.[2] We and others have previously observed this to be the case for OKE experiments in a wide range of small molecule, nonassociated liquids, for example.[7-13]

We have recently reported the results of OKE experiments performed on liquids *n*-alkyl cyanides, molecules of the form $CH_3(CH_2)nCN$.[9] While for small enough values of *n* the molecules in these liquids are expected to adopt an extended conformation, we found, unexpectedly, that extended conformations persisted in molecules with as many as 10 methylene units. In addition, our studies were suggestive of temperature dependent changes in the underlying collective structure of some of these liquids.[9]

Here we report OKE studies of 1,*n*-dicyano *n*-alkanes, i.e., molecules of the form $NC(CH_2)_nCN$. The highly polar groups at both ends of these molecules could potentially lead to significant differences in the dynamic and structural behaviors of these liquids compared to *n*-alkyl cyanides. Our results indicate, however, that the dicyanides also feature significantly extended structures in the neat liquid, with a preference for gauche conformations at the terminal methylene groups. Our data also suggest that these liquids exhibit temperature-dependent, collective structural changes.

3.2 Experimental Section

Our optical-heterodyne-detected[14,15] OKE spectrometer and data collection procedures have been described in detail elsewhere.[16,17] Temperature-dependent OKE data were collected for eight dicyanides, ranging from dicyanomethane to 1,8-dicyanooctane (Table 3.1) with pulses of 60 fs or greater duration. These relatively long pulses were employed both to increase the signal from orientational relaxation and to help remove the effects of intramolecular vibrational modes. Due to the pulse

lengths used, no attempt was made to determine the intermolecular vibrational spectra of these liquids from the OKE data.

Table 3.1 Formula Weight, Density at Room Temperature, Minimum and Maximum Temperatures Studied, and Activation Energy for Collective Reorientation for the Dicyanoalkanes Examined

liquid	FW (amu)	ρ (g/mL)	T_{min} (K)	T_{max} (K)	E_A (cm^{-1}/1000)
dicyanomethane	66.06	1.191	306	360	0.97
1,2-dicyanoethane	80.09	0.985	336	380	1.3
1,3-dicyanopropane	94.11	0.981	289	375	1.4
1,4-dicyanobutane	108.14	0.968	275	375	1.4
1,5-dicyanopentane	122.17	0.948	272	374	1.7
1,6-dicyanohexane	136.19	0.940	289	366	1.6
1,7-dicyanoheptane	150.22	0.929	306	364	1.5
1,8-dicyanooctane	164.24	0.913	297	366	1.7

All liquids were purchased in the highest purity form available from Aldrich. The liquids were colorless and were used as received, with the exception of dicyanomethane, which was brown when received. Consequently, dicyanomethane was distilled and then used promptly. After distillation, this substance was slightly reddish in color, but it did not discolor further over the course of data acquisition. The melting points of all the substances agreed well with literature values.

OKE data collected at equal but opposite heterodyne angles were subtracted to obtain the pure heterodyne signal. The data were then integrated to give the collective orientational correlation function, $C_{coll}(\tau)$,[18] where τ is the experimental delay time. In all cases, the data were taken out to delay times well beyond the point at which $C_{coll}(\tau)$ became too noisy to be fit robustly. $C_{coll}(\tau)$ was truncated at the point at which it became noisy and then was fit to a biexponential function with a variable baseline using a nonlinear-least-squares routine.[19] The early time fitting limit was varied to ensure that the fit parameters were robust. It is important to note that, with increasing alkyl chain length, the density of polarizable cyanide groups decreases, which in turn reduces the many-body polarizability of the liquid.

In addition, the orientational correlation time increases with increasing chain length. Since the OKE signal is the negative time derivative of $C_{coll}(\tau)$, liquids that relax more slowly necessarily give weaker signals. As a result, for the molecules with the longest chains it was not possible to observe decays over as many factors of *e* as for the shorter chain liquids, leading to greater uncertainty in the fit relaxation times.

Temperature-dependent viscosity data were obtained from the literature[20] and were fit to

$$\ln[\eta(T)] = A + \frac{B}{C+T} \qquad \text{(Eq. 3.2)}$$

to derive viscosities for the temperatures used here. Equilibrium molecular geometries were calculated using a molecular modeling program[21] in order to determine hydrodynamic volumes under slip boundary conditions.

*3.3 **Results***

The temperature ranges over which data were collected for each liquid are listed in Table 3.1. Shown in Figure 3.1 is a typical collective orientational correlation function obtained for one of these liquids, in this case 1,5-dicyanopentane at a temperature of 288 K. For this particular decay, the data at times $\tau \geq 20$ ps have been fit to a function of the form

$$C_{coll}(\tau) = A\exp(-\tau/\tau_1) + [1-A]\exp(-\tau/\tau_2) \qquad \text{(Eq. 3.3)}$$

where $\tau_1 > \tau_2$ and A is the normalized amplitude of the portion of the decay with the slower relaxation time. Based on the residuals plotted at the bottom of the figure, it can be seen that the fit is an excellent one. Biexponential functions were found to provide excellent fits to all of the data for each liquid. Complete tables of the temperature-dependent viscosity, parameters from biexponential fits to the OKE data, and fitting ranges are given for each liquid in the ***Appendix B***.

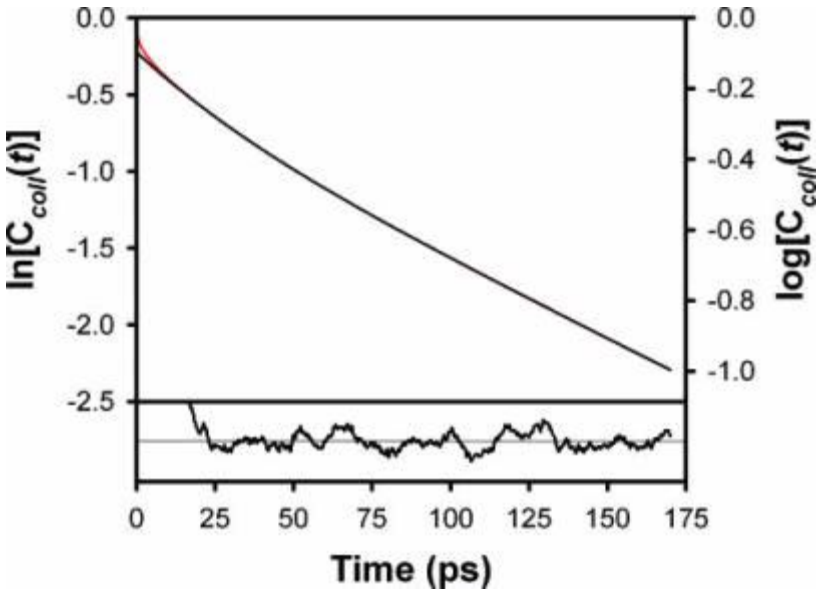

Figure 3.1 Logarithm of the collective orientational correlation function of 1,5-dicyanopentane at 288 K (red) and a biexponential fit to the data (black). The residual obtained by subtracting the fit from the data is shown at the bottom on a linear scale.

Biexponential OKE decays are commonly observed in nonnetworked, small-molecule liquids.[8-10,15,22-31] In general, the slower decay component arises from collective orientational diffusion whereas the faster component is ascribed to the socalled "intermediate" response, the source of which has not been fully established. However, it should be noted that the contribution of orientational diffusion to the OKE decay of a liquid can feature up to five exponentials, depending on the shape and orientations of the diffusion and polarizability tensors.[32] Thus, if τ_2 for the dinitriles is to be assigned to the intermediate response, it is important to verify that the dinitriles studied here exhibit single-exponential orientational diffusion. Whether a single-exponential orientational decay should be observed depends upon factors

such as the molecular conformation, the principal values of the orientational diffusion and polarizability tensors, and the principal axis systems of these tensors.[32] In the OKE spectroscopy of *n*-alkyl cyanides we did observe single-exponential orientational decays.[9] If the conformations of the dinitriles in the liquid phase are similar to those of the *n*-alkyl cyanides, then we would expect to see single-exponential orientational decays in the dinitriles as well.

For a broad range of small-molecule, nonassociated liquids, the OKE intermediate relaxation time has been observed to scale with the collective orientational correlation time.[8-10] If τ_2 for the dinitriles corresponds to the intermediate response, then it would be expected to track τ_1 with a similar scaling factor regardless of temperature or the identity of the dinitrile. In Figure 3.2 we plot τ_2 as a function of τ_1 for all of the liquids studied here. In all cases there is a linear relationship between the two times, and the constant of proportionality between the two times lies within a range of approximately [4-5], which is in good agreement with previous observations for the relation between the collective orientational correlation time and the intermediate response time.[8-10] Given the large range of aspect ratios among the molecules studied here, if τ_1 and τ_2 both corresponded to orientational diffusion, we would expect to see a much larger range of scaling factors, as reorientation about the long molecular axis should not depend significantly on molecular length whereas reorientation about the axes perpendicular to this axis should depend on length. We therefore have good evidence that τ_1 can be assigned to orientational diffusion and that τ_2 can be assigned to the intermediate response.

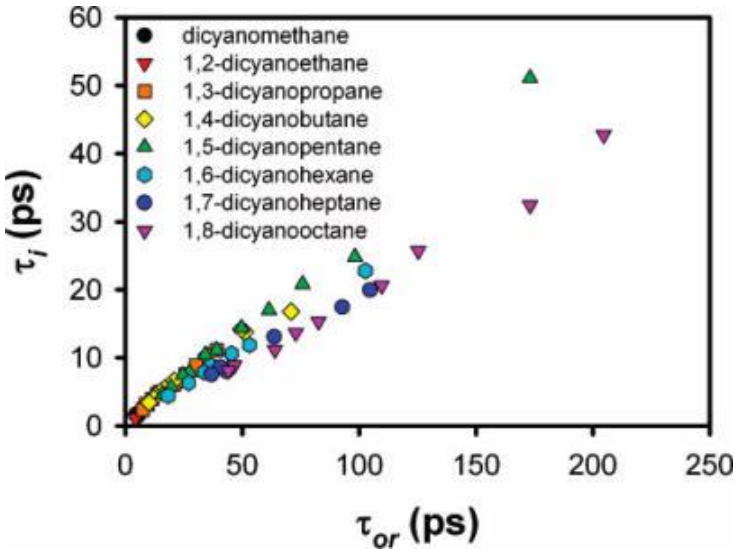

Figure 3.2 Plot of fast versus slow relaxation times for OKE decays of the dicyanoalkanes. The relationship between the two times supports the assignment of the faster time to the intermediate response and the slower time to orientational diffusion.

We should note that, in the literature, the intermediate response time originally referred to relaxation with a time constant that was generally on the order of a picosecond or less.[26] However, with improvements in laser technology it has become possible to study liquids with considerably longer relaxation times. This capability has led to the realization that the intermediate response tracks the orientational relaxation, and can therefore have a time constant that is considerably longer than a picosecond.[8-10] This is the case for most of the data presented here, and is the reason that the fit in Figure 3.1 begins only at 20 ps. In such a slowly relaxing liquid, the influence of coherently excited intermolecular modes can be observed out to delay times of many picoseconds.

To determine whether the DSE relation holds for the liquids studied here, we can

plot τ_{or} as a function of η/T for each liquid. Shown in Figure 3.3 is a representative DSE plot, in this case for 1,4-dicyanobutane. This plot is clearly not linear, but rather appears to be divided into linear regions with distinct slopes (although within the experimental uncertainty of the values of τ_{or} we cannot entirely rule out describing the DSE data for this and the other liquids studied here by smooth, monotonically decreasing curves). The plot is linear for the highest values of η/T down to approximately 0.024 cP/K, and then exhibits a transition to a new, higher slope. A second transition to an even larger slope occurs at a value of η/T near 0.005 cP/K. Similar behavior is observed for dicyanomethane through 1,6-dicyanohexane. The relaxation times for 1,7-dicyanoheptane and 1,8-dicyanooctane are so long that they could not be determined with sufficient precision to ascertain whether transitions exist for these liquids as well.

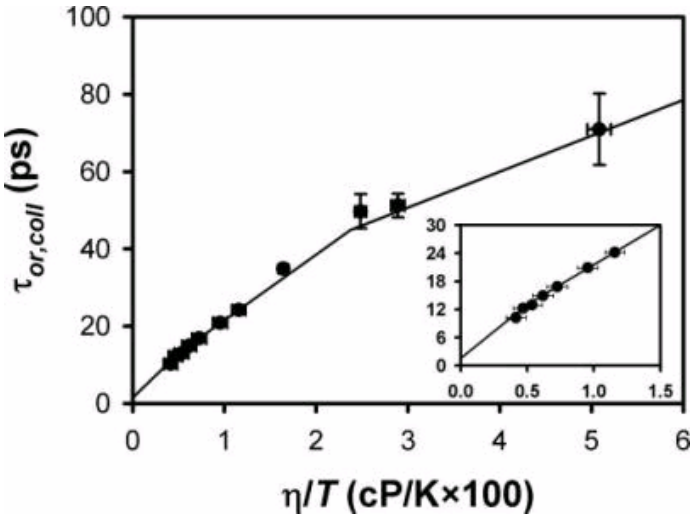

Figure 3.3 Debye-Stokes-Einstein plot for 1,4-dicyanobutane. The lines are linear-least-squares fits to the slope in each region. The inset is a blowup of the data up to η/T) 0.015 cP/K.

The DSE data for the dinitriles can be divided into three distinct regions. Slopes in region A are observed in dicyanomethane through 1,5-dicyanopentane at higher temperatures. Slopes in region B are observed in dicyanomethane through 1,3-dicyanopropane at lower temperatures, in 1,4-dicyanobutane and 1,5-dicyanopentane at intermediate temperatures, and in 1,6-dicyanohexane at higher temperatures. Slopes in region C are observed for 1,4-dicyanebutane through 1,6-dicyanohexane at lower temperatures and for 1,7-dicyanohexane and 1,8-dicyanooctane at all temperatures studied here. The slopes in each of these regions and the approximate transition temperatures between them are listed in Table 3.2 for all of the liquids studied here. We note that given our point spacing and the uncertainty in our values of τ_{or}, the transitions are not necessarily sharp, but may rather take place over a range of 5-10 K.

TABLE 3.2: DSE Slopes in Regions A, B, and C and Transition Temperatures between Regions A and B and Regions B and C for the Dicyanoalkanes Studied Here

liquid	Slope A (ns*K/cP)	Slope B (ns*K/cP)	Slope C (ns*K/cP)	T_{AB} (K)	T_{BC} (K)
dicyanomethane	0.657	0.137		323	
1,2-dicyanoethane	1.24	0.756		358	
1,3-dicyanopropane	1.90	1.27		340	
1,4-dicyanobutane	2.16	1.89	0.844	361	294
1,5-dicyanopentane	3.88	3.39	2.29	349	302
1,6-dicyanohexane		5.06	2.90	340	
1,7-dicyanoheptane			4.69		
1,8-dicyanooctane			6.47		

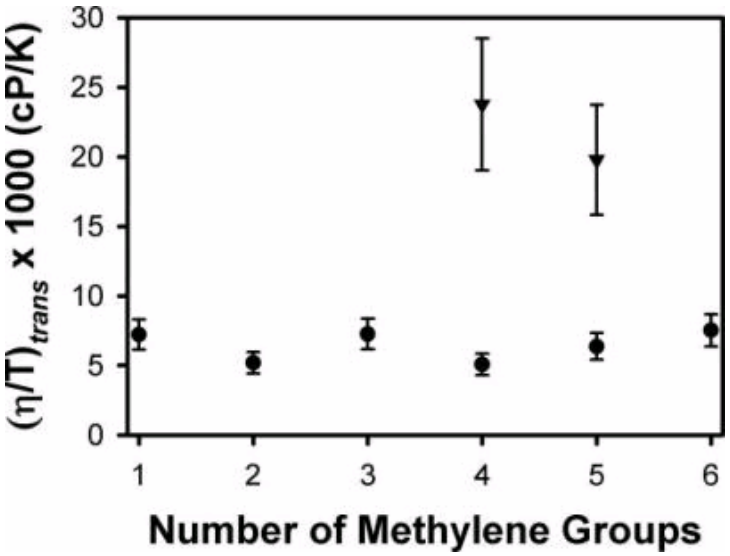

Figure 3.4 Values of η/T for the transition between regions A and B (circles) and between regions B and C (triangles) as a function of the number of methylene groups in each liquid.

In Figure 3.4 we plot the value of η/T at which the transitions between regions A and B and between regions B and C appear to occur as a function of the number of methylene groups in each molecule. The transition between regions A and B occurs at an average value of η/T of approximately 0.0065 cP/K for dicyanomethane through 1,6-dicyanohexane. The value of η/T at which the transition between regions B and C occurs appears to decrease with the number of methylene groups for 1,5-dicyanopentane and 1,6-dicyanohexane, although the two points cannot be distinguished definitively within the experimental uncertainty. Being able to obtain decays for 1,7-dicyanoheptane and 1,8-dicyanooctane out to considerably longer times would help to clarify the behavior of this transition with increasing chain length.

3.4 Discussion

Higashigaki and Wang[20] (HW) have previously studied dicyanomethane through 1,6-dicyanohexane using Rayleigh wing scattering, a technique that is related directly to OKE spectroscopy. While their results bear some similarities to ours, there are also significant differences among them. Most importantly, HW reported linear DSE plots for the six liquids that they studied, although their plots do reveal signs of slope discontinuities for some of the liquids at low values of η / T.[20] Our viscosity numbers were derived from the work of HW, so it is unlikely that these values are the cause of the discrepancies between the two studies. We must therefore focus attention on either the orientational diffusion times or the temperatures. HW found that their measured relaxation times obeyed Arrhenius behavior,[20] so in Figure 3.5 we present an Arrhenius plot of our data for the eight liquids studied here.

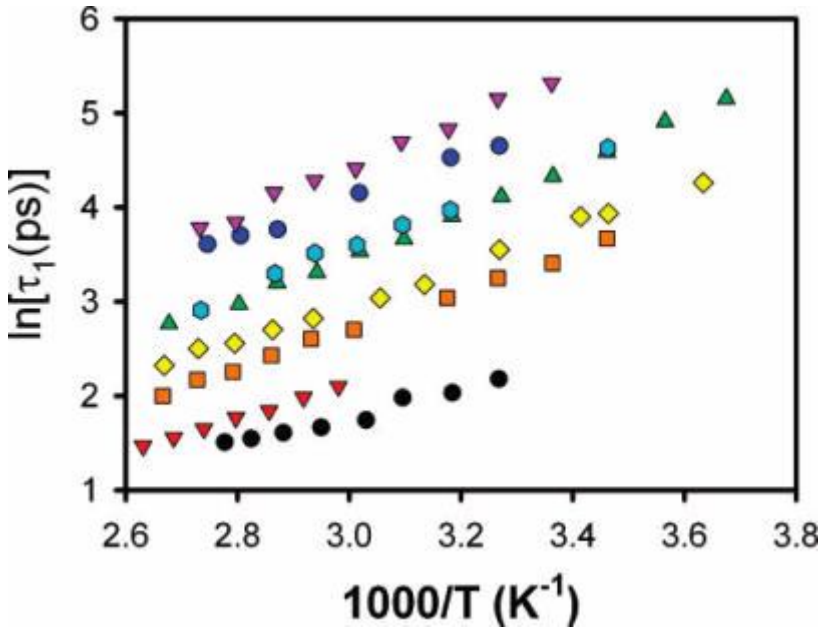

Figure 3.5 Arrhenius plot of the relaxation times of the dinitriles. The symbols are the same as in Figure 3.2.

As can be seen from this figure, we also observe Arrhenius behavior for each of these liquids, and the activation energies derived from these plots are listed in Table 3.1. However, there is no clear trend in the differences between our data and those of HW. Our data and those of HW for dicyanomethane, 1,3-dicyanopropane, and 1,5-dicyanopentane are similar, whereas those for the remaining liquids differ considerably. The similarity of the data for three liquids and the lack of a consistent pattern of differences for the remaining liquids suggests that there is not a systematic problem with the temperature determination in our experiments. The slopes of the Arrhenius plots for our data increase systematically up to 1,5-dicyanopentane and then level off, whereas there was no clear trend in the slopes of the data from HW. This leads us to conclude that it is likely that we are able to determine the collective orientational diffusion time more accurately than was possible using frequencydomain, Rayleigh-wing scattering.

We now consider the conformation of the dinitrile molecules in the liquids studied here. The two extreme possibilities are that the molecules are in a completely extended state or in a completely collapsed state. To assess which extreme is more representative of these liquids, we can plot the DSE slopes as a function of the estimated hydrodynamic volume for reorientation in the extended and collapsed states. We compute the former by using molecular modeling[21] to estimate the length of an isolated molecule in the completely extended geometry. As a proxy for hydrodynamic volume in the collapsed state, we can use the volume per molecule, as computed from the density and molecular weight of each liquid. This approximation is clearly more

accurate for larger molecules.

In Figure 3.6 we plot the DSE slopes in regions A, B, and C as a function of the estimated hydrodynamic volume for reorientation in the extended state. In each region the slope increases roughly linearly with hydrodynamic volume, although there are deviations for 1,4-dicyanobutane and 1,5-dicyanopentane. The slopes of the plots of the DSE slopes in each region are similar to one another. For comparison, in Figure 3.7 we plot the same data as a function of molecular volume. Although we must keep in mind that our estimate of the hydrodynamic volume for reorientation in the collapsed state is too low for molecules with short chain lengths, it is nevertheless clear that our data point to configurations that are toward the extended end of the continuum. This conclusion is consistent with our previous results for *n*-alkyl cyanides.

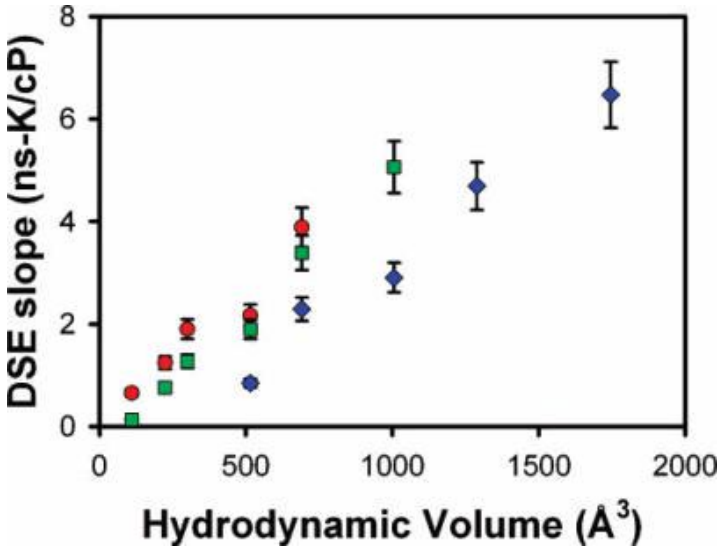

Figure 3.6 Slopes of the Debye-Stokes-Einstein plots for the liquids studied here as a function of the hydrodynamic volume for reorientation assuming that the molecules adopt a completely extended conformation. The red circles are for region A, the green squares are for region B, and the blue diamonds are for region C.

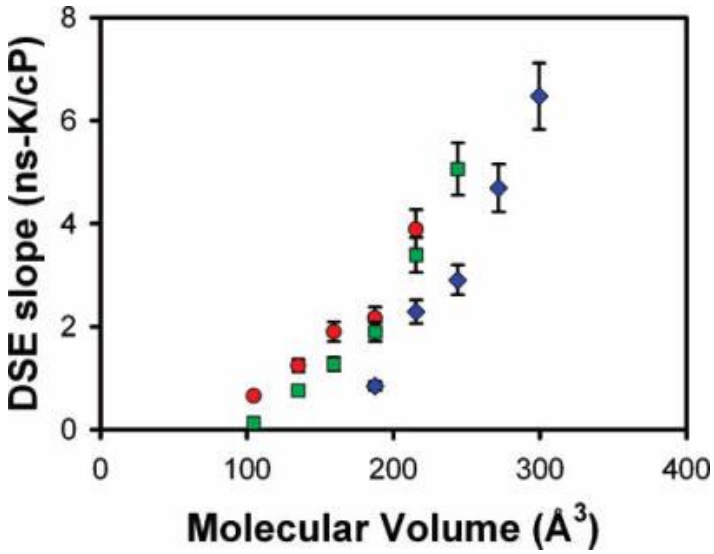

Figure 3.7 Slopes of the Debye-Stokes-Einstein plots for the liquids studied here as a function of the volume per molecule. The red circles are for region A, the green squares are for region B, and the blue diamonds are for region C.

Evidence from vibrational spectroscopic studies indicates that the lowest energy conformations for *n*-alkyl cyanides and 1,*n*-dicyanoalkanes, whether isolated or in the liquid state, are not fully extended.[33,34] Instead, the cyanide groups preferentially adopt a gauche conformation with respect to the rest of the molecule. This gauche form is favored over the trans form by on the order of 90 cm^{-1},[35] and so a significant population of the fully extended molecules is also expected to exist and has been observed spectroscopically. The gauche preference exists in isolated molecules, and it is thus believed that this conformation arises from steric effects rather than from interactions among the polar cyanide groups in the liquid.[35] A similar gauche preference is found *n*-alkyl acetylenes,[35] further supporting its steric origin.

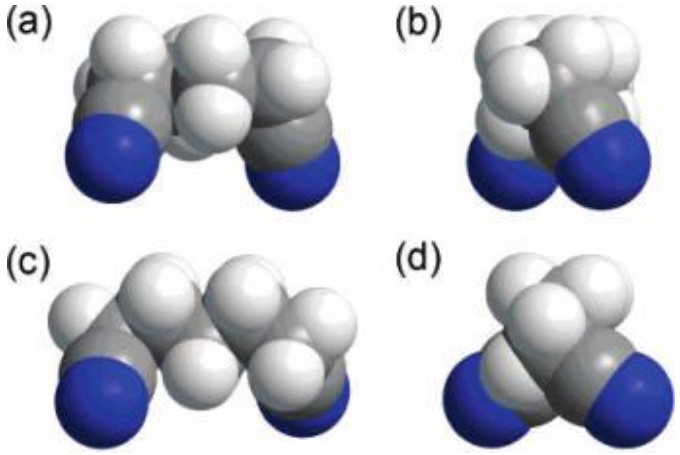

Figure 3.8 Views of the gauche-gauche structure of 1,4-dicyanobutane along the *x*-axis (a) and the *y*-axis (b) and of 1,5-dicyanopentane along the *x*-axis (c) and the *y*-axis (d). In all cases the *z*-axis is vertical.

Shown in Figure 3.8 are models of 1,4-dicyanobutane and 1,5-dicyanopentane in gauche-gauche conformations viewed from along what we denote as their *x*- and *y*-axes. Due to the angle between the cyanide groups, the polarizability is only slightly anisotropic with respect to reorientation about the *y*- and *z*-axes. However, reorientation around the *x*-axis will lead to a significant change in the polarizability. To assess whether our data are consistent with these gauche-gauche conformations, we have therefore calculated the hydrodynamic volume for reorientation about this axis for all of the molecules except for dicyanomethane (for which we have averaged the hydrodynamic volume for reorientation about each axis). A plot of the DSE slopes as a function of this gauche-gauche hydrodynamic volume is shown in Figure 3.9. The slopes for regions A, B, and C are more nearly linear in this plot than in those in Figures 3.6 and 3.7, and indeed the three slopes are all quite similar as well. We conclude that our data are consistent with the molecules preferentially adopting the

gauche-gauche conformation.

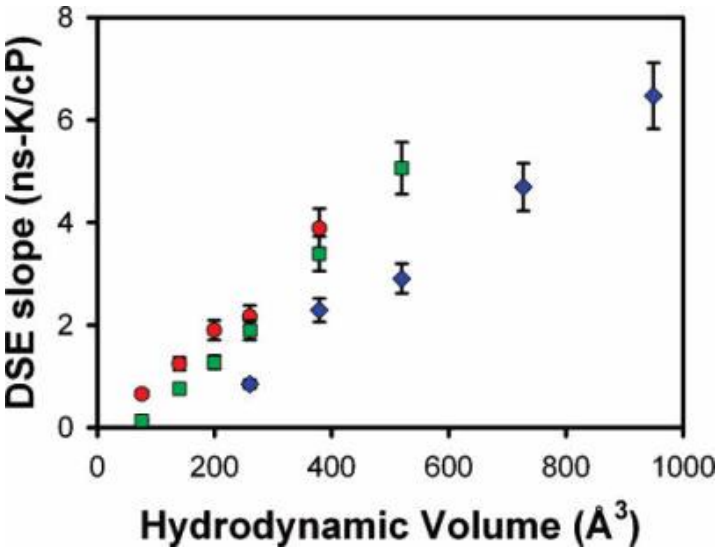

Figure 3.9 Slopes of the Debye-Stokes-Einstein plots for the liquids studied here as a function of the hydrodynamic volume for reorientation assuming that the molecules adopt an extended conformation but have gauche defects at each terminal methylene group. The red circles are for region A, the green squares are for region B, and the blue diamonds are for region C.

As was the case for *n*-alkyl cyanides,[9] we find here that when there is a transition in the slope of the DSE plot, the slope is smaller on the low-temperature side of the transition than it is on the high-temperature side. We now assess the potential causes for this behavior. One possible candidate for a change in slope would be a change in the boundary conditions for reorientation. However, if anything the boundary conditions are likely to tend more toward stick at lower temperatures and toward slip at higher temperatures, which would lead to the opposite of the observed behavior of the slope.

Given that the amount of energy by which a gauche defect is preferred is less than

room temperature thermal energy, it is possible that the conformations of the molecules become more extended at higher temperatures. More-extended molecules would have higher hydrodynamic volumes for reorientation, and therefore the DSE slope would be expected to increase at higher temperature. This mechanism would apply equally well to the cyanoalkanes that we have studied previously.[9] However, it should also be noted that dicyanomethane has only one possible conformation, and yet it displays two DSE slopes. Furthermore, conformational changes would be expected to occur gradually with temperature, rather than suddenly at a particular temperature. In addition, the linear Arrhenius behavior of these liquids argues against relatively sharp molecular conformational transitions. We therefore conclude that molecular conformational changes are unlikely to be responsible for the observed changes in DSE slopes.

Spectroscopically, the majority of the OKE signal arises from the polarizable cyanide groups. Indeed, to a good first approximation the two cyanide groups on each molecule can be thought of as being spectroscopically independent, especially for the molecules with larger numbers of methylene groups. Because OKE spectroscopy is sensitive to collective orientational motion, it measures a somewhat different quantity than do techniques such as NMR or Raman spectroscopy, which are sensitive to single-molecule orientational motion.[2] The relaxation time measured with OKE spectroscopy, τ_{OKE}, is related to the single-molecule orientational correlation time, τ_{sm}, via[2]

$$\tau_{OKE} = \frac{g_2}{j_2}\tau_{sm} \qquad \text{(Eq. 3.4)}$$

Here g_2 is the static orientational pair correlation parameter and j_2 is the dynamic orientational pair correlation parameter. It is believed that j_2 generally takes on a value near unity in simple liquids.[2] On the other hand, g_2 is a measure of the degree of parallel ordering in a liquid, and can take on values of unity or greater. The larger the value of g_2, the greater the degree of parallel ordering.

In the case of the OKE spectroscopy of dicyanoalkanes (and of cyanoalkanes[9]), the relevant ordering is that of the cyanide moieties. We have previously suggested for cyanoalkanes that the DSE slope changes are indicative of collective structural changes in the liquids affecting the degree of parallel ordering, and thereby changing the collective orientational correlation time via g_2.[9] A similar mechanism may be operating in the case of the dicyanoalkanes. The lower DSE slopes at lower temperatures would thus be indicative of a lower degree of parallel organization among the cyanide groups. The observed changes in the DSE slope can then be interpreted in terms of collective structural changes within the liquid, as we also suggested for the cyanoalkane liquids.[9] Significant changes in the slope can arise from relatively subtle changes in ordering as g_2 averages over long distances. We should also note that we have not seen any clear evidence for phase transitions using differential scanning calorimetry, indicating that any change in the liquid structure has at most a minor effect on thermodynamic properties (as might be expected for relatively subtle collective structural changes). The fact that the transition between regions A and B occurs at a value of η/T that is essentially independent of the identity of the liquid suggests that dynamic effects may be involved in the structural changes.

All of the molecules studied here have similar cross-sectional areas perpendicular to the *y*-axis (as defined in Figure 3.8). Based on the DSE equation,[1,2] we would therefore expect these molecules to have similar orientational diffusion constants about their *y*-axes for a fixed value of η/T. This axis should also be the one about which diffusion occurs most readily. As can be seen in Figure 3.8, the cross-sectional area perpendicular to *y* is somewhat larger for molecules with odd numbers of methylene groups than for those with even numbers of methylene groups. As a result, if diffusion about *y* is involved, we would expect the molecules with an odd number of methylene groups to have somewhat higher values of η/T at the transition between regions A and B. There is indeed a modest even/odd effect in these transition values, as shown in Figure 3.4. We therefore suggest that, at least for this putative structural transition, dynamic effects may play a key role. We do not have enough data on the other possible structural transition to be able to suggest a mechanism at this time.

We again reiterate that within the uncertainty of our data it is possible that the true form of the DSE plots of these liquids is a smooth curve that appears linear locally. The collective orientational correlation times for all of these liquids obey Arrhenius behavior. If the collective structure of the liquid changes smoothly with temperature, then the most plausible scenario that is consistent with this Arrhenius behavior is that both the single-molecule orientational correlation time and g_2 also have Arrhenius behavior. For data such as those in Figure 3.4, if we assume that g_2 increases in an Arrhenius manner from 1 at low temperature to 2 at high temperature, we can make approximate fits to the data. However, the locally linear fits still describe the data significantly more accurately. In either case, our data offer evidence for temperature-

dependent, collective structural rearrangements in these liquids.

3.5 Conclusions

We have presented a detailed OKE study of the orientational dynamics of dicyanoalkanes over a broad range of temperatures. Our data are consistent with these molecules preferentially adopting a gauche-gauche conformation in the liquid phase. As was the case for cyanoalkanes, we find that there are changes in the slopes of DSE plots for these liquids that are consistent with underlying, temperature-dependent, collective structural rearrangements within the liquids. It will be interesting to search for other signatures of such transitions with different experimental techniques.

3.6 References

(1) Debye, P. *Polar Molecules*; Dover: New York, **1929.**

(2) Kivelson, D.; Madden, P. A. *Annu. Rev. Phys. Chem.* **1980**, 31, 523.

(3) Righini, R. *Science* **1993**, 262, 1386.

(4) Kinoshita, S.; Kai, Y.; Ariyoshi, T.; Shimada, Y. *Int. J. Mod. Phys. B* **1996**, 10, 1229.

(5) Smith, N. A.; Meech, S. R. *Int. Rev. Phys. Chem.* **2002**, 21, 75.

(6) Hunt, N. T.; Jaye, A. A.; Meech, S. R. *Phys. Chem. Chem. Phys.* **2007**, 9, 2167.

(7) Ruhman, S.; Kohler, B.; Joly, A. G.; Nelson, K. A. *Chem. Phys. Lett.* **1987**, 141, 16.

(8) Loughnane, B. J.; Scodinu, A.; Farrer, R. A.; Fourkas, J. T.; Mohanty, U. *J. Chem. Phys.* **1999**, 111, 2686.

(9) Zhu, X.; Farrer, R. A.; Zhong, Q.; Fourkas, J. T. *J. Phys.: Condens. Matter* **2005**, 17, 4105.

(10) Loughnane, B. J.; Scodinu, A.; Fourkas, J. T. *J. Phys. Chem. B* **2006**, 110, 5708.

(11) Ricci, M.; Wiebel, S.; Bartolini, P.; Taschin, A.; Torre, R. *Philos. Mag.* **2004**, 84, 1491.

(12) Lotshaw, W. T.; McMorrow, D.; Thantu, N.; Melinger, J. S.; Kitchenham, R. *J. Raman Spectrosc.* **1995**, 26, 571.

(13) Ricci, M.; Bartolini, P.; Chelli, R.; Cardini, G.; Califano, S.; Righini, R. *Phys. Chem. Chem. Phys.* **2001**, 3, 2795.

(14) McMorrow, D. *Opt. Commun.* **1991**, 86, 236.

(15) McMorrow, D.; Lotshaw, W. T. *J. Phys. Chem.* **1991**, 95, 10395.

(16) Farrer, R. A.; Loughnane, B. J.; Deschenes, L. A.; Fourkas, J. T. *J. Chem. Phys.* **1997**, 106, 6901.

(17) Loughnane, B. J.; Farrer, R. A.; Scodinu, A.; Reilly, T.; Fourkas, J. T. *J. Phys. Chem. B* **2000**, 104, 5421.

(18) Scodinu, A.; Fourkas, J. T. *J. Phys. Chem. B* **2002**, 106, 10292.

(19) *SigmaPlot*, version 9.0; Systat: Point Richmond, CA, **2004**.

(20) Higashigaki, Y.; Wang, C. H. *Mol. Phys.* **1982**, 45, 493.

(21) *Chem 3D Pro*, version 5.0; CambridgeSoft: Cambridge, MA, **1999**.

(22) Quitevis, E. L.; Neelakandan, M. *J. Phys. Chem.* **1996**, 100, 10005.

(23) Neelakandan, M.; Pant, D.; Quitevis, E. L. *J. Phys. Chem. A* **1997**, 101, 2936.

(24) Chang, Y. J.; Castner, E. W., Jr. *J. Phys. Chem.* **1996**, 100, 3330.

(25) Cong, P.; Deuel, H. P.; Simon, J. D. *Chem. Phys. Lett.* **1995**, 240, 72.

(26) Lotshaw, W. T.; McMorrow, D.; Kalpouzos, C.; Kenney-Wallace, G. A. *Chem. Phys. Lett.* **1987**, 136, 323.

(27) McMorrow, D.; Lotshaw, W. T. *Chem. Phys. Lett.* **1993**, 201, 369.

(28) McMorrow, D.; Lotshaw, W. T.; Kenney-Wallace, G. A. *IEEE J. Quantum Electron.* **1988**, 24, 443.

(29) Kamada, K.; Ueda, M.; Ohta, K.; Wang, Y.; Ushida, K.; Tominaga, Y. *J. Chem. Phys.* **1998**, 109, 10948.

(30) Smith, N. A.; Meech, S. R. *J. Phys. Chem. A* **2000**, 104, 4223.

(31) Jaye, A. A.; Hunt, N. T.; Meech, S. R. *J. Chem. Phys.* **2006**, 124, 24506.

(32) Berne, B. J.; Pecora, R. *Dynamic Light Scattering*; Wiley: New York, **1976**.

(33) Matsubara, I. *J. Chem. Phys.* **1961**, 35, 373.

(34) Thorbjor, J.; Ellestad, O. H.; Klaeboe, P.; Torgrims. T. *Acta Chem. Scand.* **1972**, 26, 3799.

(35) Durig, J. R.; Drew, B. R.; Koomer, A.; Bell, S. *Phys. Chem. Chem. Phys.* **2001**, 3, 766.

Chapter 4: Shape and Electrostatic Effects in Optical Kerr Effect Spectroscopy of Aromatic Liquids

4.1 Introduction

Ultrafast optical Kerr effect (OKE) spectroscopy has become a broadly-used technique for probing the intrinsic dynamics of simple,[1-4] complex[4] and confined liquids.[5,6] In the most common implementation of OKE spectroscopy, a linearly-polarized pump pulse traverses a transparent liquid composed of molecules with an anisotropic polarizability. The pump pulse impulsively excites Raman active intramolecular and intermolecular modes, and creates a small net alignment of the liquid molecules. A variably-delayed probe pulse polarized at 45° is then used to probe the time dependence of collective orientational diffusion and vibrational dephasing by monitoring the decay of the birefringence induced by the pump pulse.

OKE spectroscopy is the formal time-domain equivalent of low-frequency Raman scattering. By using a Fourier-transform deconvolution technique with OKE data,[7] it is possible to derive the Bose-Einstein-corrected, low-frequency Raman spectrum of a liquid. It has become common in OKE studies to perform an approximate subtraction of the collective orientational diffusion contribution from this spectrum, leaving what has become known as the reduced spectral density (RSD).[7] The RSD contains information about the Raman-active intermolecular modes of a liquid, including librations and collective modes that appear as a result of interaction-induced scattering.

The use of OKE RSDs to develop a molecular-level interpretation of structure and dynamics in liquids has proven challenging. The RSDs are generally broad and do not have sharp features. Interpretation is further complicated by the fact that different contributions to the RSD may interfere constructively or destructively, making it difficult to isolate the influence of a particular mechanism or mode in the RSD.

Despite the challenges involved in interpreting RSDs, some progress has been made in understanding their microscopic origin. For instance, temperature-dependent OKE studies have revealed that for most liquids the RSD broadens to both higher and lower frequency as the temperature is decreased.[8-10] At the high-frequency end of the RSD, this behavior is interpreted as arising from the densification of the liquid with decreasing temperature, which leads to an increase in frequencies of librations and other intermolecular modes. At the low-frequency end of the RSD, it has been suggested that the broadening with decreased temperature arises from a decrease in the degree of motional narrowing in the spectrum.[11] However, a number of liquids have recently been shown not to exhibit the low-frequency broadening effect with decreasing temperature.[12,13] The interpretation of the temperature dependence of the low-frequency portion of RSDs for liquids thus remains an open question.

Ryu and Stratt[14] have suggested that the form of the OKE RSD can, in part, be a manifestation of molecular shape, especially insofar as the structure of liquids is dominated by effective repulsive interactions.[15] To explore this idea, we have previously reported temperature-dependent OKE studies of a series of aromatic liquids, including benzene, benzene-d_5, hexafluorobenzene (HFB), 1,3,5-trifluorobenzene (TFB), and mesitylene.[10] Despite the fact that these are all disk-like

molecules, the RSDs for benzene differ markedly from those of HFB and TFB, while the RSDs of mesitylene resemble those of benzene at low temperature and those of HFB and TFB at high temperature. By correlating the shapes of the RSDs with known structural details for these liquids,[16-22] we proposed that the higher-frequency portion of the RSDs arose from molecules with predominantly perpendicular local ordering while the lower-frequency portion of the RSDs arose from molecules with predominantly parallel ordering.[10]

Elola and Ladanyi performed simulations of benzene, HFB and TFB to test our structural proposal.[23] They found that for benzene, molecules with predominantly parallel local ordering have *higher* librational frequencies than those with perpendicular local ordering. The same effect exists in TFB, although to a lesser extent, and is absent in HFB. Elola and Ladanyi suggested that the differences in the RSDs of these three liquids arise from pairwise potentials of different depths, with a deeper potential leading to an RSD that appears more triangular.[23] Presumably the deeper pairwise potentials of HFB and TFB result from electrostatic effects. How this proposal fits in with the observed behavior of the RSDs of mesitylene is unclear, however.

Another study that is directly relevant to importance of molecular shape and electrostatics in OKE spectroscopy was performed by Smith and Meech, who looked at polar, monosubstituted benzenes including aniline, benzonitrile, and nitrobenzene.[9] All of these molecules have similar shapes, and their RSDs bear strong resemblance to one another as well. The RSDs of aniline are considerably broader than those of the other two liquids, which may be attributed to the ability of aniline to form

hydrogen bonds. Nitrobenzene and benzonitrile have both similar shapes and similar dipole moments, both of which may play a role in the similarity of their RSDs.

To investigate the relative importance of shape and electrostatic interactions further, here we report the temperature-dependent OKE spectroscopy of four more aromatic liquids, pyridine, pyridine-d_5, 2,4,6-trifluoropyridine (TFP), 2,4,6-trimethylpyridine (TMP) and 1,3,5-tris(trifluoromethyl)benzene (nonafluoromesitylene, NFM). The shapes of these molecules bear strong similarity to those of aromatic liquids that we studied previously.[10] However, the electrostatics of the molecules studied here differ from those of the molecules we studied previously, allowing us to investigate the relative importance of shape and electrostatics in OKE spectroscopy.

4.2 Experimental Section

The liquids studied here were purchased from Aldrich (except for TFP, which was purchased from Alfa Aesar) in the purest form available and were used without any additional purification. Relevant physical properties of these liquids are listed in Table 4.1. The densities reported are those given by the supplier except for that of TMP. For this liquid the density was measured with a 2 mL Gay-Lussac pycnometer.

TABLE 4.1: Formula weight, density at 298 K, molar volume and dipole moment for the liquids studied here and related liquids.

Liquid	*FW* (amu)	ρ (g/mL)	V_m (mL/mol)	*p* (Debye)
Benzene	78.11	0.874	89.4	0
Pyridine	79.10	0.978	80.9	2.15
Benzene-d_6	84.16	0.950	88.6	0
Pyridine-d_5	84.14	1.05	80.1	2.15
TFB	132.08	1.277	103.5	0
TFP	133.07	1.383	96.2	2.34
Mesitylene	120.19	0.864	139.1	0
TMP	121.18	0.917	132.1	1.96
NFM	282.11	1.514	186.3	0
HFB	186.05	1.612	115.4	0

Samples were sealed into cuvettes with a 1 mm optical pathlength and were mounted on the cold finger of a nitrogen flow cryostat. To ensure that the samples were kept at constant temperature throughout the course of an experiment, a temperature sensor was affixed to the cuvette as near as possible to the point at which data were obtained. The samples were allowed to stabilize for at least 30 minutes at a given temperature before data were collected.

We have described our optical-heterodyne-detected OKE spectrometer in detail in previous chapters.[5,8] The laser employed was a KMLabs Ti:sapphire oscillator operating at a center wavelength of approximately 800 nm. Typical pulse lengths

used were 50 fs, and second-harmonic-generation autocorrelations were measured often for purposes of Fourier-transform deconvolution of the data. Data with a large time step (typically 0.67 ps) were taken out to long delays to measure the collective orientational decays of the liquids, and data with a short time step (33 fs) were taken out to delays of a few picoseconds so that RSDs could be obtained through Fourier-transform deconvolution. Decays obtained at equal positive and negative heterodyne angles were subtracted from one another to remove the homodyne contribution from the data.

To fit the portion of the decay arising from orientational diffusion, the data were integrated to obtain the collective orientational correlation function $C_{coll}(t)$, as described previously.[24] The constant of integration was determined by ensuring that the decays were exponential at long times. The integrated decays were fit to a function of the form

$$B\left[A\exp\left(-t/\tau_{or}\right)+\left(1-A\right)\exp\left(-t/\tau_{i}\right)\right] \qquad \text{(Eq. 4.1)}$$

where B is an overall amplitude, A is a normalized relative amplitude for the two exponentials, t is the delay time, τ_{or} is the collective orientational correlation time, and τ_i is the "intermediate" relaxation time, which is shorter than τ_r. Once the integrated decays had been fit, the parameters were used to strip a tail onto the short-step data with the same point spacing as the short-step data set. This concatenated decay was used for the Fourier-transform deconvolution procedure. To derive the RSDs, a rise time of 200 fs was assumed for the diffusive portion of the OKE decays.

4.3 Results

Shown in Figure 4.1 is a typical integrated OKE decay, in this case for pyridine at 297 K (black). A biexponential fit to the data using Eq. 4.1 is shown in red, and the residuals for the fit are shown in the lower panel on a linear scale. All of the fits reported here were of similar quality, and the decays all had sufficient dynamic range to determine the fit parameters with good precision. A complete list of fit parameters at each temperature studied for each liquid can be found in the ***Appendix C.***

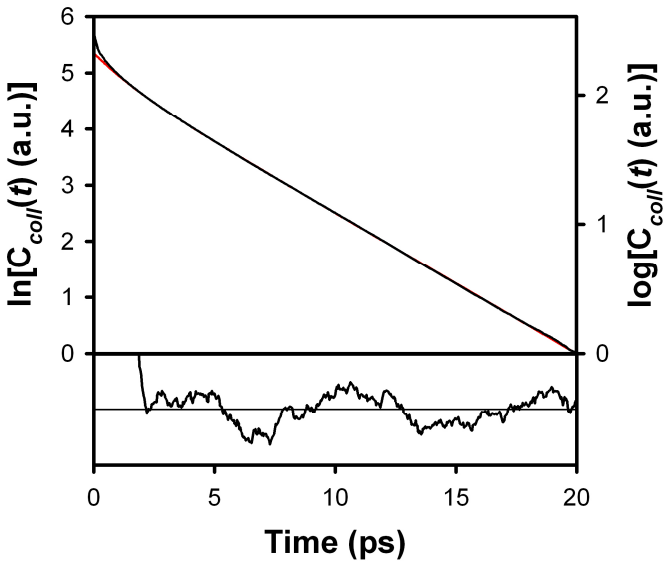

Figure 4.1 Representative integrated OKE decay for pyridine at 297 K (black) and biexponential fit (red). The residual is shown on a linear scale in the lower panel.

Exponential "intermediate" relaxation is a phenomenon that is commonly observed in the OKE spectroscopy of simple liquids.[7-9,11,13,25-34] The origin of this relaxation is still not well understood. We have shown for a broad range of simple liquids that the intermediate relaxation time is proportional to the collective orientational relaxation

time.[10,11,33,34] The constant of proportionality between these times generally falls within a relatively narrow window for most simple liquids. We have suggested that the two times are related because motional narrowing plays a major role in determining the dephasing time of coherently excited intermolecular modes.[11] As shown in Figure 4.2, for the liquid studied here τ_i is proportional to τ_{or}. The constant of proportionality is between 3 and 4, as we found previously for other aromatic liquids.[10]

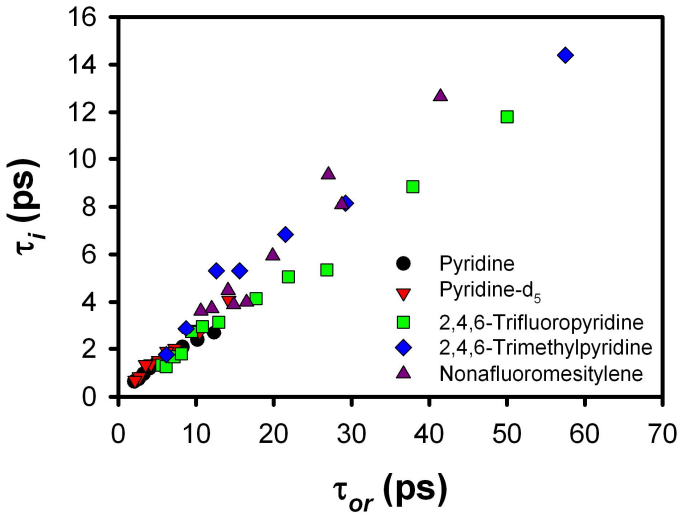

Figure 4.2 Plot of the intermediate relaxation time as a function of the collective orientational correlation time for the liquids studied here.

Shown in Figures 4.3 and 4.4 are RSDs for pyridine and pyridine-d_5, respectively, at temperatures ranging from 240 K to 349 K. The RSD of pyridine at room temperature is in good agreement with that reported previously by McMorrow and Lotshaw.[35] As is the case for other typical simple liquids, the RSDs broaden to both higher and lower frequency as the temperature is decreased. There is a strong

similarity between these RSDs and those of benzene and benzene-d_6, which are also "rectangular" at low temperature and become increasingly asymmetric at higher temperatures. The similarity between the RSDs of benzene and pyridine has been noted previously at room temperature.[35]

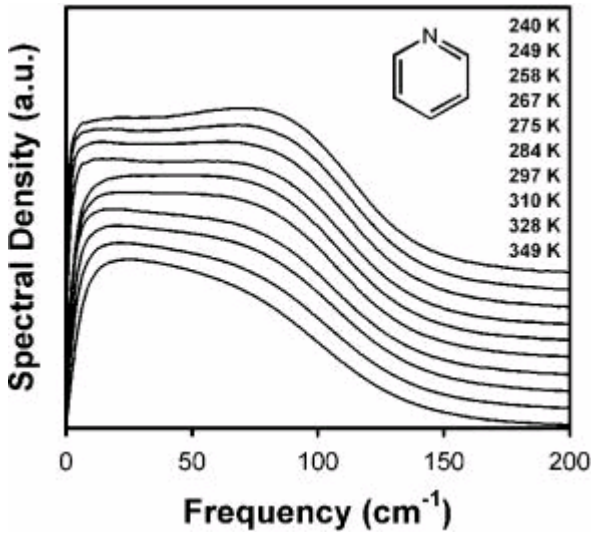

Figure 4.3 Height-normalized RSDs for pyridine at temperatures ranging from 240 to 349 K. The data have been offset for clarity.

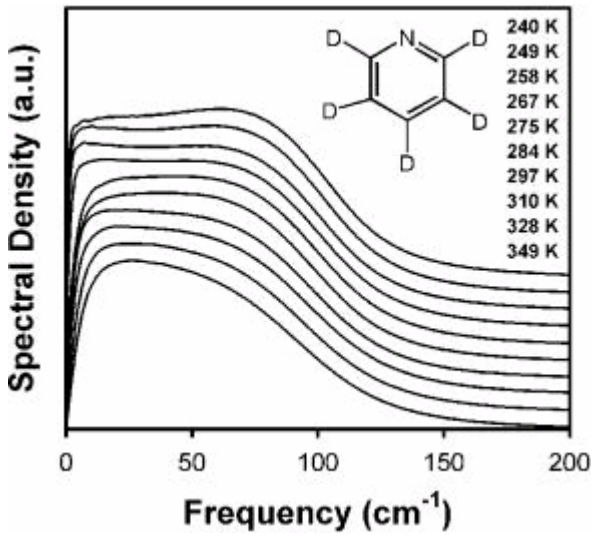

Figure 4.4 Height-normalized RSDs for pyridine-d5 at temperatures ranging from 240 to 349 K. The data have been offset for clarity.

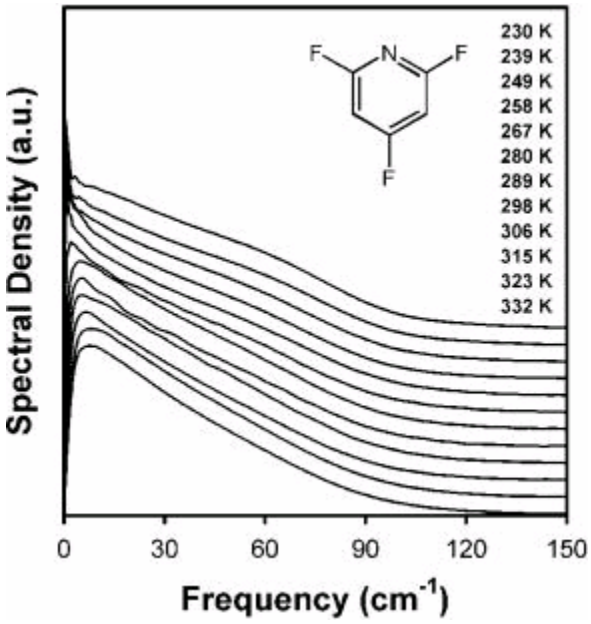

Figure 4.5 Height-normalized RSDs for TFP at temperatures ranging from 230 to 332 K. The data have been offset for clarity.

In Figure 4.5 we show the RSDs for TFP at temperatures ranging from 230 K to 332 K. As is the case for HFB and TFB, these RSDs are "triangular" in shape and change little with temperature other than to develop a slight rounded feature at high frequency at lower temperatures. Shown in Figure 4.6 are the RSDs for TMP at temperatures from 243 K to 351 K. As was the case for mesitylene,[10] these RSDs have a "rectangular" shape akin to that of the RSDs of benzene at low temperature and become "triangular" at high temperature. The RSDs for NFM, shown in Figure 4.7 at temperatures ranging from 285 K to 348 K, are also roughly triangular and

have a similar temperature dependence to that of the RSDs for TFP. However, the RSDs for NFM are considerably narrower than those for TFP.

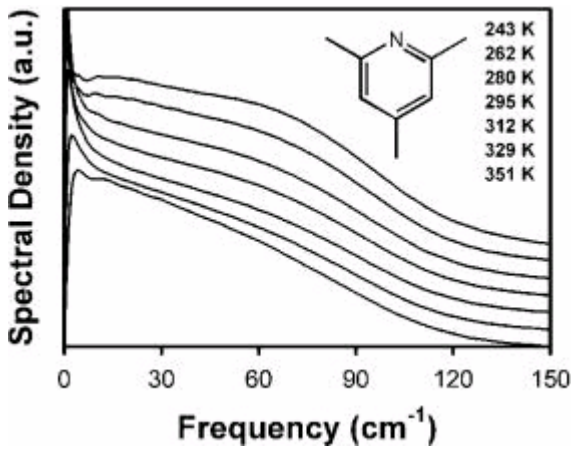

Figure 4.6 Height-normalized RSDs for TMP at temperatures ranging from 243 to 351 K. The data have been offset for clarity.

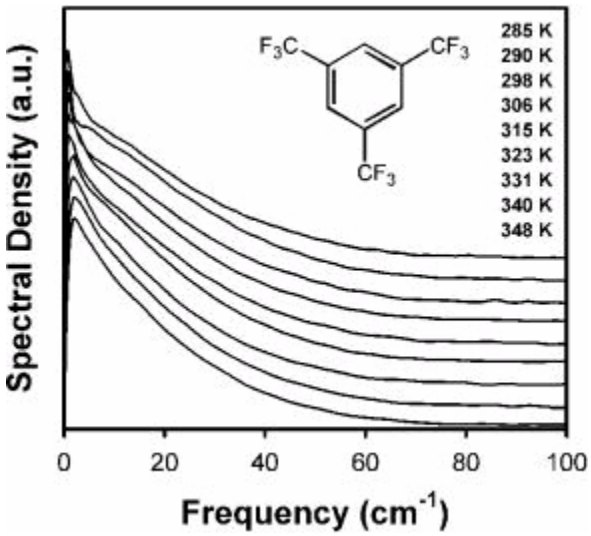

Figure 4.7 Height-normalized RSDs for NFM at temperatures ranging from 285 to 348 K. The data have been offset for clarity.

4.4 Discussion

Isotopologues such as pyridine and pyridine-d_5 have essentially the same shape and the same charge distribution. As a result, their RSDs would be expected to be quite similar, and as can be seen in Figures 4.3 and 4.4 this is indeed the case. We have found previously that the RSDs of benzene and benzene-d_6 can be overlapped nearly perfectly if the frequency axis for the latter liquid is scaled by $[I_x(\text{benzene})/I_x(\text{benzene-}d_6)]^{½}$, where I_x is the moment of inertia for tumbling.[10] The probable implication of this result is that librations dominate the RSDs of these liquids, as the librational frequency is expected to scale with $I_x^{-½}$.

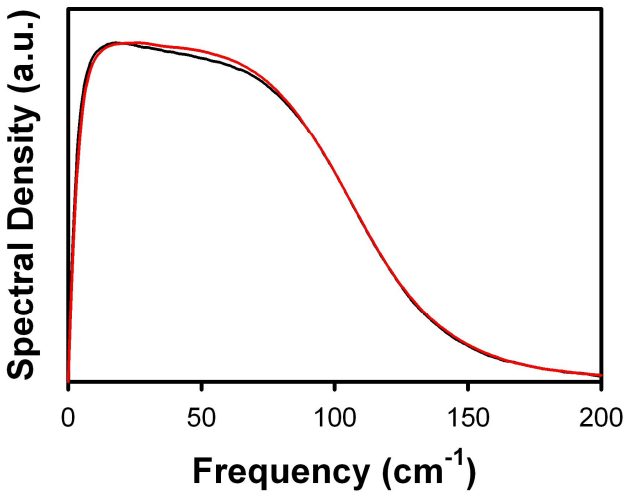

Figure 4.8 Comparison of the height-normalized RSDs for pyridine (black) and pyridine-*d*5 (red) at 297 K. The frequency axis for pyridine-*d*5 has been scaled by a factor of 1.086.

In analogy to our previous findings for benzene and benzene-d_6, in Figure 4.8 we show RSDs for pyridine and pyridine-d_5 at 297 K. The frequency axis for pyridine-d_5 has been scaled by a factor of 1.860, which is the square root of the average of the ratios of the moments of inertia about the two tumbling axes of these molecules.[36] As was the case for benzene and benzene-d_6, the RSDs for pyridine and pyridine-d_5 correspond quite closely once the frequency axes have been scaled appropriately. Thus, given molecules of nearly identical shape and charge distribution, a shift based on librational frequencies again does an excellent job of mapping the RSDs of different isotopologues onto one another.

To help understand the relative roles played by shape and electrostatics in OKE RSDs, it is instructive to compare spectra of molecules that are isoelectronic but that are not isotopologues. This strategy has been pursued previously with furan, thiophene and selenophene, but only at a single temperature.[37] Here we compare benzene and pyridine, which have shapes that are similar but charge distributions that differ considerably. Due to its symmetry, benzene has no dipole moment. Pyridine, on the other hand, has a significant dipole moment of 2.15 Debye.[38] This difference in charge distribution would be expected to be reflected in different intermolecular structures for these liquids, which in turn may influence the OKE RSDs.

Experimental data confirm the influence that the different charge distributions have on the structures of crystalline and liquid benzene[17,20,39] and pyridine.[40,41] Even the crystal structure of pyridine is[42] "unexpectedly complicated and very different from the known ones of geometrically similar molecules." By the same token, x-ray and

neutron diffraction studies have shown that the intermolecular structure in liquid pyridine[40] differs markedly from that of benzene and HFB.[39]

Despite clear differences in liquid structure, as we have already seen the RSDs of benzene and pyridine bear a strong resemblance to one another, and also have similar temperature dependences. In Figure 4.9 we show a direct comparison of the RSDs for these two liquids at 267 K and 327 K. The frequency axis of the benzene RSDs has been scaled by a factor of 1.075 at the lower temperature and 1.1 at the higher temperature in order to maximize the overlap between the spectra. Unlike in the case of isotopologues, we cannot merely scale the frequency axis of the RSDs based on moments of inertia for these liquids. Due to the dipolar nature of pyridine, it has a significantly higher density than benzene and, correspondingly, a molar volume that at room temperature is on the order of 10% smaller than that of benzene. Differences in the temperature dependence of the densities of the two liquids probably account for the change in the scaling factor for matching up the RSDs of these liquids at low and high temperatures. Issues of scaling notwithstanding, the similarities between the RSDs of these liquids at all temperatures are quite striking.

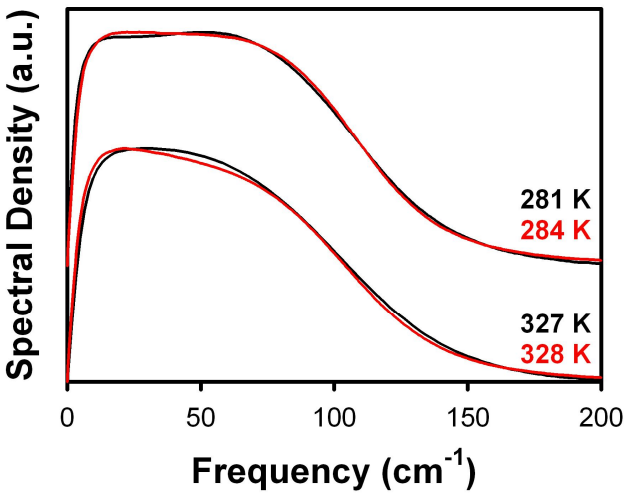

Figure 4.9 Comparison of the height-normalized RSDs for benzene (black) and pyridine (red) at two different temperatures. The frequency axis for the benzene RSDs has been scaled to make the correspondence between the RSDs as close as possible. The data at the two temperatures have been offset for clarity.

It is also instructive to compare the orientational dynamics of these liquids. For simple liquids, the orientational correlation time usually follows the Debye-Stokes-Einstein (DSE) relation[43,44]:

$$\tau_{or} = \frac{V_H \eta}{k_B T} + \tau_0 \qquad \text{(Eq. 4.2)}$$

Here, V_H is the hydrodynamic volume for reorientation, η is the viscosity, k_B is Boltzmann's constant, and τ_0 is the limiting orientational correlation time at infinite temperature (or zero viscosity). Although intended to describe the reorientation of large solutes, this relation often works well for neat liquids as well. The hydrodynamic volume term is related to the volume swept out by a molecule as it

reorients. Isotopologues generally fall on a single line on a DSE plot, and as can be seen in Figure 10 this is indeed the case of pyridine (in black) and pyridine-d_5 (in red). The solid line in this plot is a linear least-squares fit to the combined data for the isotopologues.

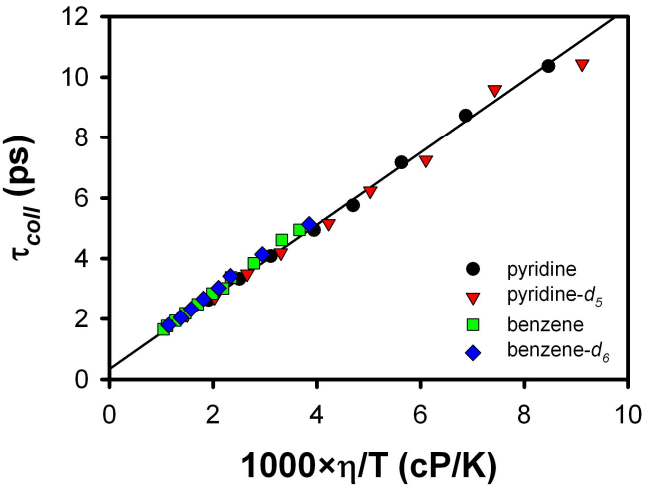

Figure 4.10 DSE plot for pyridine (black) and pyridine-*d*5 (red), along with a fit to the data (solid line). Data for benzene (green) and benzene*d*6 (blue) have also been included, but were not used in the fit.

Since benzene and pyridine are isoelectronic, we can also investigate whether they have matching DSE behavior. In Figure 4.10 we have also plotted the DSE data for benzene (green) and benzene-d_6 (blue). These data fall nearly on the plot for pyridine and pyridine-d_5, but the benzene data appear to have a slightly higher slope than do the pyridine data. The implication may be that pyridine has a slightly smaller hydrodynamic volume than does benzene.

OKE spectroscopy measures a collective orientational correlation time, but the DSE relation is intended to describe the single-molecule orientational correlation time. The relationship between these times is given by

$$\tau_{or,coll} = \frac{g_2}{j_2}\tau_{or,sm} \qquad \text{(Eq. 4.3)}$$

where g_2 is the static orientational pair correlation parameter and j_2 is the dynamic orientational pair correlation parameter.[44] It is generally believed that j_2 is near unity for simple liquids.[44] On the other hand, g_2 can vary considerably, and gives direct information on the degree of parallel ordering in a liquid.

Ito and Kato[45] (IK) have performed carbon-13 NMR and depolarized Rayleigh scattering experiments on pyridine. NMR is sensitive to the single-molecule orientational correlation time, whereas depolarized Rayleigh scattering is a frequency-domain equivalent of OKE spectroscopy, and so measures the collective orientational correlation time.[46] At temperatures of both 0 °C and 20 °C, they found that times determined by NMR and Rayleigh scattering were virtually identical, implying that g_2 is close to unity in pyridine near room temperature. The collective orientational correlation times determined by IK are in good agreement with those presented here.

Liu, Li and Jonas[47] (LLJ) performed deuterium NMR studies of reorientation in pyridine-d_5 over a larger range of temperatures than IK. The single-molecule orientational correlation times derived by LLJ are significantly smaller than the collective orientational times determined here for pyridine-d_5. It is unlikely that g_2 differs appreciably for pyridine and pyridine-d_5, particularly as both liquids fall on the

same line in a DSE plot. Thus, it is unclear whether to use the results of IK or LLJ in calculating g_2/j_2 for these liquids.

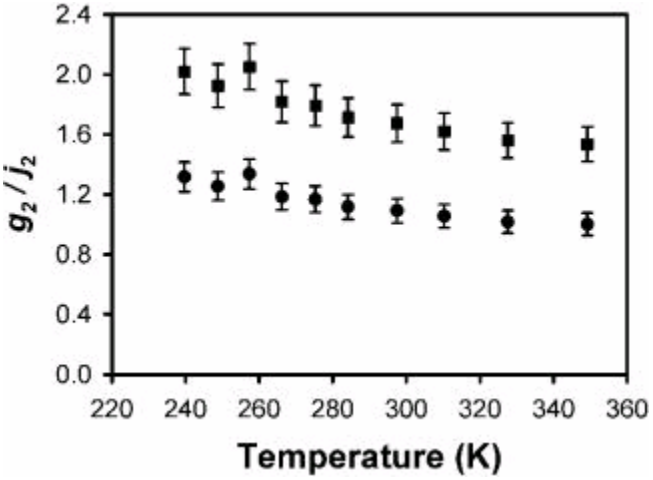

Figure 4.11 Temperature dependence of g_2/j_2 for pyridine. The data in squares are calculated directly from the results of Liu, Li, and Jonas for the single-molecule orientational correlation time, whereas the data in circles have been scaled to match the single-molecule orientational times measured by Itoh and Kato.

Since the data of LLJ cover a broader range of temperatures than those of IK, we will use them as a guideline. If we assume that the values calculated by LLJ are accurate, we find that g_2/j_2 is near 2.0 at low temperature and decreases to near 1.6 at high temperature (squares in Figure 4.11). If we assume that there is a systematic error in the numbers of LLJ and that their numbers should match those of IK at high temperature, then we find that g_2/j_2 is approximately 1.3 at low temperature and decreases to unity at high temperature (circles in Figure 4.11). These two models imply significantly different degrees of parallel ordering for pyridine, and should probably be viewed as the two extreme possible cases. Neutron and x-ray diffraction

data appear to point towards a significant degree of parallel ordering in pyridine, which tends to favor the model based directly on the data of LLJ.

Whichever model of g_2/j_2 is correct, it is clear that this quantity decreases with increasing temperature for pyridine. In contrast, g_2/j_2 is essentially independent of temperature for benzene. As we have seen, the OKE RSDs of pyridine and benzene bear strong resemblance over a broad temperature range. These results suggest that intermolecular structure does not have a large impact in determining the shape of the RSD, whereas molecular shape does play a strong role.

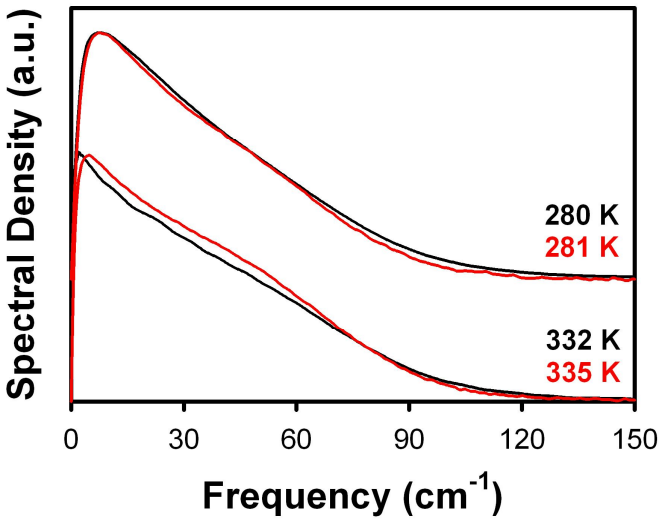

Figure 4.12 Comparison of the height-normalized RSDs for TFP (black) and TFB (red) at two different temperatures. The data at the two temperatures have been offset for clarity.

We next turn to a comparison of the OKE spectra of TFB and TFP. In Figure 4.12 we compare RSDs for these two liquids near 280 K and near 332 K. In this case

we have used no scaling of the frequency axis of the data, yet the RSDs are in strong agreement over the entire range of temperatures. This agreement arises despite the fact that the significant dipole moment of TFP[48] (2.34 Debye) causes TFP to have a significantly higher density (1.383 g/mL) than does TFB (1.277 g/mL). These results again suggest a strong role for shape in determining the appearance of the OKE RSD.

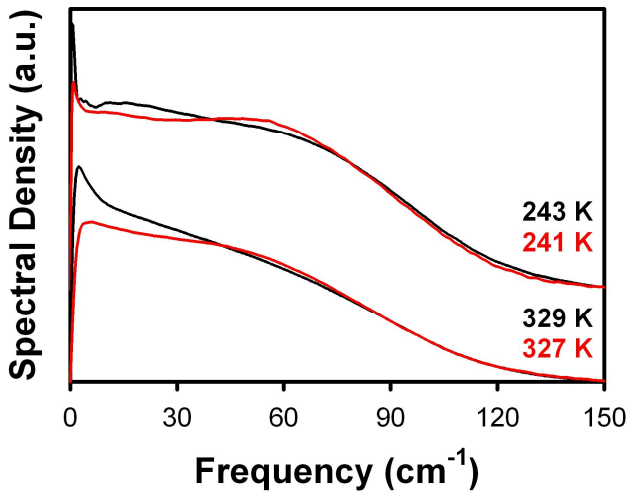

Figure 4.13 Comparison of the height-normalized RSDs for TMP (black) and mesitylene (red) at two different temperatures. The data at the two temperatures have been offset for clarity.

In Figure 4.13 we compare the RSDs for TMP and mesitylene near 243 K and 349 K. Once again there is a significant similarity between the RSDs for the two liquids, although the correspondence is not as strong as for some of the other liquids discussed here. TMP has a dipole moment of 1.96 D,[49] which leads to it having a somewhat smaller molar volume than does mesitylene. Nevertheless, as was the case for TFB and TFP, we have not scaled the frequency axis for the TMP and mesitylene RSDs.

While the shapes of the RSDs of mesitylene and TMP change considerably in going from low temperature to high temperature, this is not the case for NFM. The RSDs for NFM do show evidence of a high-frequency feature that builds in at low temperature, but this feature is not nearly as prominent as in the case of mesitylene. The RSDs of NFM are thus more reminiscent of those of HFB, TFB and TFP than they are of the RSDs of mesitylene.

We now are ready to consider the factors that work to determine the shapes of the OKE RSDs for aromatic liquids. We have suggested previously that the RSDs of aromatic liquids are reflective of their local intermolecular structure.[10] However, the results presented here show that liquids with considerably different local structures but comparable molecular shapes have OKE RSDs that are highly similar. In fact, with appropriate scaling of the frequency axes of the RSDs, these spectra can be virtually superimposed over a broad range of temperatures.

Elola and Ladanyi[23] simulated the room-temperature OKE spectra of benzene, HFB and TFB, and found good agreement with previous experimental results. Based on their simulations, they suggested that the strengths of the pairwise potentials in these liquids play a significant role in determining the shapes of the RSDs. However, the results discussed here suggest that the strength of the attraction between neighboring molecules is not the major factor driving the shape of the RSD. For instance, benzene and pyridine have intermolecular interactions that differ considerably from one another, as is evidenced by the notably smaller molar volume of pyridine. These differences in intermolecular interactions also lead to considerable differences in the intermolecular structures of these liquids. However, the OKE

RSDs for these two liquids are highly similar from low temperature up to high temperature.

Our results support the proposal of Ryu and Stratt[14] that molecular shape is a primary determinant of the shape of the OKE RSDs of non-associated liquids. We have recently found similar results for a series of alkanes and ethers as well.[13] These results suggest that OKE spectroscopy may not be a sensitive probe of intermolecular structure in liquids.

Still, a number of issues about the shapes of OKE RSDs remain to be answered. For instance, the shapes of benzene and pyridine are not vastly different from those of HFB, TFB and TFP, and yet the RSDs of the first two liquids differ markedly from those of the other three. Furthermore, the RSDs of benzene and pyridine have a relatively strong temperature dependence, whereas those of the other three liquids do not.[10] One possible explanation for this behavior is that the distribution of the polarizability in these molecules also plays a distinct role in shaping the RSDs. In addition, it is possible that only RSDs with significant content at higher frequencies are susceptible to shape changes with increasing temperature, perhaps due to motional narrowing. The RSDs of mesitylene and TMP also present an interesting puzzle, in that they resemble those of benzene at low temperature and those of HFB, TFB and TFP at high temperature. All of these issues might be examined profitably with molecular dynamics simulations.

4.5 Conclusion

We have presented a detailed, temperature-dependent OKE study of a number of aromatic liquids that complements a study of similar liquids that we have reported previously. Based on comparisons among the RSDs for these liquids, we conclude that molecular shape plays a major role in determining the shape of the OKE RSD in non-associated liquids. The effects of local structure and electrostatic forces on the spectra appear to be minor, although the manner in which the molecular polarizability is distributed may play some role in shaping the RSDs.

4.6 References

(1) Righini, R. *Science* **1993**, 262, 1386.

(2) Kinoshita, S.; Kai, Y.; Ariyoshi, T.; Shimada, Y. *Int. J. Mod. Phys. B* **1996**, 10, 1229.

(3) Fourkas, J. T. Nonresonant Intermolecular Spectroscopy of Liquids. In *Ultrafast Infrared and Raman Spectroscopy*; Fayer, M. D., Ed.; Marcel Dekker: New York, **2001**; Vol. 26; pp 473.

(4) Hunt, N. T.; Jaye, A. A.; Meech, S. R. *Phys. Chem. Chem. Phys.* **2007**, 9, 2167.

(5) Loughnane, B. J.; Farrer, R. A.; Scodinu, A.; Reilly, T.; Fourkas, J. T. *J. Phys. Chem. B* **2000**, 104, 5421.

(6) Farrer, R. A.; Fourkas, J. T. *Acc. Chem. Res.* **2003**, 36, 605.

(7) McMorrow, D.; Lotshaw, W. T. *J. Phys. Chem.* **1991**, 95, 10395.

(8) Farrer, R. A.; Loughnane, B. J.; Deschenes, L. A.; Fourkas, J. T. *J. Chem. Phys.* **1997**, 106, 6901.

(9) Smith, N. A.; Meech, S. R. *J. Phys. Chem. A* **2000**, 104, 4223.

(10) Loughnane, B. J.; Scodinu, A.; Fourkas, J. T. *J. Phys. Chem. B* **2006**, 110, 5708.

(11) Loughnane, B. J.; Scodinu, A.; Farrer, R. A.; Fourkas, J. T.; Mohanty, U. *J. Chem. Phys.* **1999**, 111, 2686.

(12) Jaye, A. A.; Hunt, N. T.; Meech, S. R. *J. Chem. Phys.* **2006**, 124, 024506.

(13) Zhong, Q.; Fourkas, J. T. *J. Phys. Chem. B* **2008**，112，8656.

(14) Ryu, S.; Stratt, R. M. *J. Phys. Chem. B* **2004**, 108, 6782.

(15) Andersen, H. C.; Chandler, D.; Weeks, J. D. *Adv. Chem. Phys.* **1976**, 34, 105.

(16) Cabaco, M. I.; Danten, Y.; Besnard, M.; Guissani, Y.; Guillot, B. *Chem. Phys. Lett.* **1996**, 262, 120.

(17) Cabaco, M. I.; Danten, Y.; Besnard, M.; Guissani, Y.; Guillot, B. *J. Phys. Chem. B* **1997**, 101, 6977.

(18) Cabaco, M. I.; Tassaing, T.; Danten, Y.; Besnard, M. *J. Phys. Chem. A* **2000**, 104, 10986.

(19) Cabaco, M. I.; Tassaing, T.; Danten, Y.; Besnard, M. *Chem. Phys. Lett.* **2000**, 325, 163.

(20) Tassaing, T.; Cabaco, M. I.; Danten, Y.; Besnard, M. *J. Chem. Phys.* **2000**, 113, 3757.

(21) Danten, Y.; Cabaco, M. I.; Tassaing, T.; Besnard, M. *J. Chem. Phys.* **2001**, 115, 4239.

(22) Cabaco, M. I.; Besnard, M.; Tassaing, T.; Danten, Y. *Pure Appl. Chem.* **2004**, 76, 141.

(23) Elola, M. D.; Ladanyi, B. M. *J. Phys. Chem. B* **2006**, 110, 15525.

(24) Scodinu, A.; Fourkas, J. T. *J. Phys. Chem. B* **2002**, 106, 10292.

(25) Kalpouzos, C.; Lotshaw, W. T.; McMorrow, D.; Kenney-Wallace, G. A. *J. Phys. Chem.* **1987**, 91, 2028.

(26) Lotshaw, W. T.; McMorrow, D.; Kalpouzos, C.; Kenney-Wallace, G. A. *Chem. Phys. Lett.* **1987**, 136, 323.

(27) Deeg, F. W.; Fayer, M. D. *J. Chem. Phys.* **1989**, 91, 2269.

(28) McMorrow, D.; Lotshaw, W. T. *Chem. Phys. Lett.* **1991**, 178, 69.

(29) Chang, Y. J.; Castner Jr., E. W. *J. Chem. Phys.* **1993**, 99, 113.

(30) Neelakandan, M.; Pant, D.; Quitevis, E. L. *J. Phys. Chem. A* **1997**, 101, 2936.

(31) Foggi, P.; Bartolini, P.; Bellini, M.; Giorgini, M. G.; Morresi, A.; Sassi, P.; Cataliotti, R. S. *Eur. Phys. J. D* **2002**, 21, 143.

(32) Ricci, M.; Bartolini, P.; Chelli, R.; Cardini, G.; Califano, S.; Righini, R. *Phys. Chem. Chem. Phys.* **2001**, 3, 2795.

(33) Zhu, X.; Farrer, R. A.; Zhong, Q.; Fourkas, J. T. *J. Phys. Cond. Mat.* **2005**, 17, S4105.

(34) Zhong, Q.; Zhu, X.; Fourkas, J. T. *J. Phys. Chem. B* **2008**, 112, 3115.

(35) McMorrow, D.; Lotshaw, W. T. *Chem. Phys. Lett.* **1993**, 201, 369.

(36) Holz, M.; Mao, X. A.; Seiferling, D.; Sacco, A. *J. Chem. Phys.* **1996**, 104, 669.

(37) Kamada, K.; Ueda, M.; Ohta, K.; Wang, Y.; Ushida, K.; Tominaga, Y. *J. Chem. Phys.* **1998**, 109, 10948.

(38) DeMore, B. B.; Wilcox, W. S.; Goldstein, J. H. *J. Chem. Phys.* **1954**, 22, 876.

(39) Bartsch, E.; Bertagnolli, H.; Schulz, G.; Chieux, P. *Ber. Bunsen-Ges. Phys. Chem.* **1985**, 89, 147.

(40) Bertagnolli, H.; Engelhardt, T.; Chieux, P. *Ber. Bunsen-Ges. Phys. Chem.* **1986**, 90, 512.

(41) Megiel, E.; Kasprzycka-Guttman, T.; Jagielska, A.; Wroblewska, L. *J. Mol. Struct.* **2001**, 569, 111.

(42) Mootz, D.; Wussow, H. G. *J. Chem. Phys.* **1981**, 75, 1517.

(43) Debye, P. *Polar Molecules*; Dover: New York, **1929**.

(44) Kivelson, D.; Madden, P. A. *Annu. Rev. Phys. Chem.* **1980**, 31, 523.

(45) Ito, N.; Kato, T. *J. Phys. Chem.* **1984**, 88, 801.

(46) Berne, B. J.; Pecora, R. *Dynamic Light Scattering*; Wiley: New York, **1976**.

(47) Liu, G.; Li, Y.; Jonas, J. *J. Chem. Phys.* **1991**, 95, 6892.

(48) Van Doren, J. M.; Kerr, D. M.; Miller, T. M.; Viggiano, A. A. *J. Chem. Phys.* **2005**, 123, 114303.

(49) Jatkar, S. K. K.; Deshpande, C. M. *J. Indian Chem. Soc.* **1960**, 37, 11.

Chapter 5: Searching for Voids in Liquids with Optical Kerr Effect Spectroscopy

5.1 Introduction

A simple liquid is generally viewed as being a dense medium in which there are no large void spaces. While there exist numerous examples of nonideal mixtures that have a volume that is smaller than that of the component liquids,[1] this phenomenon can generally be described as arising from a loss of relatively evenly distributed free volume due to favorable interactions between the two components. However, for some liquids there are indications of the existence of voids of substantial volume. For instance, recent studies have offered strong evidence for the existence of such voids in room-temperature tetrahydrofuran (THF).[2,3] Large voids are believed to be responsible for the unusual spectroscopy and photophysics of solvated electrons in THF.[2,4,5] Neutron diffraction studies[3] and simulations[2,3] indicate the presence of voids with diameters of 2.5 Å or more in this liquid.

The presence of large voids in a liquid might be expected to be manifested in an obvious manner, but the fact that these voids went undetected in THF until recently underscores the subtlety of the signatures of such empty spaces. Indeed, at room temperature the volume per molecule in THF is smaller than that for closely related liquids that are not known to exhibit significant voids, such as cyclopentane, diethyl ether, and *n*-pentane.[6] The coefficient of thermal expansion for THF at room

temperature is slightly smaller than those for the other three related liquids, as would be expected from the smaller molar volume of THF.[6] The void spaces in THF must therefore arise from an uneven partitioning of the modest free volume in this liquid.

In optical Kerr effect (OKE) spectroscopy, [7–10] a linearly polarized, nonresonant pump pulse is used to put a torque on the molecules of a liquid and to drive intramolecular and intermolecular Raman-active modes impulsively. Depolarization of a probe pulse polarized at 45° is then used to measure the time dependence of collective orientational diffusion and depolarized intramolecular and intermolecular Raman modes. By transforming the data into the frequency domain, [11] the depolarized, Bose-Einstein-corrected, low-frequency Raman spectrum can be obtained.

The presence of sizable voids might be expected to manifest itself in OKE spectra in at least two different ways. First, the frequencies of intermolecular modes are sensitive to the distribution of free volume in a liquid. If the free volume is concentrated in substantial voids that are bordered by a only a fraction of the molecules in the liquid, then the remaining molecules have less free volume surrounding them than those in a more typical liquid. These tightly packed molecules would be expected to exhibit higher-frequency intermolecular modes. Second, the time scale for diffusive reorientation is also sensitive to the free volume surrounding a molecule and so might be expected to reveal the signature of unequally distributed free volume. In addition, we might expect that both of these aspects of the OKE data might exhibit an unusual temperature dependence in a liquid with substantial voids.

To test whether OKE spectroscopy can reveal the presence of significant voids in a liquid, here we present a detailed, temperature-dependent study of eight liquids: furan,

THF, diethyl ether, *n*-pentane, cyclopentane, cyclohexane, tetrahydropyran, and hexamethylphosphoramide (HMPA).

5.2 Experimental Section

All liquids (Table 5.1) were purchased in the purest form available from Aldrich and were used without any further purification. The liquids were sealed into 1-mm path length glass cuvettes and attached to the sample mount of a nitrogen-flow cryostat. To ensure an accurate temperature measurement, a temperature probe was placed directly against the cell near the position at which data were collected. After being changed, the temperature was allowed to stabilize for at least 30 min before data collection commenced.

Table 5.1: Formula Weight, Density at 298 K, and Viscosity at 298 K for the Liquids Studied

Liquid	*FW* (amu)	ρ (g/mL)	η (cP)
furan	68.07	0.921	0.361
THF	72.11	0.902	0.472
cyclopentane	70.14	0.741	0.419
diethyl ether	74.12	0.708	0.235
pentane	72.15	0.621	0.229
tetrahydropyran	86.13	0.879	0.808
cyclohexane	84.16	0.774	0.880
HMPA	179.20	0.879	3.147

Our optical-heterodyne-detected OKE experimental apparatus has been described in detail previously.[12, 13] For the data reported here, transform-limited Ti:sapphire laser pulses with a duration of approximately 50 fs and a center wavelength of 800 nm were employed. Data collected at equivalent positive and negative heterodyne angles were subtracted from each other to obtain the pure heterodyned contribution to the signal. Typically, [10] decays were collected at each angle for a liquid at a given temperature. Second-harmonic-generation autocorrelation data were used to perform Fourier-transform deconvolution of the OKE data in order to derive the Bose-Einstein-corrected, low frequency Raman spectra.[11]

For purposes of determining the orientational relaxation and "intermediate" relaxation[14] times, the data were integrated to determine the collective orientational correlation function $C_{coll}(\tau)$,[15] where τ is the experimental delay time. Fits were made to a function of the form

$$B[A\exp(-\tau/\tau_1)+(1-A)\exp(-\tau/\tau_2)] \qquad \text{(Eq. 5.1)}$$

where the amplitude A is less than unity, B is a scaling factor, τ_1 is the orientational correlation time, and τ_2 is the intermediate relaxation time. Based on these fits, the contribution of orientational diffusion was removed from the unintegrated data, assuming a rise time of 200 fs, in order to calculate the depolarized reduced spectral density (RSD) corresponding to each low-frequency Raman spectrum.

5.3 Results

Most of the liquids studied here are not highly polarizable and therefore yield relatively weak OKE signals. Representative integrated data for THF at 285 K are shown in Figure 5.1 (black line). The long-time portion of the decay has been fit to eq. 5.1.

Values of the decay times and their corresponding amplitudes are given in the ***Appendix D***. The fit to the data is also shown in Figure 5.1 (red line), and the residual can be seen to be quite smooth.

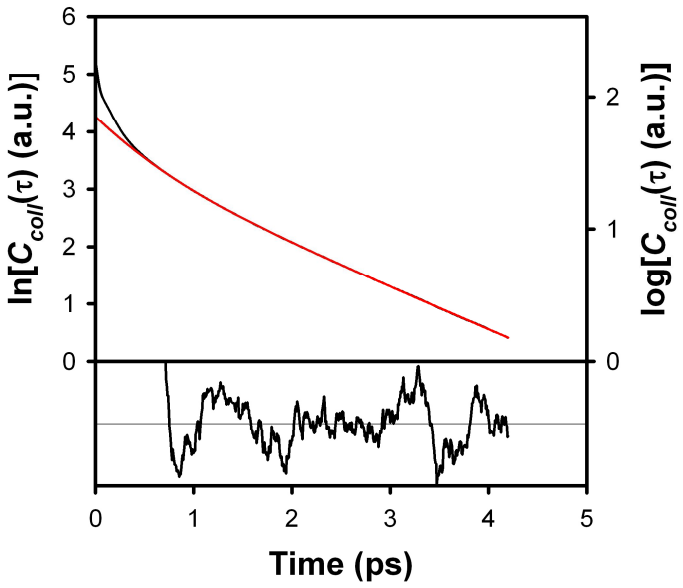

Figure 5.1 Logarithm of the collective orientational correlation function for THF at 285 K (black line, upper panel) as well as a biexponential fit to the data (red line). The residuals, shown in the lower panel on a linear scale, demonstrate the high quality of the fit to this representative data set.

OKE spectral densities usually have a relatively sharp feature below 10 cm^{-1} that is largely reorientational in origin; as such, this feature is generally not present in the reduced spectral density. However, the reorientational contribution to the OKE signal for the nonconjugated liquids studied here is weak enough that in many cases the spectral density does not have a clear low-frequency feature. As an example, we show the full spectral density and the reduced spectral density for THF at 286 K in Figure 5.2.

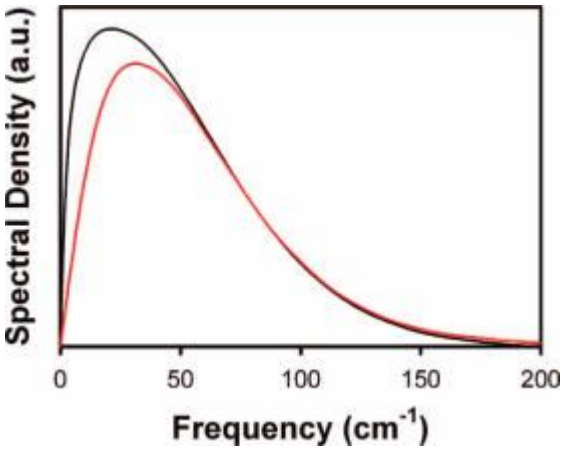

Figure 5.2 Representative Bose-Einstein-corrected spectral density (black) and reduced spectral density (red) for THF at 286 K.

For most simple liquids that have been studied to date with OKE spectroscopy, the behavior of the RSD with temperature follows a simple pattern.[12,16,17] With decreasing temperature, the RSD generally broadens, with the high-frequency portion moving to higher frequencies and the low-frequency portion moving to lower frequencies. The shift of the high-frequency portion can be attributed to the increase in density with decreasing temperature. The shift of the lower frequency portion is less well understood, but is related to the fact that the intermediate response time

generally tracks the orientational diffusion time in simple liquids.[14] The only exception to this behavior that has been reported previously is SO2, for which the entire RSD shifts to higher frequency with decreasing temperature.[18]

Shown in Figure 5.3 are RSDs for furan at temperatures ranging from 245 to 298 K; these and all other RSDs reported here have been scaled to have the same peak intensity. The room temperature RSD is consistent with a previously reported OKE spectral density.[19] This liquid exhibits a typical temperature dependence, with the RSD becoming considerably broader at low temperature than it is at high temperature. In Figure 5.4 we show RSDs for THF at temperatures ranging from 235 to 298 K. It is clear from these data that the RSDs for THF differ markedly from those for furan. The THF RSDs are substantially narrower than those of furan, and have a first moment at a considerably lower frequency. Furthermore, although the THF RSDs do become slightly broader at lower temperatures, they do so in an unusual fashion. The low-frequency portion of the THF RSDs exhibits a small shift to lower frequency with decreasing temperature (see inset of Figure 5.4), whereas the shape of the high-frequency portion is essentially constant with temperature.

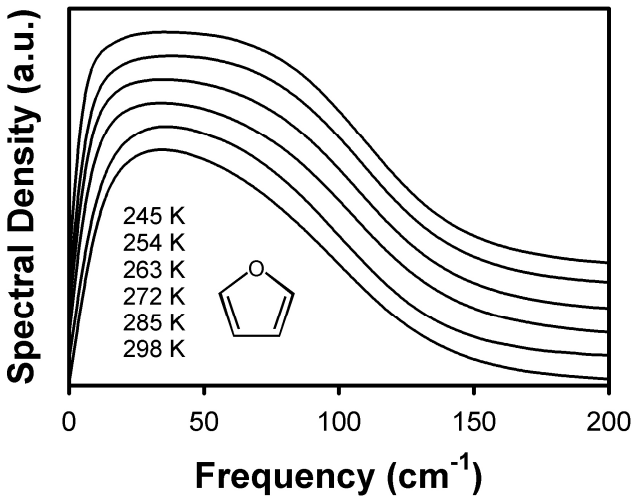

Figure 5.3 Height-normalized RSDs for furan at various temperatures. The plots have been offset vertically for clarity.

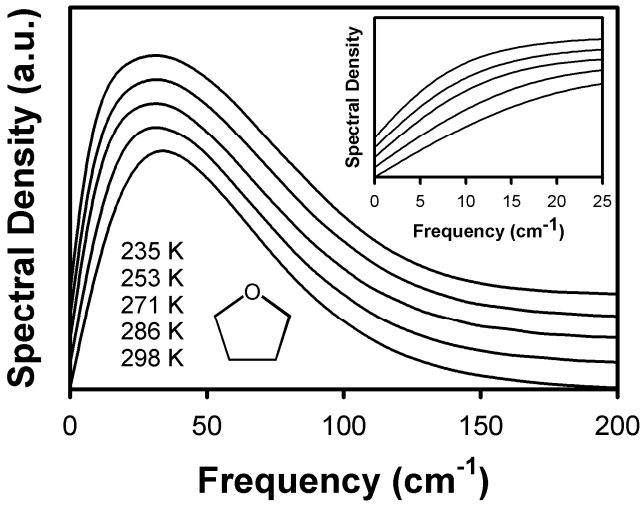

Figure 5.4 Height-normalized RSDs for THF at various temperatures. The inset gives a closer view of the lowest-frequency portions of the spectral densities. The plots have been offset vertically for clarity.

What factors account for the differences in the RSDs of furan and THF? One common proposal for bimodal OKE RSDs is that the lower-frequency feature arises from collision-induced scattering whereas the higher-frequency feature is librational in origin.[19–25] Furan's refractive index (1.423) is only modestly larger than that of THF (1.407),[6] so the polarizabilities of these liquids do not differ tremendously. As a result, collision-induced scattering may be of relatively similar importance for both liquids, yet the RSDs of THF do not appear bimodal. Indeed, given the modest refractive indices of these liquids, collision-induced scattering might not be expected to be particularly strong for either liquid. However, the relative importance of collision-induced scattering also depends on the magnitude of the polarizability anisotropy of a liquid, and it remains possible that differences in the polarizability anisotropy account for some of the differences between the RSDs of these liquids as well.

The molar volume of THF is on the order of 10% larger than that of furan, a difference that can decrease the librational frequencies and may therefore be partially responsible for the lower average frequency of the RSDs of THF. However, the differences in width and mean frequency of the RSDs of these liquids are large enough that they are unlikely to arise from density effects alone. Furan and THF also have different geometries and therefore different moments of inertia. However, the differences in moments of inertia are only large enough to account for a change in librational frequency on the order of 10%.

The differences between the furan and THF RSDs may also be related to the conjugated nature of furan. It is thus useful to compare the THF RSDs to those of

other related, nonconjugated liquids as well. We begin by considering temperature dependence of the RSDs for cyclopentane, which has a shape that is similar to that of THF. Cyclopentane is nondipolar, and therefore has a significantly lower density than THF. At room temperature, for instance, the molar volume of cyclopentane is approximately 15% greater than that of THF. The refractive index of cyclopentane (1.405)[6] is virtually identical to that of THF. RSDs for cyclopentane at 297 K and at 249 K are shown in Figure 5.5. The RSD at 249 K shows a subtle increase at lower frequencies as compared to the RSD at 297 K, but overall these spectra are remarkably similar to one another. In Figure 5.6 we compare the RSD of THF at 298 K (black) with that of cyclopentane at 297 K (red). The spectral densities peak at nearly the same frequency, but the RSD for cyclopentane is somewhat narrower than that of THF. The narrower RSD of cyclopentane at room temperature may result from its greater molar volume.

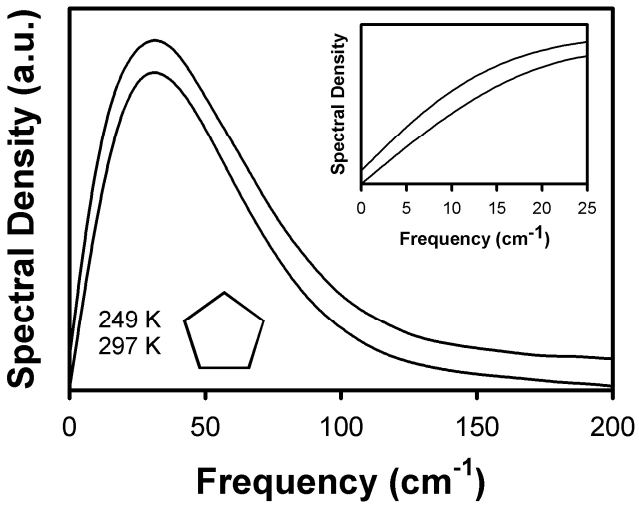

Figure 5.5 Height-normalized RSDs for cyclopentane at various temperatures. The inset gives a closer view of the lowest-frequency portions of the spectral densities. The plots have been offset vertically for clarity.

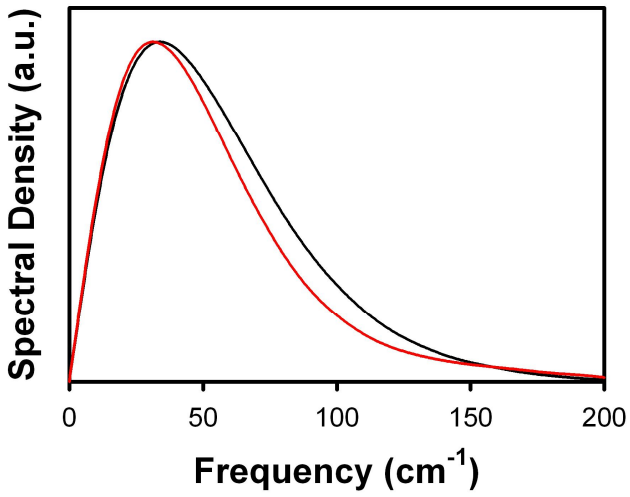

Figure 5.6 Comparison of the room-temperature RSDs for THF (black) and cyclopentane (red).

Ryu and Stratt have suggested that liquids composed of molecules with similar shapes may have similar OKE spectra, [26] and our data support this general idea for these two liquids. While the basic shapes of the RSDs are similar, the difference in widths of the RSDs of THF and cyclopentane does become more substantial at lower temperatures. The molar volume of THF increases by nearly 5% in going from 297 to 249 K, while that of cyclopentane increases by roughly 6%. Thus, the ratio of molar volumes of the two liquids remains nearly the same over this temperature range. The increasing differences in the RSDs of these liquids at lower temperatures may therefore be a signature of different distributions of free volume. The voids in THF appear to be associated with (but have surfaces that tend not to include) oxygen atoms, [3] and therefore may not be present in cyclopentane.

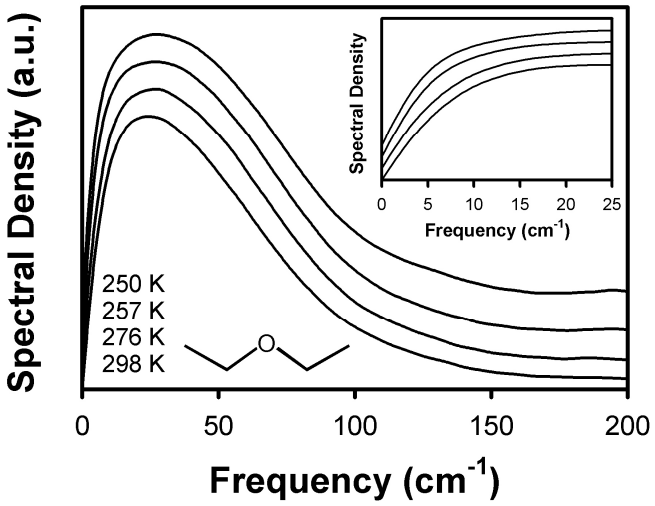

Figure 5.7 Height-normalized RSDs for diethyl ether at various temperatures. The inset gives a closer view of the lowest-frequency portions of the spectral densities. The plots have been offset vertically for clarity.

We next consider the temperature dependence of the RSD of diethyl ether, which is chemically similar to THF but is a linear molecule. RSDs for this liquid at temperatures ranging from 250 to 298 K are shown in Figure 5.7. At 298 K the diethyl ether RSD resembles that of THF, but peaks at a substantially lower frequency. This shift in peak frequency is consistent with the larger molar volume of diethyl ether, which is nearly 30% greater than that of THF at room temperature. However, it is clear from Figure 5.7 that the diethyl ether RSDs exhibit a more conventional temperature dependence, broadening to both higher and lower frequency with decreasing temperature.

Given the flexibility of diethyl ether, this liquid might not be expected to exhibit sizable voids. Neutron diffraction or other studies are needed to confirm this supposition. However, it is well-known that the structures of simple alkane liquids do not generally feature large voids.[27–29] We therefore also consider the temperature dependence of the RSD of *n*-pentane, which has strong structural similarity to diethyl ether on a molecular level. In the liquid, *n*-pentane tends to adopt an extended conformation, although not to the same extent as longer-chain alkanes.[29] In analogy, simulations suggest that more than 70% of diethyl ether molecules adopt an all-*trans* configuration in the liquid, with the majority of the remaining molecules featuring a single *gauche* defect. In Figure 5.8 we show RSDs for *n*-pentane at temperatures that range from 214 K to room temperature. Due to the weak polarizability of *n*-pentane, these RSDs are noisier than those of diethyl ether. Nevertheless, the RSDs for *n*-pentane and diethyl ether bear strong similarity, as is underscored in Figure 5.9.

Although the RSDs for *n*-pentane do not broaden quite as much to lower frequency with decreasing temperature as do those of diethyl ether, the RSDs do remain quite similar to one another over the temperature range studied here, in contrast to the RSDs for THF and cyclopentane. The similar temperature dependence of the RSDs for diethyl ether and *n*-pentane might suggest that the former liquid does not exhibit large voids. However, as opposed to *n*-pentatne, diethyl ether has a significant, localized dipole moment, and so similarities in molecular structure need not imply equally strong similarities in liquid structure.

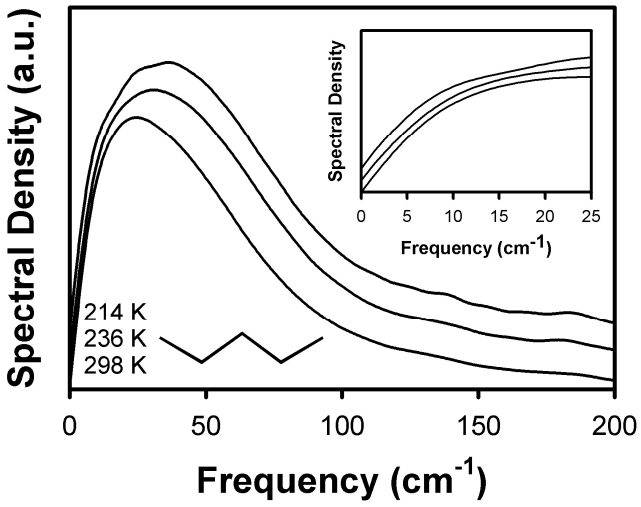

Figure 5.8 Height-normalized RSDs for *n*-pentane at various temperatures. The inset gives a closer view of the lowest-frequency portions of the spectral densities. The plots have been offset vertically for clarity.

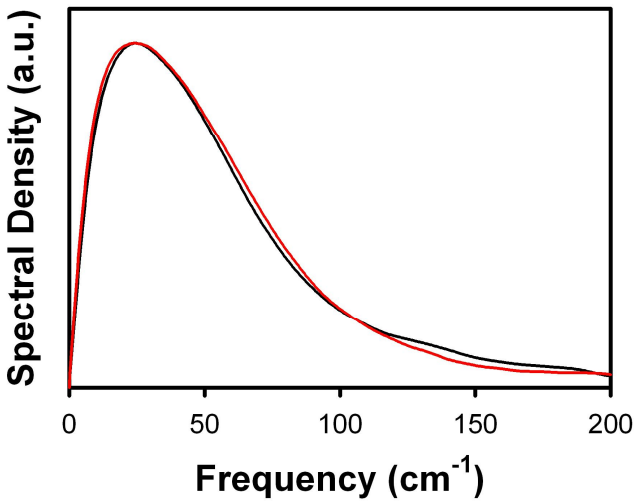

Figure 5.9 Comparison of the room-temperature RSDs for *n*-pentane (black) and diethyl ether (red).

It is possible that part of the reason that THF exhibits large voids is its near 5-fold symmetry, which prevents it from filling space efficiently. Furan and cylcopentane have similar shapes, so the near 5-fold symmetry of THF cannot alone be responsible for it unusual liquid structure. Nevertheless, it is instructive to compare THF to similar cyclic molecules with a different number of atoms. With this in mind, in Figure 5.10 we present RSDs for tetrahydropyran, a six-membered ring with a single oxygen atom, at temperatures of 242 and 297 K. This liquid exhibits a relatively conventional temperature dependence, with its RSD broadening to higher and lower frequencies with decreasing temperature. At room temperature, the RSD for tetrahydropyran is broader than that of THF and peaks at a somewhat lower frequency. One possible source of these differences might be that the free volume in tetrahydropyran is more uniformly distributed than that in THF. Again, neutron

diffraction studies will be required to investigate this issue fully.

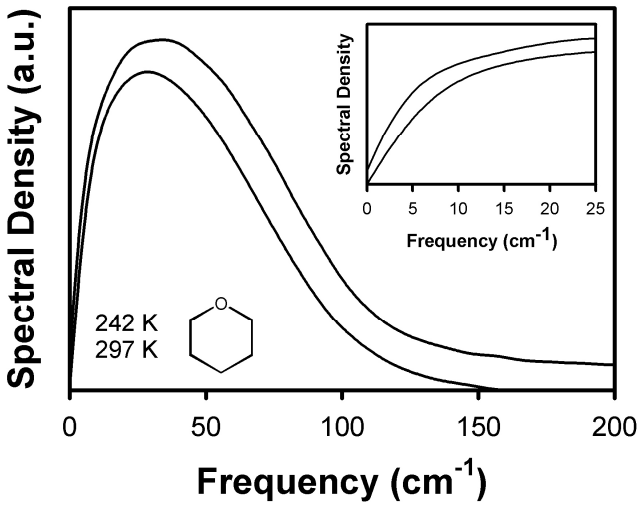

Figure 5.10 Height-normalized RSDs for tetrahydropyran at 242 and 297 K. The inset gives a closer view of the lowest-frequency portions of the spectral densities. The plots have been offset vertically for clarity.

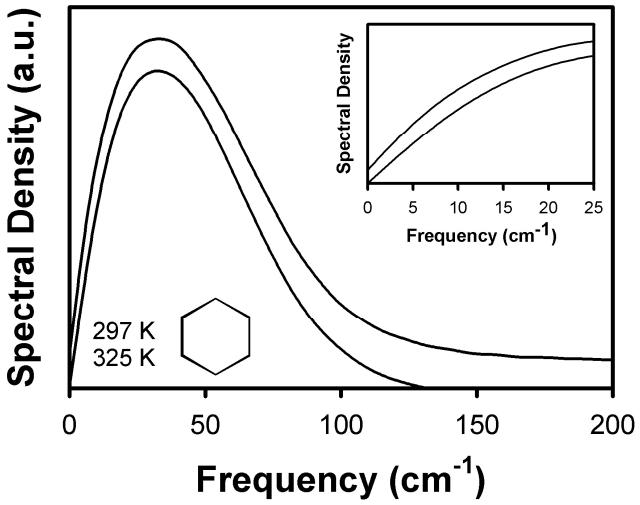

Figure 5.11 Height-normalized RSDs for cyclohexane at 297 and 325 K. The inset gives a closer view of the lowest-frequency portions of the spectral densities. The plots have been offset vertically for clarity.

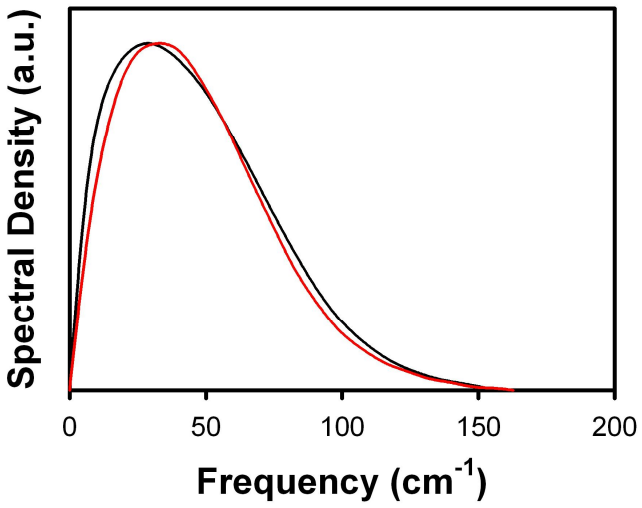

Figure 5.12 Comparison of the room-temperature RSDs for tetrahydropyran (black) and cyclohexane (red).

In Figure 5.11 we show RSDs for cyclohexane at 297 and 325 K. As was the case with cyclopentane, the cyclohexane RSD changes only modestly with temperature, suggesting that this may be common behavior for saturated cyclic hydrocarbons. In analogy with THF and cyclopentane, Figure 5.12 shows that the RSDs of tetrahydropyran and cyclohexane are similar at room temperature.

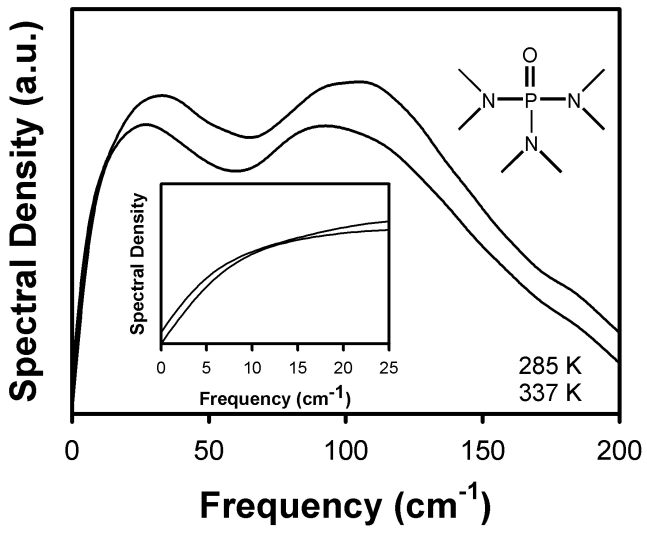

Figure 5.13 Height-normalized RSDs for hexamethylphosphoramide at 285 and 337 K. The inset gives a closer view of the lowest-frequency portions of the spectral densities. The plots have been offset vertically for clarity.

The final liquid that we consider is HMPA, which has also been proposed to contain voids of significant dimension.[2] RSDs for this liquid at 285 and 337 K are shown in Figure 5.13. The RSDs of HMPA exhibit considerable structure, presumably due to low-frequency hindered internal rotational modes. The peaks in the spectrum do appear to broaden slightly and shift to higher frequency with decreasing temperature, with some broadening to lower frequency as well. Thus, we believe that the temperature- dependent behavior of the intermolecular portion of the RSD of this liquid is somewhat different from that of THF; however, as the shape of the high-frequency intramolecular mode depends significantly upon temperature, it is difficult to make a clear determination of how the shape of the low frequency,

intermolecular portion of the spectrum changes with temperature.

Void spaces in THF, if they exist, should manifest themselves in observables beyond the OKE RSD. For instance, according to the Debye-Stokes-Einstein (DSE) equation,[30, 31] the orientational correlation time τor of a solute molecule in a simple liquid should satisfy

$$\tau_{or} = \frac{V_H \eta}{k_B T} + \tau_0 \qquad \text{(Eq. 5.2)}$$

where V_H is the hydrodynamic volume for reorientation, η is the viscosity, T is the temperature, k_B is Boltzmann's constant, and τ_0 is a constant that depends on the solute and the solvent but whose physical meaning is a subject of continuing debate. The hydrodynamic volume should be highly sensitive to the distribution of free volume in a liquid, and we might therefore expect that the temperature dependence of the orientational correlation time will be sensitive to the presence of voids in a liquid.

Although it is not intended to apply to neat liquids, the DSE equation generally does a good job of describing the temperature and viscosity dependences of the reorientation times in these systems as well.[14] In addition, the DSE equation applies to the single-molecule orientational correlation time, whereas OKE spectroscopy measures the collective orientational correlation time, $\tau_{coll.}$[32] These two times are related via[31]

$$\tau_{corr} = \frac{g_2}{j_2} \tau_{sm} \qquad \text{(Eq. 5.3)}$$

where g_2 is the static pair orientational correlation parameter and j_2 is the dynamic pair orientational correlation parameter. In general, j_2 is believed to take on a value near unity for simple liquids, whereas g_2 varies depending on the degree of parallel

ordering of the liquid molecules.[31] For liquids with no net parallel ordering, g_2 has a value of unity, while in the presence of such ordering it takes on a larger value.

We investigated the DSE behavior of all of the liquids studied here. Temperature-dependent viscosity data for each liquid were obtained from the literature.[6, 33–40] The DSE plots for the OKE relaxation times of the saturated cyclic liquids and of HMPA are shown in Figure 5.14.

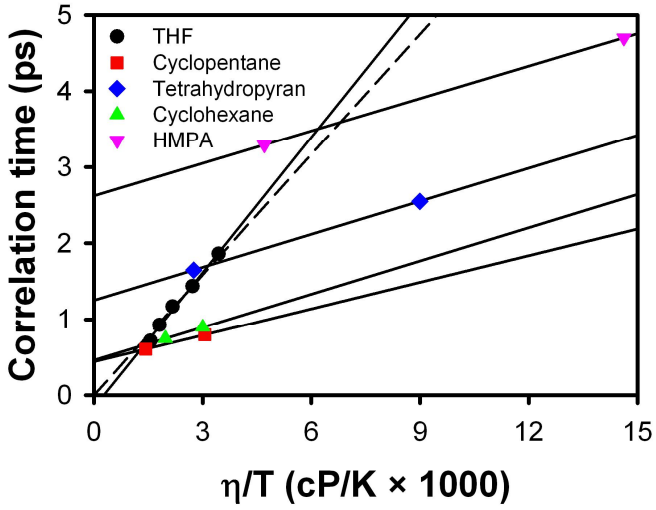

Figure 5.14 DSE plots for THF, cyclopentane, tetrahydropyran, cyclohexane, and HMPA. The solid lines are linear least-squares fits to the data. The dashed line is a linear least-squared fit to the THF data that has been constrained to pass through the origin.

The slopes of the plots for tetrahydropyran and cyclohexane are close to one another. This similarity indicates that these liquids have similar products of the hydrodynamic volumes for reorientation and g_2, as might be expected based on their similar structures. At any given value of η/T, the overall magnitude of the τ_{coll} for

tetrahydropyran is on the order of 0.8 ps greater than that of cyclohexane, a difference that is reflected in different values of τ_0 for these two liquids. The DSE plot for cyclopentane has a smaller slope than those for tetrahydropyran and cyclohexane, which is in line with the smaller size, and presumably smaller hydrodynamic volume, of cyclopentane. The limiting orientational correlation time, τ_0, for cyclopentane is virtually identical to that of the chemically similar cyclohexane. The DSE plot for HMPA has a slope that is similar to those of tetrahydropyran and cyclohexane, and has a limiting orientational correlation time that is considerably greater than that for any of the other liquids. The DSE plot for THF differs substantially from those for the other saturated cyclic liquids. First, the limiting value of the orientational correlation time τ_0 for this plot is negative (although a fit that is constrained to pass through the origin also does a good job of fitting these data; see the dashed line in Figure 5.14). More importantly, the slope of the DSE plot for this liquid is considerably steeper than those for the other three liquids. The steeper slope of the DSE plot for THF is too large to be accounted for by a large value g_2 for this liquid, and the structure derived from neutron diffraction studies suggests that g_2 should be near unity.[3] The slope must therefore be indicative of an increase in the hydrodynamic volume for reorientation. Such an increase may arise from a change in the boundary conditions for reorientation from slip in the other three liquids to stick in THF.

It is tempting to conclude that the reason that the DSE plot for THF differs greatly from those for the other liquids is that a transition in boundary conditions for reorientation results from an uneven distribution of free volume that causes the molecules in THF to have to reorient in a collective manner. However, it is also

important to note that the DSE plot for OKE reorientation times for THF is not atypical of similar plots obtained for a wide range of simple molecular liquids. For example, DSE plots derived from OKE data for acetonitrile, benzene, carbon disulfide, chloroform and methyl iodide[14] all have small τ_0 values and slopes that are similar to that of the THF DSE data presented here. To underscore this point, in Figure 5.15 we compare the DSE plot of the OKE relaxation times for THF with those of furan, diethyl ether, and *n*-pentane. The slope of the DSE plot for furan is similar to that for THF, although furan has a slightly higher value of τ_0. The DSE plots for diethyl ether and *n*-pentane are nearly superimposable. These plots have a considerably higher slope that that for THF, presumably because diethyl ether[41] and *n*-pentane[29] adopt relatively straight conformations in the liquid phase and therefore have a larger hydrodynamic volume for reorientation, and potentially a larger value of g_2. As is the case with THF, the values of τ_0 for the DSE plots of diethyl ether and *n*-pentane are near zero.

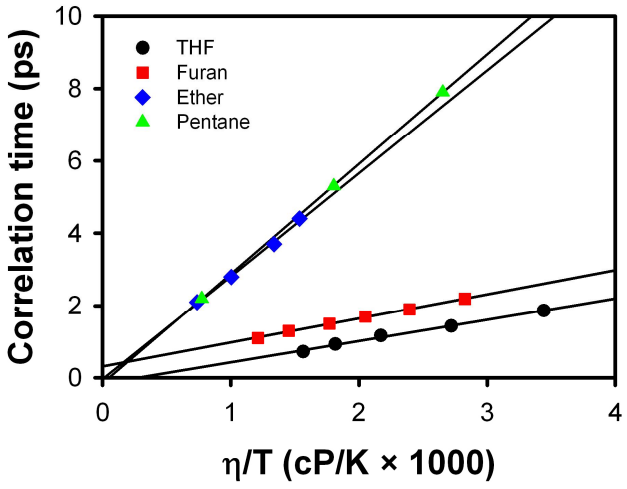

Figure 5.15 DSE plots for THF, furan, diethyl ether, and *n*-pentane. The solid lines are linear least-squares fits to the data.

5.4 Discussion

The RSDs for THF do not differ radically from those of other liquids studied here. Furan's RSDs display a "conventional" temperature dependence, broadening significantly to higher and lower frequencies with decreasing temperature. The behavior of the high-frequency portion of the furan RSD can be rationalized in terms of the density increase that goes along with decreasing temperature. This densification leads to a decrease in free volume, increasing the frequencies of librations and hindered translational motions. The low-frequency behavior is another manifestation of the temperature-dependent behavior of the intermediate response. As the temperature is decreased, the frequency at which motional narrowing dominates the spectrum becomes smaller, thereby making the RSD become more intense at lower frequencies. The RSDs of the linear molecules diethyl ether and *n*-pentane do show notable broadening at lower temperatures. For the saturated, cyclic liquids, the RSDs exhibit a considerably more subtle temperature dependence, and the behavior of the THF RSDs does not stand out among them.

To gain further insight into these data, it is useful to consider what is known about the structure of liquid THF based on neutron diffraction studies coupled with empirical potential structure refinement.[3] THF molecules are twisted but essentially planar in the liquid. There is a significant propensity for pairs of neighboring molecules to adopt a T-like configuration in the liquid, which leads to the expectation that g_2 should be near unity. The positions of the oxygen atoms presumably play

some role in determining the preferred relative orientations of pairs of molecules in T configurations. The surfaces of the largest voids (of 3 Å diameter) in the liquid are composed virtually entirely of hydrogen atoms from all four of the methylene groups and of the carbon atoms bonded to the oxygen atoms. In somewhat smaller voids with a 2.5 Å diameter, the surfaces do have a small representation from the oxygen atoms and from the carbon atoms that are opposite the oxygen atoms.[3] Thus, the void surfaces are enriched in portions of the molecules with a partial positive charge, to the relative exclusion of both the oxygen atoms, which have a partial negative charge, and the near neutral carbon atoms that are not bonded to the oxygen atoms.

Given that the RSDs for the saturated, cyclic molecules are relatively insensitive to temperature, it is interesting to consider whether it is possible that cyclopentane, tetrahydropyran and cyclohexane also exhibit substantial voids, perhaps due to their relative lack of conformational freedom as compared to linear molecules. This question must ultimately be addressed by neutron diffraction and/or simulation studies, but we can gain some useful insights based on what is known currently.

The extremely low probability of finding oxygen atoms in the voids of THF suggests that these atoms do play a role in the formation of the voids. Thus, it is not unreasonable to imagine that tetrahydropyran should exhibit similar voids. It is important to keep in mind, however, that tetrahydropyran is considerably more flexible than THF. In addition, since THF is nearly planar, its roughly 5-fold symmetry may contribute to making it difficult to pack these molecules efficiently. Such constraints do not exist to the same extent for tetrahydropyran.

Although the oxygen atoms in liquid THF clearly play a role in the formation of

voids, we should not entirely discount the possibility that cyclopentane also contains such voids. It is well known that the structures of simple liquids can be described as being determined by effective repulsive interactions.[42] While the effective repulsive shapes of THF and cyclopentane must certainly differ, the similarities may still be great enough to lead to voids in cyclopentane as well.

Another possibility is that RSDs for liquids, and the temperature dependences of these RSDs, are relatively insensitive to the presence of voids. While voids make up a notable portion of the free volume of the liquid, they do not account for a sizable fraction of the total volume of the liquid. As a result, such voids may not have a strong influence on the low-frequency Raman spectra of these liquids. Within this picture, the similarity in the RSDs of the liquids may arise from the similar molecular shapes, and the relative insensitivity of the RSDs to temperature may be a manifestation of the low degree of conformational freedom of cyclic molecules.

Other than furan, the cyclic liquids studied here do not exhibit significant broadening of their RSDs as the temperature is decreased. Such broadening has been a near-universal feature in previous OKE studies of simple liquids. The source of the different temperature behavior of the RSDs of these saturated, cyclic liquids merits further investigation. Although based on their refractive indices, furan and THF have similar polarizabilities, it is still likely that these liquids differ significantly in their polarizability anisotropies. It is therefore possible that the weak temperature dependence of the RSDs of THF and other cyclic liquids studied here is a sign of a relatively small polarizability anisotropy, although the fact that a significant reorientational decay is observed in all of the liquids studied here suggests that the

polarizability anisotropy is not negligible in any of these substances. Linear molecules such as diethyl ether and *n*-pentane would be expected to adopt extended conformations and therefore have larger polarizability anisotropies that the cyclic liquids, and indeed the linear molecules do show a greater temperature dependence in their RSDs than do the saturated, cyclic molecules.

We should also note that the intermolecular modes and orientational diffusion to which OKE spectroscopy is sensitive occur on essentially the same time scale as does rearrangement of voids.[2] Indeed, these motions are probably involved intimately in this rearrangement. This similarity in time scales may be responsible for the lack of a clear signature of voids in the OKE spectra. A technique that is sensitive to structure on a shorter time scale may have greater sensitivity to the presence of voids.

As is the case with the RSDs, the orientational behavior of THF does not provide a clear signature of void spaces. We have found that the DSE plot for THF differs substantially from those for cyclopentane, tetrahydropyran, cyclohexane and HMPA. However, the behavior of the DSE plot of THF is rather typical of those for nonassociated, small-molecule liquids, including furan, diethyl ether, and *n*-pentane. We should note that the orientational dynamics of the liquids studied here have been described by single exponentials, whereas in theory up to five exponentials may be needed.[32] However, for the vast majority of simple liquids a single-exponential treatment appears to work well. Furthermore, even if we are only measuring that slowest exponential of a multiexponential decay, DSE behavior would still be expected to hold. Thus, the substantial limiting values of τ_0 observed for some of the liquids studied here are rather unexpected.

5.5 Conclusion

Based on simulations and techniques such as neutron diffraction, there is strong evidence that substantial voids exist in THF at room temperature.[2,3] We have studied THF and a number of related liquids over a range of temperatures to determine whether or not these voids have a clear OKE spectroscopic signature. The temperature dependence of the OKE spectra of THF differs significantly from that of its close relative furan. However, other related cyclic liquids that lack double bonds have RSDs that have a temperature dependence that is not readily distinguishable from that of THF. It remains possible that all of these liquids have significant void spaces, and this possibility should be investigated with other techniques.

The dependence of the orientational correlation time of THF on viscosity and temperature does not display any sort of anomalous behavior that can be linked to the presence of voids. A number of the other liquids studied here do have somewhat surprising DSE behavior, and this is another topic that also merits further investigation.

Our studies offer no clear evidence that the voids spaces in THF are manifested in any obvious manner in OKE spectra of THF. Although the liquid structure of THF is unusual, the influence of the voids on OKE spectra and orientational correlation times is subtle enough that that we must conclude that OKE spectroscopy is not likely to be a useful means of searching for such voids in other liquids.

5.6 References

(1) Marcus, Y. *Solvent Mixtures: Properties and Selective Solvation*; Marcel Dekker: New York, **2002**.

(2) Bedard-Hearn, M. J.; Larsen, R. E.; Schwartz, B. J. *J. Chem. Phys.* **2005**, 122, 134506.

(3) Bowron, D. T.; Finney, J. L.; Soper, A. K. *J. Am. Chem. Soc.* **2006**, 128, 5119.

(4) Martini, I. B.; Barthel, E. R.; Schwartz, B. J. *Science* **2001**, 293, 462.

(5) Jou, F. Y.; Freeman, G. R. *J. Phys. Chem.* **1977**, 81, 909.

(6) Weast, R. C. *CRC Handbook of Chemistry and Physics*, 66th ed.; CRC Press: Boca Raton, **1985**.

(7) Righini, R. *Science* **1993**, 262, 1386.

(8) Kinoshita, S.; Kai, Y.; Ariyoshi, T.; Shimada, Y. *Int. J. Mod. Phys. B* **1996**, 10, 1229.

(9) Fourkas, J. T. Nonresonant Intermolecular Spectroscopy of Liquids. In *Ultrafast Infrared and Raman Spectroscopy*; Fayer, M. D., Ed.; Marcel Dekker: New York, **2001**; Vol. 26; p 473.

(10) Hunt, N. T.; Jaye, A. A.; Meech, S. R. *Phys. Chem. Chem. Phys.* **2007**, 9, 2167.

(11) McMorrow, D.; Lotshaw, W. T. *J. Phys. Chem.* **1991**, 95, 10395.

(12) Farrer, R. A.; Loughnane, B. J.; Deschenes, L. A.; Fourkas, J. T. *J. Chem. Phys.* **1997**, 106, 6901.

(13) Loughnane, B. J.; Farrer, R. A.; Scodinu, A.; Reilly, T.; Fourkas, J. T. *J. Phys. Chem. B* **2000**, 104, 5421.

(14) Loughnane, B. J.; Scodinu, A.; Farrer, R. A.; Fourkas, J. T.; Mohanty, U. *J. Chem. Phys.* **1999**, 111, 2686.

(15) Scodinu, A.; Fourkas, J. T. *J. Phys. Chem. B* **2002**, 106, 10292.

(16) Loughnane, B. J.; Scodinu, A.; Fourkas, J. T. *J. Phys. Chem. B* **2006**, 110, 5708.

(17) Ricci, M.; Bartolini, P.; Chelli, R.; Cardini, G.; Califano, S.; Righini, R. *Phys. Chem. Chem. Phys.* **2001**, 3, 2795.

(18) Jaye, A. A.; Hunt, N. T.; Meech, S. R. *J. Chem. Phys.* **2006**, 124, 024506.

(19) Kamada, K.; Ueda, M.; Ohta, K.; Wang, Y.; Ushida, K.; Tominaga, Y. *J. Chem. Phys.* **1998**, 109, 10948.

(20) Chang, Y. J.; Castner Jr., E. W. *J. Chem. Phys.* **1993**, 99, 113.

(21) Chang, Y. J.; Castner Jr., E. W. *J. Chem. Phys.* **1993**, 99, 7289.

(22) Chang, Y. J.; Castner Jr., E. W. *J. Phys. Chem.* **1994**, 98, 9712.

(23) Neelakandan, M.; Pant, D.; Quitevis, E. L. *J. Phys. Chem. A* **1997**, 101, 2936.

(24) Neelakandan, M.; Pant, D.; Quitevis, E. L. *Chem. Phys. Lett.* **1997**, 265, 283.

(25) Smith, N. A.; Meech, S. R. *J. Phys. Chem. A* **2000**, 104, 4223.

(26) Ryu, S.; Stratt, R. M. *J. Phys. Chem. B* **2004**, 108, 6782.

(27) Brady, G. W.; Fein, D. B. *J. Appl. Crystallogr.* **1975**, 8, 261.

(28) Rigby, D.; Roe, R. J. *J. Chem. Phys.* **1988**, 89, 5280.

(29) Small, D. M. *The Physical Chemistry of Lipids*; Plenum: New York, **1986**.

(30) Debye, P. *Polar Molecules*; Dover: New York, **1929**.

(31) Kivelson, D.; Madden, P. A. *Annu. Rev. Phys. Chem.* **1980**, 31, 523.

(32) Berne, B. J.; Pecora, R. *Dynamic Light Scattering*; Wiley: New York, **1976**.

(33) Holland, R. S.; Smyth, C. P. *J. Phys. Chem.* **1955**, 59, 1088.

(34) Sinha, A.; Roy, M. N. *J. Chem. Eng. Data* **2006**, 51, 1415.

(35) Giner, B.; Gascon, I.; Villares, A.; Cea, P.; Lafuente, C. *J. Chem. Eng. Data* **2006**, 51, 1321.

(36) Assael, M. J.; Dalaouti, N. K.; Dymond, J. H. *Int. J. Thermophys.* **2000**, 21, 621.

(37) Froba, A. P.; Pellegrino, L. P.; Leipertz, A. *Int. J. Thermophys.* **2004**, 25, 1323.

(38) Comelli, F.; Francesconi, R.; Bigi, A.; Rubini, K. *J. Chem. Eng. Data* **2007**, 52, 639.

(39) Aminabhavi, T. M.; Patil, V. B.; Aralaguppi, M. I.; Phayde, H. T. S. *J. Chem. Eng. Data* **1996**, 41, 521.

(40) Bhadani, S. N. *Indian J. Chem.* **1972**, 10, 88.

(41) Briggs, J. M.; Matsui, T.; Jorgensen, W. L. *J. Comput. Chem.* **1990**, 11, 958.

(42) Andersen, H. C.; Chandler, D.; Weeks, J. D. *Adv. Chem. Phys.* **1976**, 34, 105.

Chapter 6: Preliminary Study of Liquids under Tension

6.1 Introduction

The seminal work of Weeks, Chandler and Andersen[1-3] demonstrates that in the absence of specific interactions such as hydrogen bonds, the local structure of molecular liquids is determined predominantly by the net repulsive pairwise interactions between molecules. Yet it is the attractive interactions between molecules that hold a liquid together. Is it possible to find a structural signature (ie. an experimental signature that depends on structure) of these attractive interactions? The local structure of liquids is undeniably dependent on temperature, but this is arguably more a matter of which structures are thermally accessible rather than a density effect. Liquids can be densified isothermally by applying pressure, but this only increases the importance of repulsive interactions. Thus, in order to increase the importance of attractive interactions, one must find a way to decrease the density of a liquid at constant temperature.

This problem was solved over 150 years ago by Berthelot.[4] In his experiment, water was sealed in a cell under vacuum, and the temperature was raised until the water occupied the entire cell volume. When the cell was cooled down to its original temperature, the water continued to occupy the entire cell volume due to the energy barrier that had to be overcome to nucleate a vapor bubble. This inability to reach its equilibrium volume caused the water to be in a state of tension. At some point the tension eventually led to a vapor bubble nucleating either heterogeneously (on a cell

wall) or homogeneously (when the tensile strength of the liquid is reached).

Heterogeneous nucleation[5,6] is typical in stretched liquids and occurs often. It generally occurs at nucleation sites located on surfaces contacting the liquid or vapor. Suspended particles or minute bubbles also provide nucleation sites. Homogeneous nucleation has no preference for nucleation sites, and it generally occurs in the interior of a uniform substance, with much more difficulty than heterogeneous nucleation. Homogeneous nucleation occurs spontaneously and randomly, and is rare compared to heterogeneous nucleation. In order to keep liquids under tension for a time long enough to perform spectroscopic experiments, understanding nucleation, especially heterogeneous nucleation is necessary.

Water was the first liquid to be studied to any significant extent under extreme tension.[7-14] Water is an ideal liquid for such studies in many ways. For instance, it has an extremely high tensile strength for a liquid due to the high degree of hydrogen bonding. However, heterogeneous nucleation generally prevents water from being stretched to its intrinsic tensile strength. Furthermore, water is not readily amenable to study using OKE spectroscopy due to its extremely low polarizability anisotropy. The same holds true for other hydrogen-bonded liquids that would have high tensile strengths. As a result, little spectroscopic work has been done on these types of liquids.

Aromatic liquids could be excellent candidates for initial experiments on liquids under tension. Simple aromatic liquids such as benzene have medium to high surface tensions for organic liquids,[15] yet they also have small contact angles on silica. The small contact angles indicate a large enough affinity for glass that should facilitate

liquid large tensions in silica cells. The fact that the contact angles on silica are so small despite these liquids having healthy surface tensions is also an indication that these liquids are likely to have relatively large tensile strengths even though they are not dipolar. Indeed, previous measurements on benzene show that it has a tensile strength of at least 150 atm,[16] although the authors of this study believed that heterogeneous nucleation of vapor bubbles prevented the homogeneous nucleation limit from being reached in their experiments. While the tensile strength of benzene is substantially less than that of water (believed to be greater than 1000 atm[10]), 150 atm still represents a substantial tension. Under such big tension, the density of benzene will be reduced and the intermolecular interactions will change dramatically. Thus, OKE experiments on aromatic liquids should yield clear signatures due to the effects of negative pressure. These signatures should be evident in reduced spectral density (RSD) which provides intermolecular dynamics information.

For initial experiments, we used glass tubes (1 mm inner diameter) with one end sealed as the sample cell. Ultra pure, degassed aromatic liquids are employed. The cells are filled to some level, and the liquid is frozen using liquid nitrogen. The cell is then evacuated prior to being sealed just above the original fill line with a torch. Aromatic liquids have a number of advantages over water in the construction of a Berthelot cell in this manner: not only do aromatic liquids contract upon crystallization, but they also have much higher thermal expansion coefficients than water.[15] We can therefore employ a considerably larger vapor volume in Berthelot cells of aromatic liquids than is the case for water.

One issue that we need to address is how to measure the tension to which a liquid

sample is subjected. The tensions we are exploring are too small to measure reliably with Raman scattering from a ruby chip, and we would rather not add such a chip to a Berthelot cell for fear that it will provide heterogeneous nucleation sites. It is straightforward to obtain a reasonable estimate of the volume of the cell and the amount of liquid in it, but we must know the equation of state in order to turn this information into a tension at a given temperature. Given that the tensions that the liquids we will study can sustain are likely to be on the order of a few hundred atm, we might reasonably estimate the tension from pressure-volume-temperature data for these liquids at positive pressures, when such data is available. Also, Henderson and Speedy[8] designed a clever cell that has a spiral arm that changes its degree of winding depending on the pressure in the liquid it holds, allowing for accurate measurement of the tension in a liquid. In our method, we use a regular capillary tube with 1 mm inner diameter as the sample cell. The length of liquid in the cell can be used to represent the volume of the liquid. After the cell is sealed, the liquid and the vapor phase will be in equilibrium. If we know the temperature, we can determine the pressure. Thus, we will have all the data (temperature-volume-pressure) for the initial liquid state. For the final state (under tension), we know the temperature and volume, and its pressure can be determined (see below).

6.2 Experimental Section

To place liquids under negative pressure, we have developed a method based on the Bertherlot tube technique. A diagram of our experimental setup is shown in Figure 6.1. The pure liquid is placed in a reservoir hooked up to a vacuum line (Ace Glass Inc.), and then this liquid is degassed using several (4-6) freeze-pump-thaw

cycles. The sample tube is made from a capillary tube (1 mm inner diameter) by sealing one side of the tube. After being annealed in an oven at about 500 °C for about 2 hours, the tube is connected to the vacuum line. The final length of the tube is usually about 35 cm.

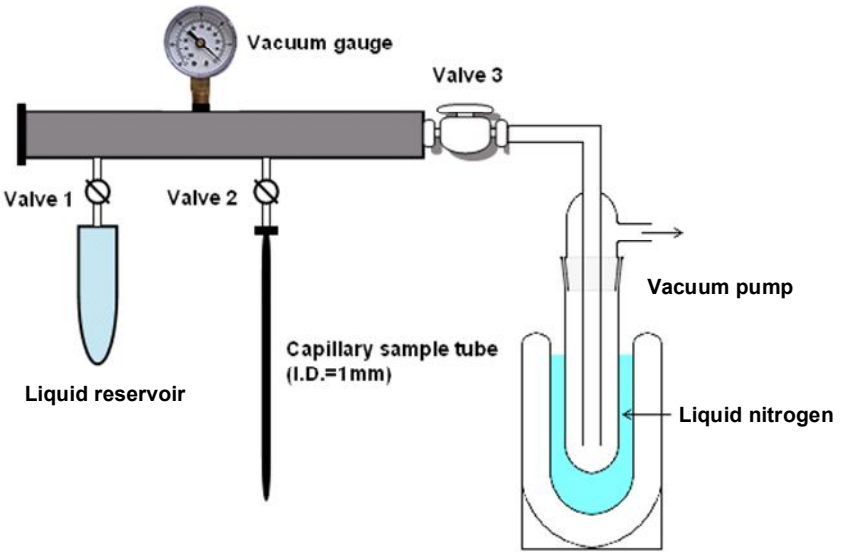

Figure 6.1 Experimental setup for preparing liquid samples under tension

The detailed procedure for producing a liquid sample under tension can be described by four steps:

(1) The liquid must be degassed using the following freeze-pump-thaw procedure:

(a) Fill the liquid container with about 10 ml liquid, and hook it up to the vacuum line (see Figure 6.1);

(b) Freeze the liquid using liquid nitrogen, and then open valve 3 to reduce

the pressure in that liquid container;

(c) Close valve 1, thaw the frozen sample until it melts using a water bath (You will see gas bubbles evolve from the liquid). After the frozen liquid completely melts, repeat step (b) – (c) until you no longer see bubbles form as the frozen liquid thaws (usually about five cycles).

(2) The degassed liquid needs to be transferred to the capillary sample tube:

(a) Close valves 1 and 2 and open valve 3 (see Figure 6.1). Evacuate the chamber (shown in gray in Figure 6.1) to ~ 50 torr. Then keep the pump on but close valve 3;

(b) Open valves 1 and 2, at the same time. Put the empty bottom part (few centimeters) of the capillary sample tube inside the mixture of water and ice (0 °C) in a dewar. Some liquid will be deposited into the bottom of the tube after a few minutes;

(c) Repeat steps (a) – (b) several times until 80% of the tube (25-30 cm) is filled up. Remove the dewar, and mark the point of the liquid level at room temperature.

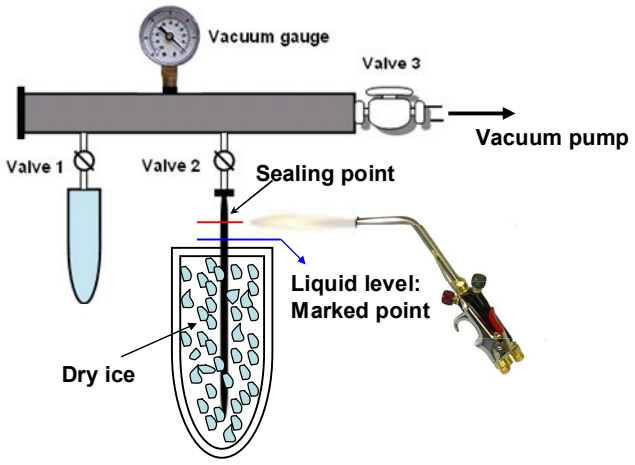

Figure 6.2 Experimental setup for sealing the capillary sample tube.

(3) Sealing process: The capillary sample tube should be sealed at a point about 1 cm above the the height of the liquid level at room temperature.

(a) Place an empty dewar below the sample tube, and adjust the height of the dewar such that the top of the dewar at or a little bit lower than the marked point (blue line in Figure 6.2);

(b) Fill the dewar with crushed dry ice. The liquid will freeze and shrink;

(c) Seal the tube at the sealing point (red line in Figure 6.2) with a torch and take the sealed tube away.

(4) When the sealed tube returns to the room temperature, the liquid level will return to the marked point (ie. its original height at room temperature). Warm the liquid slowly until it expands and occupies the whole tube.

Record the temperature T_{fill} at which the liquid just occupies the whole tube. Wait until the liquid goes back to room temperature, if it still occupies the whole tube, then the liquid is under tension and the sample is ready for further experiments.

The curved surface of the sample tube causes scattering and diffraction of laser beam and this presents challenges to performing OKE experiments. This problem is solved by placing the tube in a fluorescence cell (see Figure 6.3) filled with glycerin (refractive index: 1.473), which has similar refractive index as Pyrex glass (1.474). Our optical-heterodyne-detected[17,18] OKE spectrometer and data collection procedures have been described in detail elsewhere,[19,20] and OKE data for acetonitrile under tension have been collected at room temperature (297 K).

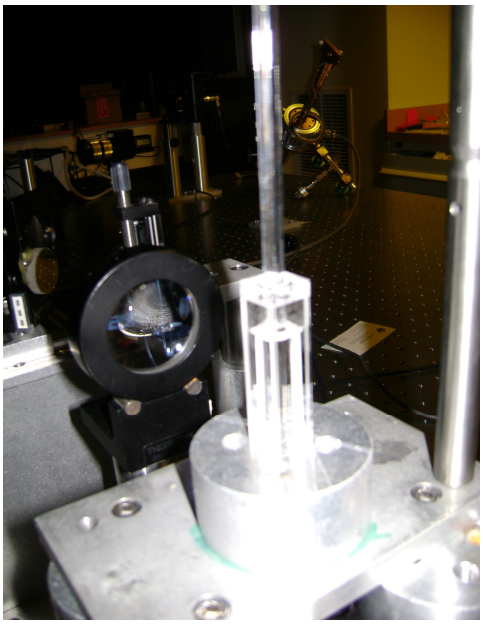

Figure 6.3 Design of the sample holder

6.3 Preliminary Results and Discussion

Benzene is the first liquid that was placed under tension. Benzene has a medium surface tension, a small contact angle on the glass, and a large thermal expansion coefficient (see Table 6.1). OKE data for benzene under ambient conditions are also available for comparison[21].

Table 6.1 Physical parameters of benzene and acetonitrile

Liquids	Surface tension σ / (mN/m), 298K	Contact angle on glass (degree, 295K))	Thermal expansion coefficient (α / 10^{-5} $K^{-1,}$ 293K)
Benzene	28.57[1]	12±5	121
Acetonitrile	28.16[2]	4±4	

1. Nath, S.: J. Coll. Interf. Sci. 209 (1999) 116.
2. Kinart, C.M., Kinart, W.J., Kolasinski, A., Cwiklinska, A.: Phys. Chem. Liq. 38 (2000) 583.

Samples of benzene under tension were created successfully. However, these samples only tended to remain stretched for a few (1-2) minutes. The sample tube was 27 cm long in total, and the benzene inside was 26 cm long under room temperature T_1 (293.8 K). The benzene inside expanded to just occupy the whole tube after being warmed to some well-defined filling temperature T_{fill} (which depends on the initial fluid/vapor ratio and the thermal expansivity of the liquid). Further heating of the benzene places the liquid under positive pressure and may lead to breakage of the tube; cooling benzene to some temperature lower than T_{fill}, for example room temperature T_1, should lead to a contraction to its original volume, but the surface adhesive forces between the liquid and the wall will hold the liquid under tension,

which accounts for the negative pressure.

At T_{fill}, equilibrium will be achieved between benzene and its vapor, so $P = P_v$. At T_1, the negative pressure can be calculated[22] from the thermal properties of benzene using the thermal pressure coefficient, Γ.

$$\Gamma = (\partial P / \partial T)_V = -(\partial V / \partial T)_P / (\partial V / \partial P)_T = \alpha / \kappa \qquad \text{(Eq. 6.1)}$$

here α is the isobaric expansivity, $\alpha = (\partial \ln V / \partial T)_P$ and κ is the isothermal compressibility, $\kappa = -(\partial \ln V / \partial P)_T$. Both α and κ are weakly dependent on P and T.

As an approximation, one can make the assumption that $\Gamma_{fill} \sim \alpha_{fill} / \kappa_{fill}$. Then the negative pressure which results from cooling the liquid from T_{fill} to T_1 (room temperature) can be calculated by[22]

$$\int dP \sim P - P_{fill} \sim \Delta P \sim \int \Gamma_{fill} dT \sim \Gamma_{fill} (T_1 - T_{fill}) \qquad \text{(Eq. 6.2)}$$

For benzene, $\alpha \sim 10^{-3}$ K^{-1}, $\kappa \sim 10^{-9}$ Pa^{-1}, T_1=293.8 K. If we know T_{fill}, we can estimate the negative pressure for benzene. A rough value for T_{fill} can be obtained from experiment. Usually after the sample was warmed by about 10 °C, the benzene liquid occupied the whole tube, so the tension achieved was on the order of 100 atm.

A more accurate determination of T_{fill} is also possible: The benzene liquid and vapor phase are always in equilibrium during the expansion process. Therefore on the phase diagram, the pressure and temperature should always follow the curve between the liquid and vapor phases. At T_1, we can determine the corresponding pressure and find out the density d_1 using NIST Chemistry Webbook. After the liquid just occupies the whole tube at T_{fill}, we can determine the density d_2 ($d_2 = d_1 * L_1 / L_2$, where L is the length of the column of liquid benzene). Based on d_2, we can ascertain T_{fill} and the corresponding pressure.

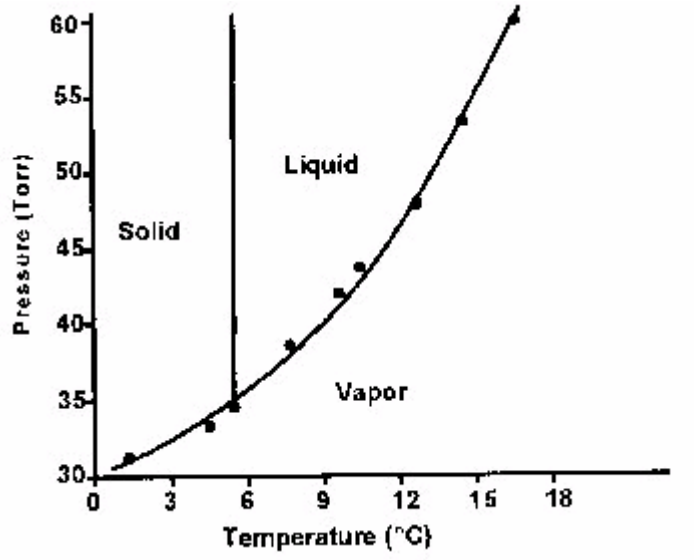

Figure 6.4 Phase diagram of bezene

In order to perform OKE experiments on a liquid sample under tension, we need to stop nucleation to hold the liquid under tension for longer time, which is a big challenge. Homogeneous nucleation occurs spontaneously, randomly and extremely rarely, and generally occurs with much more difficulty in the interior of a uniform substance. Heterogeneous nucleation occurs much more often than homogeneous nucleation and is the major challenge. The creation of a nucleus implies the formation of an interface at the boundaries of a new phase, and this process requires free energy. The balance between the free energy available from driving force and the energy consumed in creating new interface will decide whether the nucleation can happen. The free energy available is mainly released by the transformation process. In our case, liquid that was originally under tension returns to its normal condition after a bubble is generated due to nucleation. During this process free energy is gained for creating new volume, and the amount of the released free energy is proportional to

the volume. The free energy cost due to creation of a new interface is proportional to the surface area of the bubble and the interfacial energy, γ. If the nucleating bubble is treated as a sphere, the net change in free energy can be written as:

$$\Delta G = -4\pi/3\, r^3\, \Delta G_V + 4\pi r^2\, \gamma \qquad \text{(Eq. 6.3)}$$

where ΔG_V is free energy released for creating unit new volume, and r is the radius of the nucleating bubble. When the overall change in free energy, ΔG, is negative, nucleation is favored.

Heterogeneous nucleation occurs at preferential sites, such as phase boundaries or impurities (e.g. dust). It requires less energy than homogeneous nucleation. At such preferential sites, there is a pre-existing interface or the effective surface energy is lower, thus diminishing the free energy barrier and facilitating nucleation. Our study about nucleation first focuses on how to stop heterogeneous nucleation.

As Eq. 6.3 shows, if we want to stop the heterogeneous nucleation, we need to make ΔG positive or less negative. We anticipated this could be done by increasing the second term $4\pi r^2\gamma$. To test this hypothesis, we tried another liquid, acetonitrile. Acetonitrile has a smaller contact angle on the glass than benzene, which means there is a stronger interaction between acetonitrile molecules and glass surface. Acetonitrile therefore requires more free energy to create a new interface, making nucleation more difficult compared to benzene. This effect should allow acetonitrile to be maintained under tension for a longer time than benzene.

The experimental results are consistent with our prediction. For the acetonitrile sample we made, the total length of the sample tube was 27.7 cm, and the liquid length under room temperature (293.8 K) was about 27.5 cm. We measured how long

acetonitrile could be held under tension on three different days. The results are shown in Table 6.2:

Table 6.2 Time period (minutes) Acetonitrile can sustain tension at 293.8 K

	Time duaration (minutes)
Day 1	51, 35, 50, 42, 15
Day 2	67, 65
Day 3	45, 13, 73

In most cases, the acetonitrile can sustain tension for longer than 50 minutes. Only for a few experiments was the time period for sustaining tension less than 15 minutes. We pressume that nucleation may be due to thermal fluctuations in the environment, which provide extra energy for heterogeneous nucleation to occur. Nevertheless, 50 minutes is still not a long enough time period to perform an intermolecular dynamics study using the OKE method. However, it is enough time for us to measure the reorientational diffusion. Under normal conditions, the orientational correlation time for acetonitrile is about 1.67 ps at room temperature (297 K). The biexponential fitting result for acetonitrile under ambient condition is:

$$0.67\ \mathrm{Exp}(-t/\mathbf{1.67})+0.33\ \mathrm{Exp}(-t/0.42) \qquad \text{(Eq. 6.4)}$$

When acetonitrile is under tension, the reorientatinal diffusion becomes faster and the fitting result is:

$$0.70\ \mathrm{Exp}(-t/\mathbf{1.52})+0.30\ \mathrm{Exp}(-t/0.32) \qquad \text{(Eq. 6.5)}$$

This result can be explained reasonably. When a liquid is under tension, the

molecules are stretched and less crowded than in the liquid is in a normal state, so after the birefringence is induced, it should be easier and faster for molecules to return to the random orientation. Unfortunately, 50 minutes is still not long enough to study the intermolecular dynamics, which should give us more information.

More efforts can be made to avoid heterogeneous nucleation of a vapor bubble. Since heterogeneous nucleation occurs at preferential sites, such as phase boundaries or impurities like dust, we need to reduce concerntration of these sites in the sample: Some precautions, such as distillation and Millipore filtration, should be taken for the liquid to get rid of the hydrophobic impurities. Treatment of the sample tube with a solution of hydrofluoric acid before it is used[8] will drive away the gas in any hydrophobic crevices. Also, surface modification techniques can be employed to achieve even higher adhesion to the cell surfaces.[23] For instance, there is a strong attraction between benzene and hexafluorobenzene[24], so modification of the wall of our sample tube with trichloropentafluorophenylsilane may further decrease the contact angle of benzene on silica.

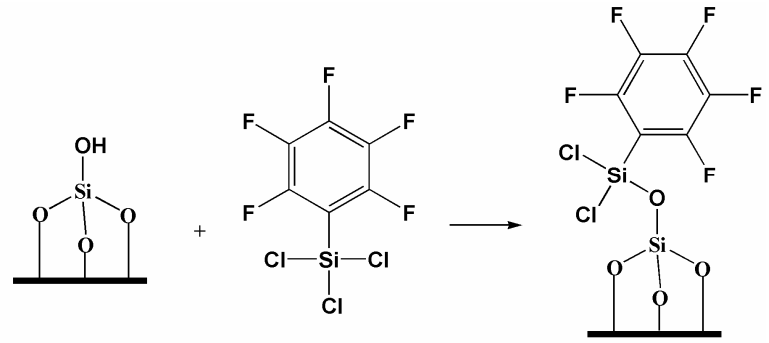

Another potential cause of heterogeneous nucleation is cosmic rays.[8] If heterogeneous nucleation presents difficulties, we can also test whether shielding with lead bricks helps to prevent this problem.

If any of these precautions permit a sample to be stretched for a suitable amount of time, we will perform an intermolecular dynamics study on this sample using OKE method. As mentioned in the introduction to this chapter, while a liquid is under tension, its density will be decreased and the attractive interactions will become more important. All these changes should be reflected in the reduced spectral density (RSD) (e.g., in the breadth and the shape of RSD), based on our former intermolecular dynamics studies of simple liquids.[25-27] This effect will help us to discover and distinguish different microscopic information behind the RSD. However, if all these precautions are still not enough to make a sample for an intermolecular dynamics study, then we may need to focus on how to reduce the homogeneous nucleation.

6.4 Conclusions

A method based on the Berthelot tube technique[4] was developed to make liquid samples under tension. Benzene and acetonitrile were successfully stretched with this method. The tensile strength of benzene achieved in our experiment was about 100 atm. Acetonitrile was found to be able to maintain a stretched state for much longer time than benzene. This made it possible to perform OKE experiments on acetonitrile. The orientational correlation time for acetonitrile at room temperature was shorter under tension than it was for unstretched samples, which is consistent with our predictions. However, the time interval under tension is still not long enough for an intermolecular dynamics study. In order to solve this problem, heterogeneous nucleation must be suppressed. Some ways to supress heterogeneous nucleation have

been suggested. Hopefully these possible solutions will make an intermolecular dynamics study for liquids under tension feasible in future.

6.5 References

(1) Andersen, H. C.; Weeks, J. D.; Chandler, D. *Phys. Rev. A* **1971**, 4, 1597.

(2) Weeks, J. D.; Chandler, D.; Andersen, H. C. *J. Chem. Phys.* **1971**, 54**,** 5237.

(3) Andersen, H. C.; Chandler, D.; Weeks, J. D. *Adv. Chem. Phys.* **1976,** 34, 105.

(4) Berthelot, M. *Ann. Chim. Phys.* **1850,** 30, 232.

(5) Abraham, F. F. **1974**, *Homogeneous nucleation theory* (Academic Press, NY)

(6) Rollett, A. D. **2002**, *Microstructure-properties: II Nucleation rate* (lecture notes)

(7) Trevana, D. H. *Contemp. Phys.* **1976,** 17, 109.

(8) Henderson, S. J.; Speedy, R. J. *J. Phys. E* **1980,** 13, 778.

(9) Green, L.; Durben, D. J.; Wokf, G. H.; Angell, C. A. *Science* **1990,** 249, 649.

(10) Zheng, Q.; Durben, D. J.; Wolf, G. H.; Angell, C. A. *Science* **1991,** 254, 829.

(11) Alvarenga, A. D.; Grimsditch, M.; Bodnar, R. J. *J. Chem. Phys.* **1993,** 98, 8392.

(12) Ruocco, G.; Sampoli, M.; Torcini, A.; Vallauri, R. *J. Chem. Phys.* **1993,** 99, 8095.

(13) Sciortino, F.; Essmann, U.; Stanley, H. E.; Hemmati, M.; Shao, J.; Wolf, G. H.; Angell, C. A. *Phys. Rev. E* **1995,** 52, 6481.

(14) Parker, M. E.; Heyes, D. M. *J. Chem. Phys.* **1998,** 108, 9039.

(15) Weast, R. C. "CRC Handbook of Chemistry and Physics" 66th edition (CRC Press, Boca Raton, **1985**).

(16) Donoghue, J. J.; Vollrath, R. E.; Gerjuoy E. *J. Chem. Phys.* **1951,** *19*, 55.

(17) McMorrow, D. *Opt. Commun.* **1991**, 86, 236.

(18) McMorrow, D.; Lotshaw, W. T. *J. Phys. Chem.* **1991**, 95, 10395.

(19) Farrer, R. A.; Loughnane, B. J.; Deschenes, L. A.; Fourkas, J. T. *J. Chem. Phys.* **1997**, 106, 6901.

(20) Loughnane, B. J.; Farrer, R. A.; Scodinu, A.; Reilly, T.; Fourkas, J. T. *J. Phys. Chem. B* **2000**, 104, 5421.

(21) Zhu, X.; Farrer, R. A.; Fourkas, J. T. *J. Phys. Chem. B* **2005,** 109, 12724.

(22) Imre, A.; Van Hook, W. A. *Chem. Soc. Rev.* **1998**, 27,117.

(23) Majors, R. E.; Hopper, M. J. *J. Chromat. Sci.* **1974,** 12, 767.

(24) Patrick, C. R.; Prosser, G. S. *Nature* **1960**, 187, 1021.

(25) Loughnane, B. J.; Scodinu, A.; Fourkas, J. T. *J. Phys. Chem. B* **2006**, 110, 5708.

(26) Zhong, Q.; Zhu, X.; Fourkas, J. T. *J. Phys. Chem. B* **2008**, 112, 3115.

(27) Zhong, Q.; Fourkas, J. T. *J. Phys. Chem. B* **2008**，112，15529.

Chapter 7: Antiresonant-Ring Kerr Spectroscopy

7.1 Introduction

Ultrafast optical Kerr effect (OKE) spectroscopy [1-4] has become a broadly-used tool for studying dynamics in bulk liquids [5-7], liquid mixtures [8-11], polymer solutions [12, 13], confined liquids [14, 15], and other fluid systems [13, 16, 17]. In this technique, a pump laser pulse passes through a transparent sample, inducing a change in refractive index that is measured with a time-delayed probe pulse. In its most common implementations, OKE spectroscopy is used to monitor the *xyxy* tensor element of the third-order response as a function the delay time between the pump and probe pulses. This so-called depolarized response is sensitive to effects that include collective molecular reorientation, scattering from depolarized Raman-active intramolecular vibrations, and librational and collective scattering from depolarized intermolecular modes. The depolarized response corresponds to the transient birefringence induced by the pump pulse.

In many instances it is of interest to measure tensor elements of the OKE response other than *xyxy*. The most important additional tensor element of the OKE response is *xxmm*, where *m* is the "magic" angle (54.7°). This tensor element is known as the isotropic response [18], and it arises from isotropic changes that the pump pulse induces in the refractive index. Any tensor element of the OKE response in an isotropic system can be described using a linear combination of the depolarized response and the isotropic response [18].

While the isotropic response is insensitive to reorientation, it is affected by

intramolecular and intermolecular modes with the appropriate symmetry. In some samples, such as proteins [19], the isotropic response from intramolecular modes is considerably more pronounced than the depolarized response. As a result, there is great interest in developing spectroscopic techniques that can cleanly separate the depolarized and isotropic OKE responses. A number of techniques for measuring the isotropic response have been reported previously, based on effects such as lensing [20] or spatial shifting of the probe pulse [21, 22].

Here we present a new strategy for determining different OKE tensor elements. The inspiration for this approach comes from the work of Trebino and Hayden on antiresonant ring transient electronic spectroscopy [23]. In their setup, a Sagnac interferometer was used to create counterpropagating probe pulses for pump/probe spectroscopy. The sample was positioned away from the center of the ring, such that the probe pulse that propagated in the opposite direction from the pump pulse arrived at the sample considerably earlier than the pump pulse, whereas the other probe pulse arrived in proximity to or after the pump pulse. All of the light that enters such an interferometer exits in the same direction unless the probe pulses experience different absorption. This difference in absorption is the signal of interest in an electronic pump/probe experiment. Since the probe beams travel exactly the same path the interferometer is highly stable, and each beam experiences identical distortions due to any imperfect optics. Any deviation of the input beam splitter from perfect 50% reflectivity serves to create a local oscillator for the signal electric field [23].

Here we present an antiresonant ring scheme for measuring phase changes rather than absorption. We call our technique antiresonant-ring Kerr spectroscopy (ARKS).

Our setup employs a double Sagnac interferometer, such that both probe beams propagate through the sample in the same direction. As a result, ARKS can be used to measure different tensor elements of the OKE response, and can even be used to combine responses at two different delay times in order to enhance or suppress particular contributions to the OKE decay.

7.2 Experimental Section

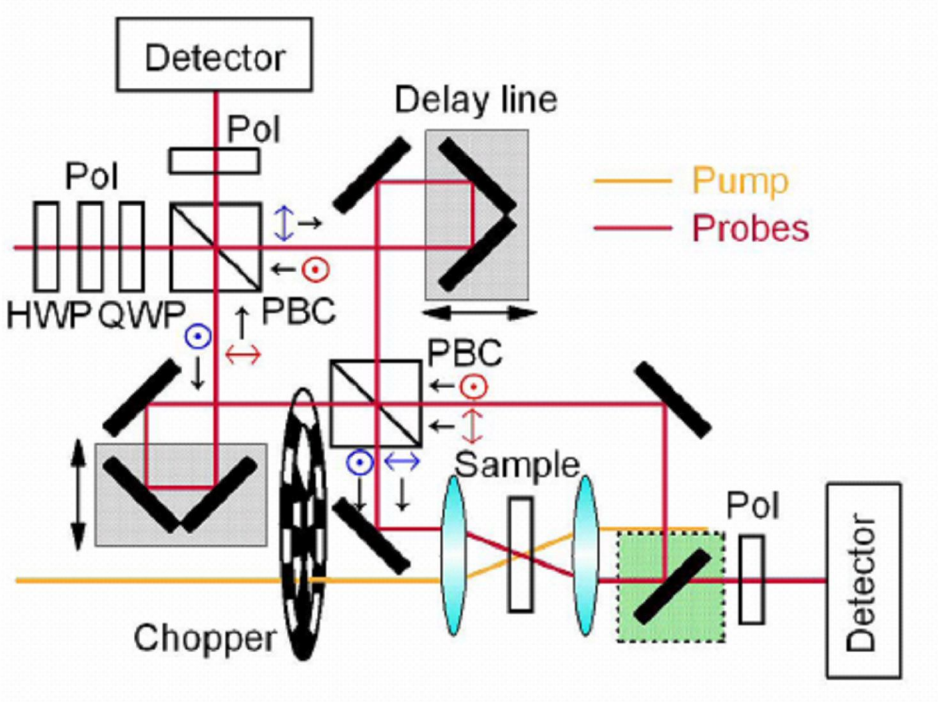

Figure 7.1 Experimental setup for ARKS. HWP = half-wave plate, Pol = polarizer, QWP = quarter-wave plate, PBC = polarizing beam cube, ⊙ = vertical polarization, ↔ = horizontal polarization. Blue denotes polarizations before the sample and red polarizations after the sample. The mirror in the green block can be removed to measure the depolarized OKE response.

A diagram of our experimental setup is shown in Figure 7.1. A KMLabs Ti:sapphire laser generates 50 fs pulses with a center wavelength near 800 nm. After a prism dispersion compensator and spatial filtering, the laser output is split into a strong pump beam and a weak probe beam. The pump beam traverses a computer-controlled optical delay line. The probe beam passes through a half-wave plate, a polarizer set at 45°, and then a quarter-wave plate (QWP) before entering the dual-ring interferometer via a polarizing beam cube (PBC). Orthogonal polarizations travel down each leg of the interferometer. The lengths of the two legs can be changed to adjust the timing of the probe pulses, and are generally set so that one probe pulse arrives at the sample several picoseconds or more before the other. The two probe beams are recombined in a second PBC, after which they are focused into the sample at the same spot as the pump beam. The probe beams are recollimated after the sample.

For collecting the depolarized OKE signal, the input optics for the interferometer are set such that there is a single, horizontally-polarized probe beam. The pump polarization is set to 45°. An analyzer polarizer is placed immediately after the recollimating lens and is set to pass light that is vertically polarized. The input polarizer and QWP are then adjusted to implement a local oscillator for optical heterodyne detection (OHD) of the OKE signal [6,24]. To measure other tensor elements of the OKE response, one axis of the QWP is set such that the polarization state of the input light is unaffected. After the sample the recollimated probe beams are fed back into the second PBC such that they are collinear with the incoming probe beams (see Figure 7.1). The horizontally- and vertically-polarized components of the probe beam

once again travel separate paths and are recombined at the original PBC. The two different polarization components ultimately travel along the exact same path, albeit in different directions, regardless of the delay between the probe pulses at the sample. Because the beams travel along identical paths, the dual-ring interferometer is relatively insensitive to vibration, as no significant motion of optics can occur during a single round trip of the interferometer. However, the laser must have good pointing stability so that the optical path through the interferometer is similar from pulse to pulse.

In the limit of weak probe beams, the output polarization of the dual-ring interferometer in the absence of a pump pulse should be identical to the input polarization (barring a 180° flip of the horizontal component of the polarization for each reflection). An analyzer polarizer is therefore placed after the output face of the first PBC and adjusted to pass light with a polarization that is orthogonal to the input polarization. In the presence of the pump beam, the two probe beams can experience different phase shifts in the sample, due to their different arrival times and different polarizations. Any differential phase shift introduces a polarization component that is orthogonal to the input polarization, and therefore leaks through the analyzer polarizer.

To optimize the signal-to-noise ratio of the data, we use a scheme that is similar to one we have reported previously [14]. The pump and probe beams are chopped at different frequencies with different rings of the same chopper wheel (Figure 7.1). A small portion of the chopped probe beam is picked off to form a reference beam (not shown in Figure 7.1) and is sent to a separate detector. The output of the reference

detector is subtracted from that of the signal detector using an analog preamplifier. The output of the preamplifier is sent to a lock-in amplifier that is referenced to the sum of the chopping frequencies. Care is taken to match the shape of the chopped signal and reference waveforms as well as possible.

The extinction ratio of polarizing beam cubes is not as high as that of other polarizing optics. Typical cubes we have employed have an extinction ratio for horizontal: vertical polarization on the order of 200 in the transmitted direction; in the reflected direction the extinction ratio for vertical:horizontal polarization is considerably lower. As a result, leakage of vertically-polarized light can be ignored, but there are significant reflections of the horizontal polarization component that propagate through the interferometer in undesired directions. It is important to understand the effects of these reflections in evaluating the performance of the spectrometer.

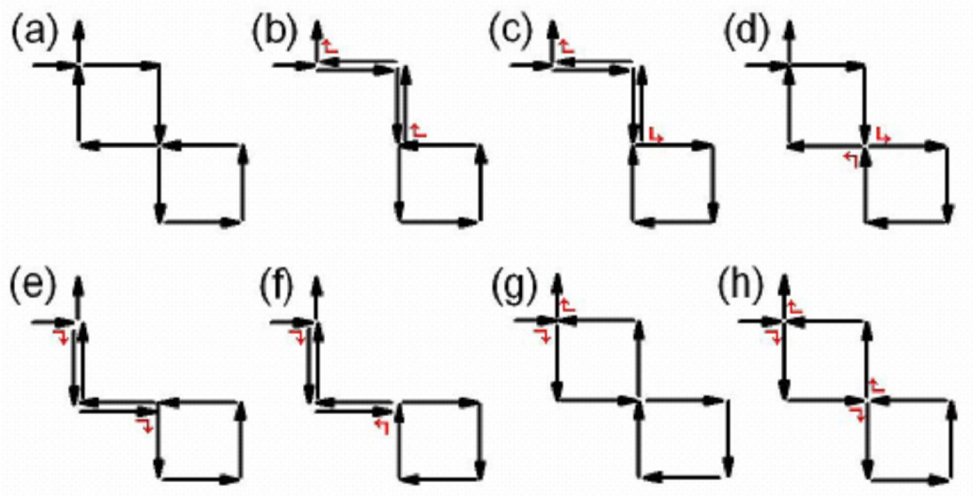

Figure 7.2 Pathways through which horizontally-polarized light that enters the ARKS apparatus can exit in the direction in which the signal is detected. Reflections of the predominantly transmitted horizontal polarization are indicated with red arrows.

In Figure 7.2 we consider all pathways that will allow horizontally-polarized light that enters the interferometer to exit in the direction in which the signal is detected. The desired path is labeled (a) in Figure 7.2. The influence of the other pathways is minimized by a number of factors. First, there must be an even number of reflections for the beam to exit the dual-ring interferometer in the same direction as the signal, which limits the number of potential interfering pathways to seven, paths (b) through (h). Second, many of the paths involve reflections also change the path length of the probe beam such that it arrives at the detector at a significantly different time from the signal; this is the case for paths (b), (c), (e) and (h). These non-time-coincident reflections can reduce the dynamic range of the detection to some extent, but they do not interfere with the signal optically. Paths (d) and (g) do not contribute significantly to the signal because the probe pulse passes through the sample in the wrong direction. Path (h) passes through the sample in the proper direction, but involves four reflections and so is very weak.

Based on the above reasoning, we do not expect imperfect extinction of the PBCs to interfere with the desired signal. However, we must also consider a second effect of such leakage, namely that it can act as a local oscillator. The PBCs are composed of dielectric materials, and the leakage of horizontally-polarized light due to its reflection from the diagonal interfaces in these optics leads to a phase shift. The laser wavelength is far from any absorption in the PBS material, and so the phase of this reflection is not expected to have any significant dependence on wavelength over the bandwidth of the laser pulses. We have found that this phase shift is consistent for a

given PBC, but varies among PBCs. The phase of the local oscillator therefore cannot be controlled, but the quadrature component of the nonresonant OKE signal is so much greater than the in-phase component that only the quadrature componenent of the local oscillator acts to amplify the signal. Introducing a variable wave plate in place of the input quarter-wave plate to control the phase of the local oscillator did not change the shape of OKE decays, and led only to a modest increase in signal intensity.

7.3 Results and Discussion

To measure the depolarized OKE response we use the procedure described above. To measure OKE response functions of the form *xxkk*, where *k* refers to any direction in the *xy* plane, the dual-ring interferometer is employed. One probe beam (generally the one that is reflected from the first PBC, whose polarization we will call *y*) is set to arrive at the sample before the other (whose polarization we will call *x*). The time between the probe beams is set to be greater than the longest delay of interest. The pump beam, which is polarized in the *k* direction, is scanned from times slightly after the later probe beam out to the greatest delay desired, and data are collected as a function of delay time. In this scheme, the pump pulse does not affect the earlier probe pulse, and so only the later probe pulse experiences a phase change due to the pump. The *xxkk* tensor element of the OKE response is therefore probed. So different tensor elements can be measured by simply changing the polarization and timing of all three pulses. In Table 7.1, we list some examples of the tensor elements that can be measured by the spectrometer.

Table 7.1 Expected performance of ARKS

Pump polarization	probe 1		probe 2		Tensor elements
	polarization	timing	polarization	timing	
x	y	Before pump	x	After pump	$\mathbf{R_{xxxx}(\tau)}$
m	y	Before pump	x	After pump	$\mathbf{R_{xxmm}(\tau)}$
y	y	Before pump	x	After pump	$\mathbf{R_{xxyy}(\tau)}$
x	y	Same time	x	Same time	$\mathbf{R_{xyxy}(\tau)}$
x	y	τ_2 after	x	τ_1 after	$\mathbf{R_{xxxx}(\tau_1)- R_{yyxx}(\tau_2)}$

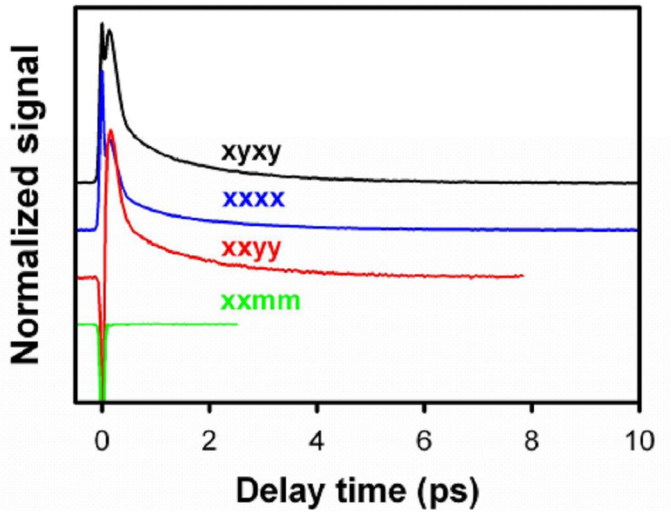

Figure 7.3 Normalized ARKS data for CS_2 under difference polarization conditions. The data have been offset vertically for clarity.

Shown in Figure 7.3 are typical data for carbon disulfide (CS_2) at room temperature. The intensities of the decays have been normalized. The depolarized response is in

good agreement with previous OHD-OKE data for this liquid [5,25]. The *xxxx* (polarized) and *xxyy* responses are similar to the depolarized response, although the magnitude (and sign) of the electronic signal near zero time changes with respect to that of the nuclear signal at positive delay times for the different tensor elements. The fact that the electronic response is negative for some tensor elements of the response is expected, and indicates that the signal is indeed heterodyned. The isotropic response is quite small, in agreement with previous results [20,26]. The dominance of the depolarized response in this liquid accounts for the strong similarities among the *xyxy*, *xxxx* and *xxyy* tensor elements. The lack of any component of the isotropic response that decays with the time scale of collective reorientation indicates that we can discriminate strongly against any contamination from the depolarized response.

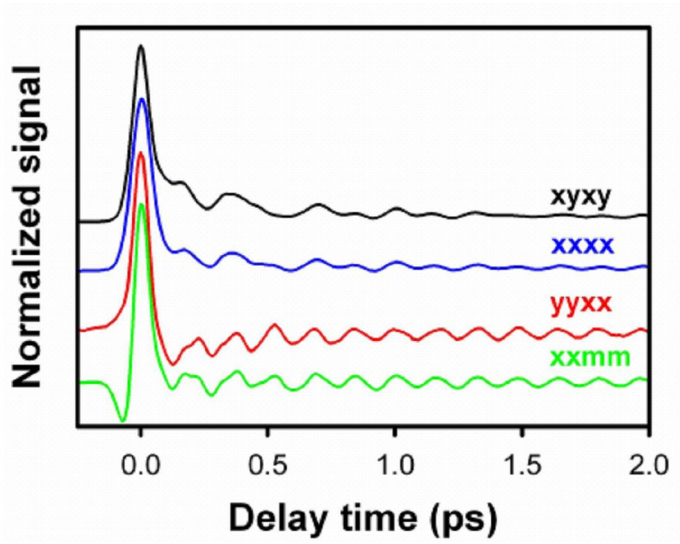

Figure 7.4 Normalized ARKS data for S_2Cl_2 under difference polarization conditions. The data have been offset vertically for clarity.

To further assess the quality of the isotropic response measured with ARKS, in Figure 7.4 we present data for sulfur monochloride (S_2Cl_2). Once again the decays

have been normalized to the same maximum intensity. For this liquid, the contribution of Raman-active intramolecular vibrational modes to the OKE response is considerably stronger than that of collective orientational relaxation or intermolecular modes. The depolarized response exhibits oscillations due to a number of different vibrational modes [27-29]. The polarized response is similar to the depolarized response. The *yyxx* and isotropic responses are also similar to one another, but in contrast to the other two responses are dominated largely by the contribution of a single vibrational mode that is highly polarized. The fact that the isotropic decay oscillates around the baseline of the scan is additional evidence that the signal is heterodyned.

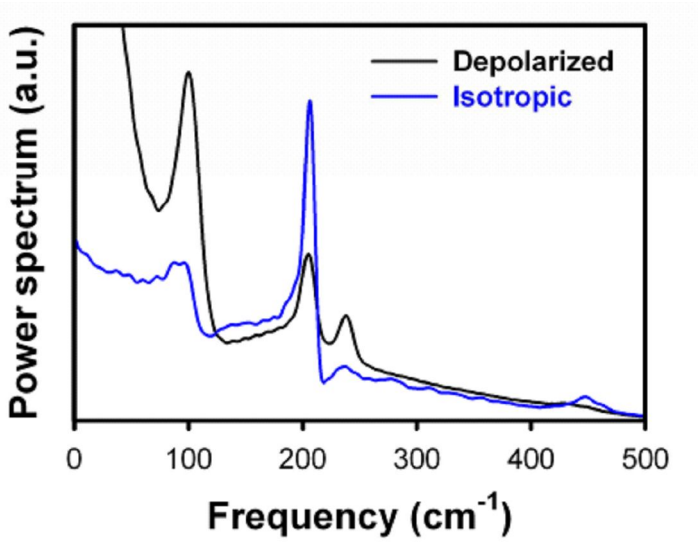

Figure 7.5 Depolarized and isotropic OKE power spectra for S_2Cl_2. The two spectra are not to scale.

To examine the spectral content the OKE decays for S_2Cl_2, we computed the power spectra corresponding to the depolarized and isotropic response functions. These power spectra, which are shown in Figure 7.5, confirm the presence of a number of

vibrational modes. The peaks at 102 cm^{-1}, 205 cm^{-1}, and 446 cm^{-1} are assigned to the ν_4 (torsion), ν_3 (S-S-Cl symmetric angle deformation) and ν_2 (S-Cl symmetric stretch) modes, respectively, all of which have *A* symmetry in the C_2 point group of this molecule [29]. These modes are all polarized and, as is clear from Fig. 5, ν_2 and ν_3 are strongly so. The peaks at 238 cm^{-1} and 434 cm^{-1} belong to the ν_6 (S-S-Cl asymmetric angle deformation) and ν_5 (S-Cl asymmetric stretch) modes, which have *B* symmetry and therefore should be completely depolarized [29]. The power spectra in Figure 7.5 confirm the depolarized nature of these vibrations. It is important to note that peaks do not appear in the power spectrum at the second harmonic of the fundamental frequencies, indicating again that our signal is proportional to the response rather than to its magnitude squared.

While the data in Figure 7.5 are power spectra, we should also note that it is possible to perform Fourier-transform deconvolution on ARKS data to obtain the Bose-Einstein-corrected, low-frequency spectral density [6,24]. To do so, however, requires that the pump and probe pulses be transform-limited at the sample. Due to the dispersion introduced by the PBCs, attaining transorm-limited pulses requires separate dispersion compensation of the pump and probe beams. While compensation of each beam is readily possible, we have not attempted it here.

We have previously demonstrated that by having two pump pulses of controllable polarization and intensity, it is possible to perform optical addition of two depolarized OKE response functions with a time shift between them [27,30]. This strategy can be employed for enhancing or suppressing particular contributions to the depolarized response, which may be useful, for instance, in OKE microscopy. In the technique

presented here, we instead have used two probe pulses. While for all of the measurements discussed above one probe pulse always arrives before the pump pulse, it is also possible to have both probe pulses arrive after the pump. In this manner, we can perform optical subtraction of two *different* tensor elements of the OKE response function with a time shift between them.

ARKS data for S_2Cl_2 illustrating the implementation of optical subtraction are shown in Figure 7.6. For reference we show the *xxxx* and *yyxx* response functions obtained with one probe pulse arriving significantly before the pump pulse. In the lower two traces both probe pulses arrive after the pump pulse. By adjusting the relative timing of the two probe pulses, we can either enhance the response from the ν_2 vibration (red trace) or suppress it virtually completely (green trace). By combining this technique with the previously demonstrated use of pump pulse pairs [27, 30], it will be possible to control the contribution of vibrational modes of any symmetry to the OKE signal.

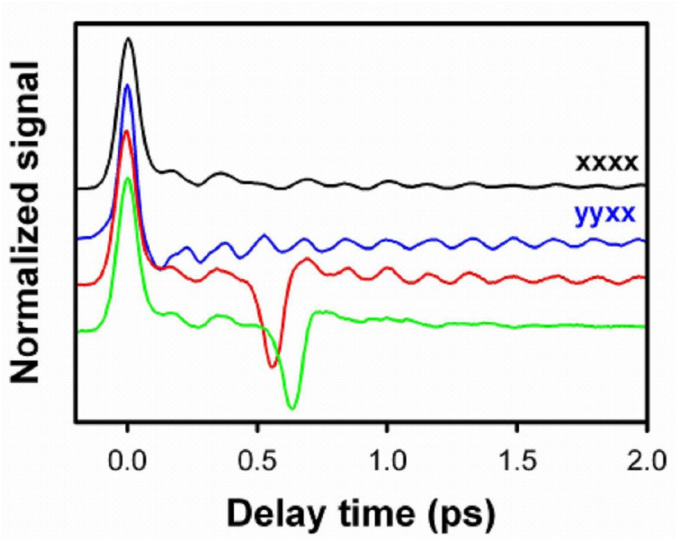

Figure 7.6 Normalized S2Cl2 ARKS data for the *xxxx* and *yyxx* tensor elements, as well as scans in which these tesnor elements are optically subtracted with different

time shifts to enhance or suppress the contribution of the ν_3 mode.

7.4 Conclusions and Future Work

We have presented a new technique for obtaining different tensor elements of the OKE response function. Employing a dual-ring Sagnac interferometer makes possible the optical subtraction of the response functions from two different probe beams. ARKS is a versatile method of collecting OKE data, and also makes possible the enhancement or suppression of different contributions to the response when both probe pulses arrive after the pump pulse.

We will work on implementing ARKS in an OKE microscope in future. We have developed mode-selective OKE spectroscopy[27,30], in which two-pump geometry is used: By controlling the timing and polarizations of the two pumps, particular mode of liquid molecules can be selectively excited. The combination of ARKS and techniques for mode-selective excitation will provide us with the ability to perform OKE microscopy with high contrast.

The first step in conversion from spectroscopy to microscopy will be to incorporate microscope objectives rather than lenses into the ARKS setup. For applications in microscopy we will need to design an objective mounting system that will allow us to control the distance between objectives readily for dealing with samples of different thickness or index of refraction. Long working distance, polarization-preserving objectives will be employed, although we will need to perform some characterization experiments to determine the experimental geometry that minimizes any depolarization. Once we have a handle on these issues from experiments in bulk

liquids, we will incorporate a sample-scanning nanostage into the setup so that we can perform imaging experiments. For samples to characterize the resolution of the microscope, we will attach polymer nanobeads to microscope cover slips and make sealed cells that can hold solvent. We will then perform a series of experiments to determine the resolution and signal to noise in different contrast modes. When our microscope has been fully characterized, we will explore our ability to generate contrast for different types of biological samples. In terms of intramolecular vibrations, we expect OKE microscopy to be complementary to CARS microscopy, which tends to be used to observe modes with frequencies of 1000 cm^{-1} and greater. We will perform experiments to determine which types of modes can most readily be interrogated in different types of biological materials, including proteins, nucleic acids, polysaccharides, and lipids.

*7.5 **References***

(1) Righini R. *Science* **1993,** 262, 1386.

(2) Fourkas, J. T. "Nonresonant Intermolecular Spectroscopy of Liquids," in *Ultrafast Infrared and Raman Spectroscopy*, M. D. Fayer, ed. (Marcel Dekker, New York, **2001**), pp. 473-512.

(3) Smith, N. A.; Meech, S. R. *Int. Rev. Phys. Chem.* **2002,** 21, 75.

(4) Kinoshita, S.; Kai, Y.; Ariyoshi T.; Shimada, Y. Int. *J. Mod. Phys. B* **1996,** 10, 1229.

(5) Loughnane, B. J.; Scodinu, A.; Farrer, R. A.; Fourkas, J. T.; Mohanty U. *J. Chem. Phys.* **1999,** 111, 2686.

(6) McMorrow, D.; Lotshaw, W. T. *J. Phys. Chem.* **1991**, 95, 10395.

(7) Castner, Jr. E. W.; Maroncelli, M. *J. Mol. Liq.* **1998**, 77, 1.

(8) Kalpouzos, C.; McMorrow, D.; Lotshaw, W. T.; Kenney-Wallace, G. A., *Chem. Phys. Lett.* **1988**, 150, 138.

(9) Steffen, T.; Meinders, N. A. C. M.; Duppen, K. *J. Phys. Chem. A* **1998,** 102, 4213.

(10) Scodinu, A.; Fourkas, J. T. *J. Phys. Chem. B* **2003,** 107, 44.

(11) Neelakandan, M.; Pant, D.; Quitevis, E. L. *Chem. Phys. Lett.* **1997,** 265, 283.

(12) Shirota, H.; Castner, Jr. E. W. *J. Am. Chem. Soc.* **2001,** 123, 12877.

(13) Hunt, N. T.; Jaye, A. A.; Hellman, A.; Meech, S. R., *J. Phys. Chem. B* **2004,** 108, 100.

(14) Loughnane, B. J.; Farrer, R. A.; Scodinu, A.; Reilly, T.; Fourkas, J. T. *J. Phys. Chem. B* **2000,** 104, 5421.

(15) Farrer, R. A.; Fourkas, J T. *Acc. Chem. Res.* **2003,** 36, 605.

(16) Hunt, N. T.; Jaye, A. A.; Meech, S. R. *J. Phys. Chem. B* **2003,** 107, 3405.

(17) Hunt, N. T.; Meech, S. R. *J. Chem. Phys.* **2004,** 120, 10828.

(18) Murry; R. L.; Fourkas, J. T. *J. Chem. Phys.* **1997,** 107, 9726.

(19) Eaves, J. D.; Fecko, C. J.; Stevens, A. L.; Peng, P.; Tokmakoff, A. *Chem. Phys. Lett.* **2003,** 376, 20.

(20) Fecko, C. J.; Eaves, J. D.; Tokmakoff, A. *J. Chem. Phys.* **2002,** 117, 1139.

(21) Chang, Y. J.; Cong, P.; Simon, J. D. *J. Chem. Phys.* **1997,** 106, 8639.

(22) Cong, P.; Chang, Y. J.; Simon, J. D. *J. Phys. Chem.* **1996,** 100, 8613.

(23) Trebino, R.; Hayden, C. C. *Opt. Lett.* **1991,** 16, 493.

(24) McMorrow, D. *Opt. Commun.* **1991,** 86, 236.

(25) Farrer, R. A.; Loughnane, B. J.; Deschenes, L. A.; Fourkas, J. T. *J. Chem. Phys.* **1997,** 106, 6901.

(26) Murry, R. L.; Fourkas, J. T.; Keyes, T. *J. Chem. Phys.* **1998,** 109, 2814.

(27) Zhu, X.; Farrer, R. A.; Gershgoren,E.; Kapteyn, H. C.; Fourkas, J. T. *J. Phys. Chem. B* **2004,** 108, 3384.

(28) Frankiss, S. G. *J. Mol. Struct.* **1968,** 2, 271.

(29) Bradley, E. B.; Mathur, M. S.; Frenzel, C. A. *J. Chem. Phys.* **1967,** 47, 4325.

(30) Zhu, X.; Farrer, R. A.; Fourkas, J. T. *J. Phys. Chem. B* **2005,** 109, 8481.

Chapter 8: Conclusion and Future Prospect

8.1 Conclusions and Future Prospects

As the above studies illustrate, OKE spectroscopy has developed into a powerful method for probing microscopic dynamics in simple liquids[1]. It has become a well-established, sensitive tool for studying orientational diffusion in transparent liquids. The temperature-dependent orientational dynamics of 1, *n*-dicyano *n*-alkane liquids ranging from dicyanomethane to 1,8-dicyanooctane have been studied[2], and the results suggest that a *gauche-gauche* conformation is adopted by the molecules in the liquids phase and a possible underlying, temperature-dependent, collective structural rearrangements within the liquids may exist .

We are also trying to gain a solid understanding of the information available from RSDs. Based on the results of former OKE experiments on benzene and its derivatives[3], we have proposed a model that connects the shape of the OKE reduced spectral density to local structure in liquids. The general validity of this model has been tested by performing OKE experiments on more aromatic liquids[4]. Our conclusion from these studies is that molecular shape plays a major role in determining the shape of the OKE RSD, although moment of inertia may play a role in determining its breadth. Some other factors, such as the distribution of the polarizability in a molecule, may play an additional role in determining whether the RSD will be "rectangular", "triangular", or somewhere in between. Nevertheless, it appears likely that it is molecular properties rather than local structural properties that tend to influence the shape of the RSD in simple, non-networked liquids.

OKE spectroscopy has also proven to be a powerful means of studying the influence of different media on liquid dynamics. One of our interests is how nanoconfiement affects the microscopic properties of liquids. We have used OKE spectroscopy to study a sizable number of liquids in nanoconfinement, and the reorientational dynamics are greatly changed[5]. We expect some effects should be observed for intermolecular dynamics, and a good comparison between the intermolecular portion of OKE spectrum in confinement and in bulk will be quite suggestive. Another interest is in liquids under tension, in which the attractive forces are dominant between molecules instead of repulsive forces, so the intermolecular dynamics should be affected. We have developed a method to make liquid samples under tension based on a Berthelot tube technique[6], reorientational diffusion data have been collected for acetonitrile under tension. We need to improve this method to maintain the liquid under tension for longer times so that we can perform intermolecular dynamics studies with OKE spectroscopy, which should provide interesting results. Besides these, additional experiment such as pressure-dependent studies would be also quite helpful for learning the microscopic properties of liquids in complex environments.

The second-generation ARKS spectrometer that we have built[7] not only offers advantages for obtaining different tensor elements of the optical Kerr response of liquids, but will also be a major element of the proposed OKE microscope. In combination with the multiple-pulse excitation schemes, this instrument should be capable of imaging with a high signal to noise ratio in a number of different contrast modes. The beam-shaping technique will further enhance the resolution of this

instrument.

We foresee one of the most exciting applications of OKE spectroscopy in the coming years to be its use in higher-order nonlinear-optical techniques. For instance, there has been great interest in a fifth-order version of OKE spectroscopy first proposed by Tanimura and Mukamel.[8] This technique employs five laser pulses and two time delays, and has the potential to rephrase intermolecular modes in order to reveal information about the degree of inhomogeneous broadening in these modes. Implementing this technique in a manner that does not produce experimental artifacts proved difficult but was eventually accomplished.[9] However, the signal in this spectroscopy is generally quite weak, and it has only been possible to obtain high-quality data for highly polarizable molecules such as CS_2. Further experimental advances may broaden the applicability of this type of spectroscopy.

Another approach to the use of the optical Kerr effect in higher-order spectroscopies is to combine this technique with other optical processes. As an example, techniques called RaPTORS (resonant pump third-order Raman spectroscopy) developed by Blank and co-workers[10] and PORS (polarizability response spectroscopy) developed by Scherer and co-workers[11] use the optical Kerr effect to probe the response of a solvent to the electronic excitation of a solute. RaPTORS and PORS are revealing new details of the solvent response to a localized change in charge distribution. These techniques demonstrate the power of using the optical Kerr effect in one or more steps of a more complex, nonlinear-optical pulse sequence, and we look forward to the development of other methods based on this general approach to be developed in the near future.

8.2 References

(1) Zhong, Q., Fourkas, J. T. *J. Phys. Chem. B* **2008,** 112, 15529.

(2) Zhong, Q., Zhu, X., Fourkas, J. T. *J. Phys. Chem. B* **2008,** 112, 3115.

(3) Loughnane, B. J.; Scodinu, A.; Fourkas, J. T. *J. Phys. Chem. B* **2006**, 110, 5708.

(4) Zhong, Q., Fourkas, J. T. *J. Phys. Chem. B* **2008**, 112, 15342.

(5) Zhu X., Farrer, R. A., Fourkas, J. T. *J. Phys. Chem. B*, **2005**, 109, 12724.

(6) Berthelot M., *Ann. Chim. Phys.* **1850,** 30, 232.

(7) Zhong, Q., Zhu, X., Fourkas, J. T. *Opt. Expr.* **2007**, 15, 6561

(8) Tanimura, Y.; Mukamel, S. *J. Chem. Phys.* **1993**, 99, 9496.

(9) Kaufman, L. J.; Heo, J. Y.; Ziegler, L. D.; Fleming, G. R. *Phys. Rev. Lett.* **2002**, 88, 207402.

(10) Schmidtke, S. J.; Underwood, D. F.; Blank, D. A. *J. Phys. Chem. A* **2005**, 109, 7033.

(11) Moran, A. M.; Nome, R. A.; Scherer, N. F. *J. Chem. Phys.* **2007**, 127, 184505.

Appendices

Appendix A: OKE Data Analysis Procedure Using LabView Program

A) *Process the Raw data*

For each sample at each temperature, we have three sets of data:

1) Long step-size data for reorientational diffusion analysis: The step size is 50, 100, or 150, we usually collect 10-20 of them, sum them together then get the average, save the average data as a txt file named as "long.txt";

2) Short step-size data for intermolecular dynamics study: The step size is 1, and we usually collect 2 or 4 of them, sum them together, get the average, and then save as "short.txt";

3) Autocorrelation data for Fourier transform: The step size is 1, usually we need to collect autocorrelation data twice, once before and once after we collect short step-size data, sum the two data, get the average and save as "auto.txt".

All the three data files are one-column txt file.

B) *Input files*

1) "Run"
2) Input "long", "short", and "autocorrelation" data for desired data sets.
3) Choose appropriate time steps (used in experiment) for long and short time-step data. (For example, if the step-size for the "long" data is 50, you should input 5 on the corresponding box.)
4) "Start".

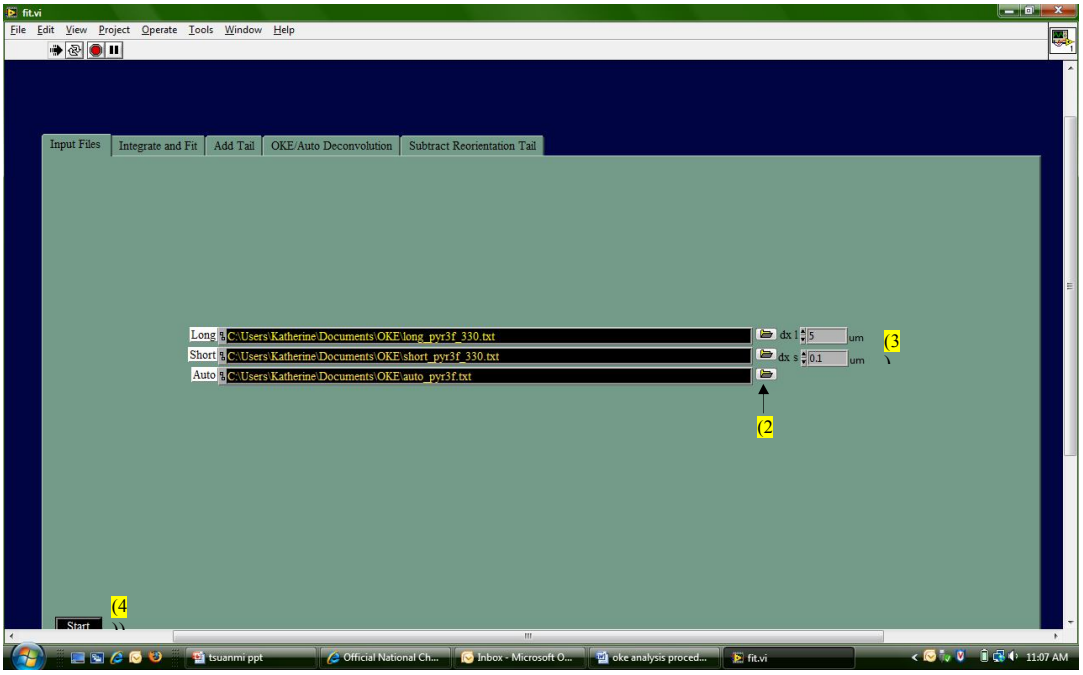

C) *Integrate and Fit*

1) Set "weight" = 1/y
2) Input you initial guess for the tri-exponential decay; if you plan to use bi-exponential decay to fit data, "amp 3" should be set at 0.

   (In most cases, we use bi-exponential decay to fit data, so for the following procedures, bi-exponential decay is the default case.)
3) Adjust cursors to choose the section of the graph that best corresponds to reorientational diffusion (usually $1.5\tau_1$ ps to > $4\tau_2$ ps, where $\tau_1<\tau_2$)
   a. Note: there is often a "Fitting Error" – choose larger range on the graph and double click the red box to correct.
4) View as "log" graph.
5) Adjust cursors until the fit line matches the data line (there should be no deviations and the data should look smooth).

a. The time constants should be stable even when varying the cursors slightly.

6) "next"

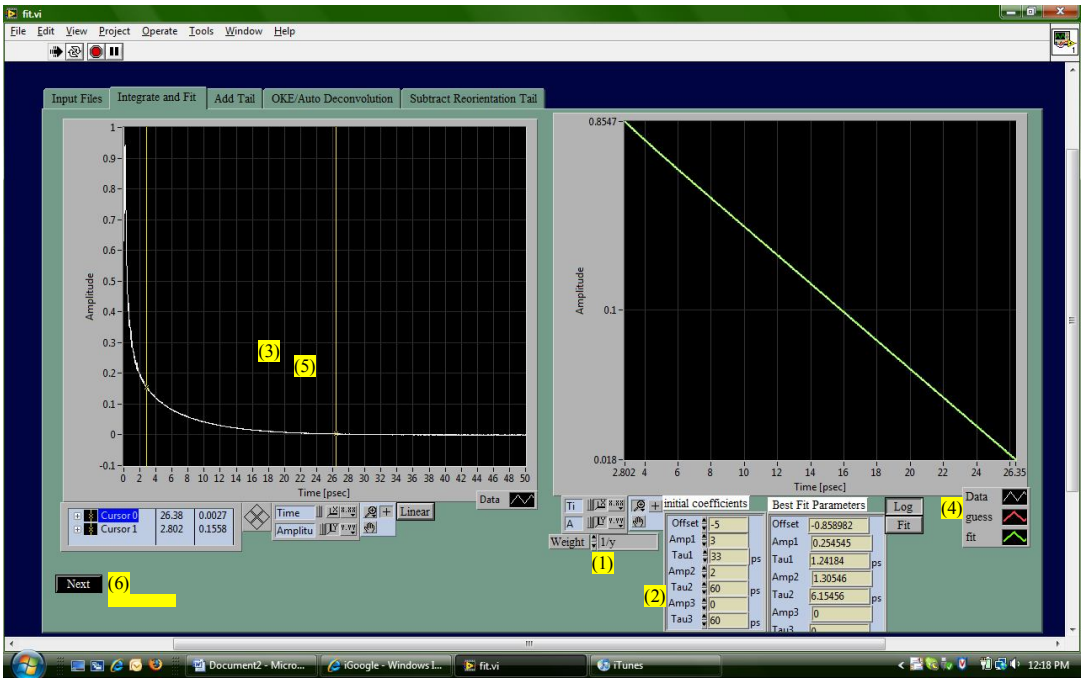

D) *AddTail*

1) Zoom out to look at entire graph (use x-axis and y-axis buttons next to "time" and "amplitude");

2) Move cursor to trailing edge of data graph (white) and zoom in horizontally

3) Adjust "gain" until the red fit line matches up with the data (may need to continue zooming in)

Note: if gain is too high, can try to decrease range size in Step 2

4) "join files"

[This step of the procedure adjusts the biexponential decay function more precisely to match the short step-size data.]

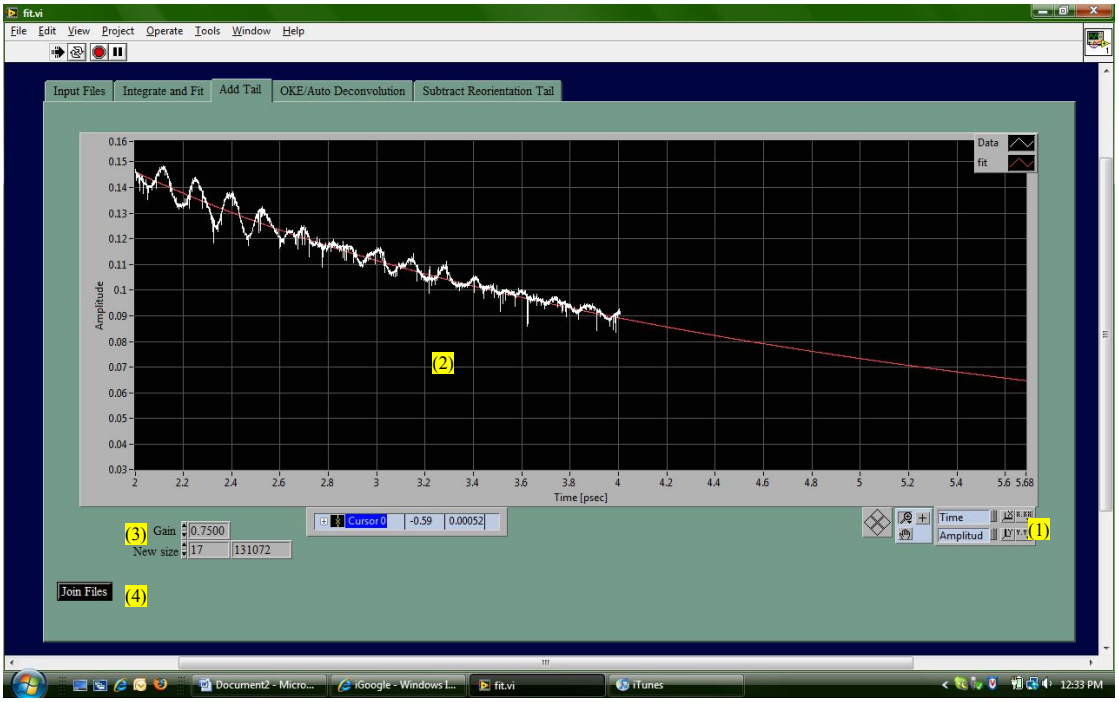

E) *Fourier Transform (Time-domain data to frequency-domain spectrum)*

1) Adjust OKE zero value on bottom left graph until the right end of the broad low frequency spectrum goes smoothly to zero. Place the cursor somewhere between the low frequency spectrum and the Raman-active vibrational peaks; this will remove the contributions to OKE signal from low-frequency Raman-active modes. [This graph shows the frequency-domain Fourier transform of the signal]
2) Adjust auto zero until the bottom right graph has smallest amplitude
3) "Done"

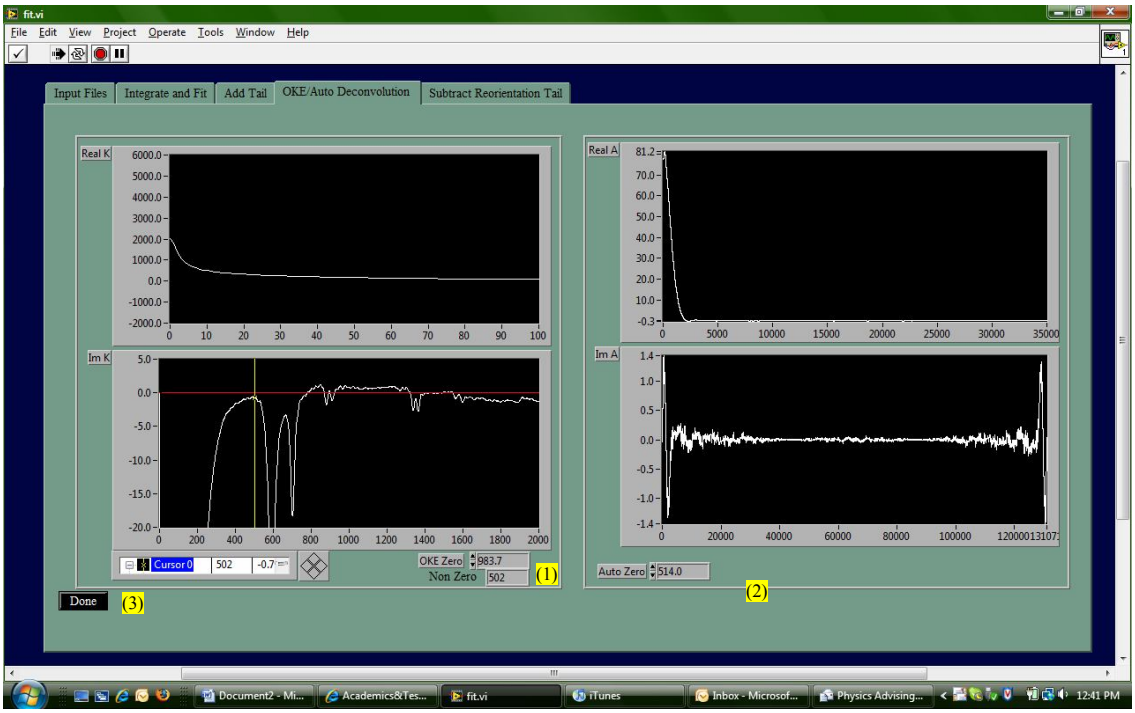

F) *Remove Reorientation Contribution (After inverse FT, back to the time domain)*

[The white line on the left of the yellow cursor is the time-domain data after inverse Fourier transform, with low frequency Raman-active modes removed; The white line on the right of the cursor is the tail of OKE data simulated using the bi-exponential decay formula.]

1) Move the cursor to around 30 ps to cut the tail of the data on the left. Then, add a tail modeled by the bi-exponential decay formula by adjusting the "gain" until the two white lines are connected continuously and smoothly.

2) Set "Amp1" = 0 and "Rise Time" = 200 fs. [By adjusting Amp1, the red line is only the reorientational diffusion part of the bi-exponential decay formula.]

3) Adjust the "Gain" until the tail of the red line fits the white curve.

4) At the bottom left corner, change "Time domain" to "RSD" and unzoom/zoom as necessary to see RSD plot

5) "Save"

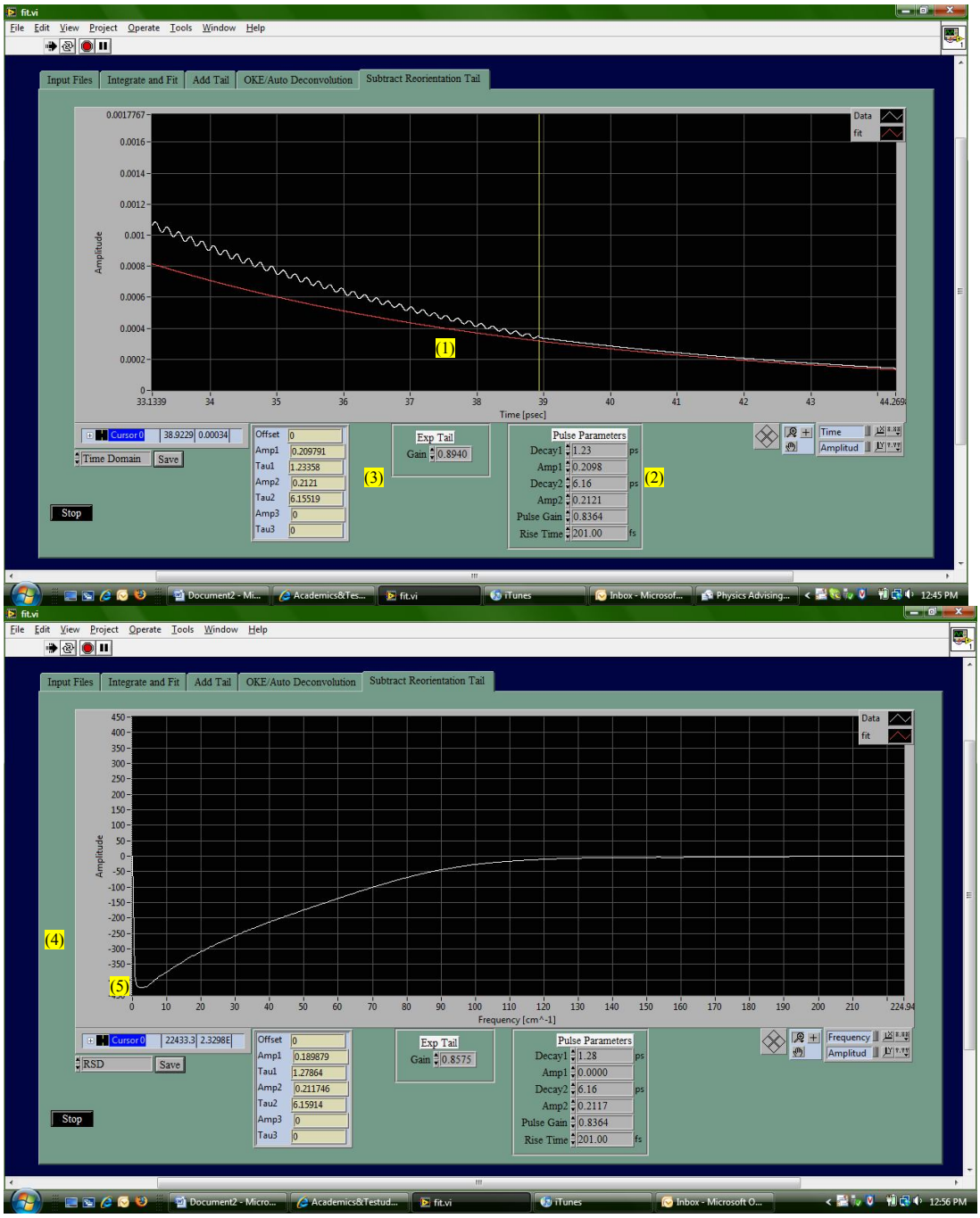

G) *Excel: normalization and finalization of RSD plot*

1) Open text file with Excel [saved from LabView program]

2) Column A is the x-axis (frequency) and Column B is y-axis (amplitude)

3) We want positive amplitudes, so for Column C input" =-B1" and extend to all cells

4) To normalize, for Column D input "=C1/max($C$1:$C$200)"

5) Plot Column A vs. Column D (probably only need the first 500 points)

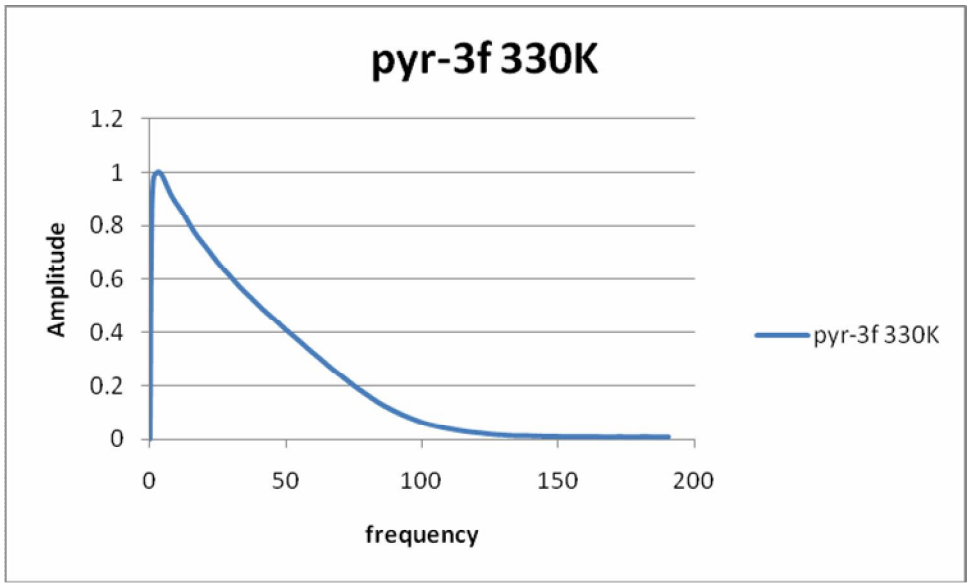

Appendix B: Temperature-dependent viscosity, parameters from biexponential fits to the Integrated OKE data, and fitting ranges for 1, n-Dicyano n-Alkanes Studied in Chapter 3

Table B.1: Fit parameters, single-molecule orientational correlation times and viscosities for integrated dicyanomethane OKE decays.

Temperature (*K*)	*A*	τ_1 (*ps*)	τ_2 (*ps*)	η (*cP*)	Fit start (*ps*)	Fit end (*ps*)
306	0.74	8.8(2)	3.1(1)	5.83	3.2	28.0
314	0.75	7.6(2)	2.7(1)	3.32	3.0	25.0
323	0.74	7.2(3)	2.3(2)	2.33	2.2	18.0
330	0.77	5.7(2)	1.9(1)	1.86	2.0	15.0
339	0.76	5.3(2)	1.7(1)	1.56	2.0	15.0
347	0.71	5.0(2)	1.7(1)	1.37	2.0	14.0
354	0.70	4.7(2)	1.7(1)	1.26	1.8	14.0
360	0.69	4.5(2)	1.6(1)	1.19	1.8	12.5

Table B.2: Fit parameters, single-molecule orientational correlation times and viscosities for integrated 1, 2-dicyanoethane OKE decays.

Temperature (*K*)	*A*	τ_1 (*ps*)	τ_2 (*ps*)	η (*cP*)	Fit start (*ps*)	Fit end (*ps*)
336	0.82	8.2(3)	2.3(1)	2.79	2.5	22.0
343	0.82	7.3(3)	1.9(1)	2.36	2.0	20.0
350	0.83	6.3(2)	1.7(1)	2.07	2.0	17.0
358	0.82	5.9(2)	1.6(1)	1.86	2.0	17.0
365	0.83	5.2(2)	1.4(1)	1.70	1.8	16.0
372	0.84	4.8(1)	1.2(1)	1.57	1.6	15.0
380	0.80	4.4(2)	1.2(1)	1.47	1.2	10.0

Table B.3: Fit parameters, single-molecule orientational correlation times and viscosities for integrated 1, 3-dicyanopropane OKE decays.

Temperature (*K*)	*A*	τ_1 (*ps*)	τ_2 (*ps*)	η (*cP*)	Fit start (*ps*)	Fit end (*ps*)
289	0.76	39(4)	11(2)	7.93	10.0	70.0
297	0.75	30(2)	8.9(8)	6.16	5.0	65.0
306	0.73	25(3)	7.5(16)	4.87	8.0	45.0
315	0.72	21(1)	6.1(4)	3.97	4.0	53.0
332	0.68	14.9(2)	5.0(1)	2.80	3.0	62.0
341	0.64	13.6(5)	4.7(3)	2.41	3.0	37.5
350	0.67	11.4(3)	4.0(2)	2.11	2.8	37.0
358	0.71	9.5(3)	3.2(3)	1.87	2.5	26.0
367	0.67	8.8(2)	3.3(2)	1.68	2.6	30.0
375	0.72	7.4(2)	2.4(2)	1.51	2.4	22.6

Table B.4: Fit parameters, single-molecule orientational correlation times and viscosities for integrated 1, 4-dicyanobutane OKE decays.

Temperature (K)	A	τ_1 (ps)	τ_2 (ps)	η (cP)	Fit start (ps)	Fit end (ps)
275	0.83	71(9)	17(3)	14.0	10.0	110.0
289	0.80	51(3)	14(1)	8.35	10.0	110.0
293	0.73	50(4)	14(2)	7.28	8.0	90.0
306	0.72	35(1)	10.4(6)	5.02	5.0	95.0
319	0.73	24.2(7)	6.9(3)	3.69	4.5	70.0
327	0.69	20.9(6)	6.6(4)	3.12	3.5	60.0
341	0.68	16.8(5)	5.4(3)	2.47	3.0	47.0
349	0.66	14.9(4)	5.0(2)	2.16	3.0	47.0
358	0.66	12.9(3)	4.4(3)	1.92	3.0	40.0
366	0.62	12.2(2)	4.1(2)	1.72	2.5	45.0
375	0.66	10.2(2)	3.4(1)	1.56	2.5	40.0

Table B.5: Fit parameters, single-molecule orientational correlation times and viscosities for integrated 1, 5-dicyanopentane OKE decays.

Temperature (K)	A	τ_1 (ps)	τ_2 (ps)	η (cP)	Fit start (ps)	Fit end (ps)
272	0.74	173(12)	51(5)	18.3	30.0	350.0
281	0.75	136(42)	32(14)	12.6	20.0	160.0
289	0.71	98(11)	25(4)	9.14	20.0	170.0
297	0.70	76(6)	21(3)	6.93	15.0	145.0
306	0.66	61(3)	17(2)	5.42	12.0	135.0
314	0.65	50(2)	14(1)	4.35	10.0	120.0
323	0.66	39(2)	11(1)	3.56	8.0	90.0
331	0.62	34(2)	10(1)	2.99	8.0	80.0
340	0.65	27(1)	7.9(8)	2.55	5.0	70.0
348	0.62	24.6(7)	7.5(5)	2.22	5.0	72.0
357	0.67	19.5(8)	5.7(6)	1.95	4.0	50.0
374	0.64	15.9(7)	4.6(5)	1.56	4.0	40.0

Table B.6: Fit parameters, single-molecule orientational correlation times and viscosities for integrated 1,6-dicyanohexane OKE decays.

Temperature (*K*)	*A*	τ_1 (*ps*)	τ_2 (*ps*)	η (*cP*)	Fit start (*ps*)	Fit end (*ps*)
289	0.74	102(12)	23(4)	10.1	10.0	160.0
314	0.70	53(6)	12(2)	4.57	7.0	85.0
323	0.67	45(9)	11(3)	3.70	5.0	60.0
332	0.67	37(4)	9(2)	3.06	5.0	60.0
340	0.65	33(6)	8(3)	2.59	5.0	47.0
349	0.67	27(8)	6(2)	2.22	5.0	33.0
366	0.71	18(1)	4.4(5)	1.70	5.0	45.0

Table B.7: Fit parameters, single-molecule orientational correlation times and viscosities for integrated 1, 7-dicyanoheptane OKE decays.

Temperature (*K*)	*A*	τ_1 (*ps*)	τ_2 (*ps*)	η (*cP*)	Fit start (*ps*)	Fit end (*ps*)
306	0.70	104(24)	20(6)	6.48	10.0	130.0
314	0.65	93(15)	17(4)	5.12	10.0	130.0
331	0.64	64(9)	13(4)	3.42	8.0	95.0
348	0.63	43(4)	8.0(13)	2.47	6.0	78.0
357	0.61	41(5)	8.6(24)	2.15	5.0	65.0
364	0.62	37(7)	7.6(28)	1.91	5.0	40.0

Table B.8: Fit parameters, single-molecule orientational correlation times and viscosities for integrated 1,8-dicyanooctane OKE decays.

Temperature (*K*)	*A*	τ_1 (*ps*)	τ_2 (*ps*)	η (*cP*)	Fit start (*ps*)	Fit end (*ps*)
297	0.59	205(60)	43(13)	10.0	30.0	245.0
306	0.58	173(22)	32(6)	7.49	25.0	270.0
315	0.59	125(28)	26(8)	5.84	20.0	150.0
323	0.59	110(10)	21(4)	4.66	15.0	190.0
332	0.61	83(5)	15(2)	3.79	12.0	175.0
340	0.60	73(6)	14(2)	3.18	10.0	135.0
349	0.60	64(5)	11(2)	2.70	8.0	120.0
358	0.62	47(5)	9(2)	2.32	6.0	80.0
366	0.60	44(2)	8(1)	2.03	5.0	100.0

Appendix C: Fit Parameters of Integrated OKE Data for All Five Aromatic Liquids Studied in Chapter 4

Table C.1: Viscosity[1] and fit parameters for integrated pyridine OKE decays.

Temperature (K)	Viscosity (cP)	A	τ_{or} (ps)	τ_i (ps)	Fit start (ps)	Fit end (ps)
249	2.11	0.75	10.4(6)	2.8(5)	5	35
258	1.77	0.73	8.7(5)	3.0(5)	5	28
267	1.50	0.73	7.2(5)	2.6(4)	4.2	28
275	1.29	0.75	5.8(4)	1.8(3)	3	22
284	1.12	0.71	4.9(3)	1.4(3)	2.8	20
297	0.926	0.73	4.1(3)	1.5(3)	2.8	16
310.	0.778	0.72	3.3(2)	1.1(2)	2.5	15
328	0.628	0.72	2.6(2)	0.86(8)	2.5	12
349	0.496	0.71	2.1(2)	0.79(7)	2	10

[1] From Ito, N.; Kato, T. *J. Phys. Chem.* **1984**, *88*, 801.

Table C.2: Viscosity[2] and fit parameters for integrated pyridine-*d5* OKE decays.

Temperature (*K*)	Viscosity (*cP*)	*A*	τ_{or} (*ps*)	τ_i (*ps*)	Fit start (*ps*)	Fit end (*ps*)
240	2.76	0.72	14.2(8)	4.1(5)	6	45
249	2.27	0.73	10.4(7)	2.7(4)	4	35
257	1.91	0.72	9.6(7)	2.8(5)	4	35
266	1.62	0.72	7.3(6)	2.0(3)	4	27
275	1.39	0.73	6.2(4)	1.9(3)	3.5	22
284	1.20	0.74	5.2(3)	1.5(3)	3.5	21
298	0.983	0.73	4.2(3)	1.4(2)	3.6	20
310	0.825	0.73	3.5(3)	1.3(2)	3	16
328	0.664	0.70	2.7(2)	0.83(8)	2.8	12
349	0.523	0.69	2.1(2)	0.69(7)	2.2	10

[2] From Holz, M.; Mao, X.-A.; Seiferling, D.; Sacco, A., *J. Chem. Phys.* **1996**, *104*, 669.

Table C.3: Fit parameters for integrated 2,4,6-trifluoropyridine OKE decays.

Temperature (*K*)	*A*	τ_{or} (*ps*)	τ_i (*ps*)	Fit start (*ps*)	Fit end (*ps*)
230	0.90	50(5)	12(1)	15	140
239	0.89	38(4)	8.8(8)	10	90
249	0.90	27(3)	5.3(6)	10	100
258	0.88	22(3)	5.1(6)	8	85
267	0.88	17(2)	4.1(5)	5	70
280	0.88	13(1)	3.2(4)	5	50
289	0.88	10.8(8)	3.0(4)	5	42
298	0.88	9.4(7)	2.7(4)	5	40
306	0.86	8.1(6)	1.8(3)	4	35
315	0.85	7.2(5)	1.7(3)	4	35
323	0.84	6. 2(5)	1.3(2)	3.5	25
332	0.84	5.6(4)	1.3(2)	3	24

Table C.4: Fit parameters for integrated 2,4,6-trimethylpyridine OKE decays.

Temperature (*K*)	*A*	τ_{or} (*ps*)	τ_i (*ps*)	Fit start (*ps*)	Fit end (*ps*)
243	0.82	58(5)	14(2)	11	125
262	0.84	29(3)	8.1(9)	10	75
278	0.76	21.5(9)	6.8(9)	9	60
295	0.75	15.6(7)	5.3(7)	5.5	44
312	0.64	12.6(8)	5.3(9)	5.4	48
329	0.77	8.7(5)	2.9(5)	3.5	30
351	0.80	6.2(4)	1.8(3)	2	22

Table C.5: Fit parameters for integrated 1,3,5-tris(trifluoromethyl)benzene OKE decays.

Temperature (*K*)	*A*	τ_{or} (*ps*)	τ_i (*ps*)	Fit start (*ps*)	Fit end (*ps*)
285	0.64	41(7)	13(3)	8	75
290	0.79	29(4)	8(2)	8	98
298	0.70	27(4)	9(2)	8	50
306	0.80	20(3)	6(1)	8	58
315	0.81	16(2)	4(1)	5	40
323	0.80	15(1)	4(1)	5	49
331	0.73	14(1)	4(1)	4	38
340	0.74	12.0(6)	3.7(5)	4	37.5
348	0.75	10.6(5)	3.6(4)	4	32

Appendix D: Viscosity and Fit Parameters of Integrated OKE Data for All Liquids Studied in Chapter 5

Table D.1: Viscosity[1] and fit parameters for integrated furan OKE decays.

Temperature (*K*)	Viscosity (*cP*)	*A*	τ_1 (*ps*)	τ_2 (*ps*)	Fit start (*ps*)	Fit end (*ps*)
246	0.693	0.55	2.2(2)	0.57(8)	0.85	6.5
254	0.608	0.54	1.9(2)	0.51(8)	0.78	5.5
263	0.539	0.53	1.7(2)	0.48(8)	0.76	5.5
272	0.481	0.53	1.5(2)	0.41(8)	0.65	4.5
285	0.414	0.53	1.3(1)	0.38(7)	0.6	4.0
298	0.361	0.51	1.1(1)	0.34(7)	0.6	4.0

[1] From Holland, R. S.; Smyth, C. P. *J. Phys. Chem.* **1955**, *59*, 1088.

Table D.2: Viscosity[2] and fit parameters for integrated THF OKE decays.

Temperature (*K*)	Viscosity (*cP*)	*A*	τ_1 (*ps*)	τ_2 (*ps*)	Fit start (*ps*)	Fit end (*ps*)
235	0.809	0.54	2.6(3)	0.67(8)	1.00	8.0
253	0.689	0.50	2.1(3)	0.59(8)	0.86	6.4
271	0.588	0.47	1.6(2)	0.48(7)	0.77	4.8
285	0.517	0.47	1.3(2)	0.41(7)	0.70	4.2
298	0.466	0.49	1.1(1)	0.33(6)	0.65	3.25

[2] From Sinha, A.; Roy, M. N. *J. Chem. Eng. Data* **2006**, *51*, 1415 and Giner, B.; Gascon, I.; Villares, A.; Cea, P.; Lafuente, C. *J. Chem. Eng. Data* **2006**, *51*, 1321.

Table D.3: Viscosities[3] and fit parameters for integrated cyclopentane OKE decays.

Temperature (*K*)	Viscosity (*cP*)	*A*	τ_1 (*ps*)	τ_2 (*ps*)	Fit start (*ps*)	Fit end (*ps*)
249	0.763	0.82	0.80(5)	0.23(4)	0.6	2.2
297	0.423	0.74	0.61(5)	0.15(3)	0.56	2

[3] From Assael, M. J.; Dalaouti, N. K.; Dymond, J. H. *Int. J. Thermophys.* **2000**, *21*, 621.

Table D.4: Viscosities[4] and fit parameters for integrated diethyl ether OKE decays.

Temperature (*K*)	Viscosity (*cP*)	*A*	τ_1 (*ps*)	τ_2 (*ps*)	Fit start (*ps*)	Fit end (*ps*)
250	0.384	0.81	4.4(4)	1.0(1)	1.5	11
258	0.345	0.76	3.7(3)	0.61(8)	0.8	7.5
276	0.277	0.73	2.8(2)	0.51(7)	0.8	5.2
298	0.220	0.67	2.1(2)	0.45(6)	0.8	5

[4] From Weast, R. C. *CRC Handbook of Chemistry and Physics*, 66th ed.; CRC Press: Boca Raton, 1985.

Table D.5: Viscosities[5] and fit parameters for integrated *n*-pentane OKE decays.

Temperature (*K*)	Viscosity (*cP*)	*A*	τ_1 (*ps*)	τ_2 (*ps*)	Fit start (*ps*)	Fit end (*ps*)
215	0.571	0.78	7.9(8)	0.85(5)	1.5	12
236	0.426	0.75	5.3(6)	0.69(5)	1.2	9
297	0.230	0.57	2.2(4)	0.47(4)	1	5

[5] From Froba, A. P.; Pellegrino, L. P.; Leipertz, A. *Int. J. Thermophys.* **2004**, *25*, 1323.

Table D.6: Viscosities[6] and fit parameters for integrated tetrahydropyran OKE decays.

Temperature (*K*)	Viscosity (*cP*)	*A*	τ_1 (*ps*)	τ_2 (*ps*)	Fit start (*ps*)	Fit end (*ps*)
242	2.17	0.63	2.55(7)	0.58(6)	0.75	5
297	0.819	0.46	1.65(5)	0.43(5)	0.7	4.8

[6] From Comelli, F.; Francesconi, R.; Bigi, A.; Rubini, K. *J. Chem. Eng. Data* **2007**, *52*, 639.

Table D.7: Viscosities[7] and fit parameters for integrated cyclohexane OKE decays.

Temperature (*K*)	Viscosity (*cP*)	*A*	τ_1 (*ps*)	τ_2 (*ps*)	Fit start (*ps*)	Fit end (*ps*)
297	0.893	0.44	0.90(5)	0.27(5)	0.5	2.5
324	0.638	0.48	0.75(4)	0.27(4)	0.5	2.25

[7] From Aminabhavi, T. M.; Patil, V. B.; Aralaguppi, M. I.; Phayde, H. T. S. *J. Chem. Eng. Data* **1996**, *41*, 521.

Table D.8: Viscosities[8] and fit parameters for integrated HMPA OKE decays.

Temperature (*K*)	Viscosity (*cP*)	*A*	τ_1 (*ps*)	τ_2 (*ps*)	Fit start (*ps*)	Fit end (*ps*)
285	4.16	0.72	4.7(5)	0.66(9)	1	8
337	1.59	0.63	3.3(4)	0.59(8)	1	7

[8] From Bhadani, S. N. *Indian J. Chem.* **1972**, *10*, 88.

Glossary

Four-wave Mixing

Heterodyne

Libration

Nonlinear Optics

Nonlinear Spectroscopy

Optical Kerr Effect (OKE)

Reorientational Diffusion

Reduced Spectral Density (RSD)

Spectrometer

Tension

Bibliography

- **Qin Zhong**, Xiang Zhu and John T. Fourkas, *"Antiresonant-Ring Kerr Spectroscopy," Opt. Exp.* **2007**, 15, 6561.
- **Qin Zhong**, Xiang Zhu and John T. Fourkas, *"Temperature-Dependent Orientational Dynamics of 1,* n-*Dicyano* n-*Alkanes," J. Phys. Chem. B*, **2008**, 112, 3115.
- **Qin Zhong** and John T. Fourkas, *"Searching for Voids in Liquids with Optical Kerr Effect Spectroscopy," J. Phys. Chem. B*, **2008**, 112; 8656.
- Xiang Zhu, Richard A. Farrer, **Qin Zhong** and John T. Fourkas, *"Orientational Diffusion of n-Alkyl Cyanides," J. Phys. Cond. Matt.* **2005**, 17, 4105.
- **Qin Zhong** and John T. Fourkas, *"Shape and Electrostatic Effects in Optical Kerr Effect Spectroscopy of Aromatic Liquids," J. Phys. Chem. B.* **2008**, 112, 15342.
- **Qin Zhong** and John T. Fourkas, *"Optical Kerr Effect Spectroscopy of Simple Liquids," J. Phys. Chem. B.* **2008**, 112, 15529.
- Feng Ding, **Qin Zhong**, Michael R. Brindza, John T, Fourkas and Robert A. Walker, *"Ti: Sapphire, Broadband Vibrational Sum Frequency Generation Spectrometer with a Counter-propagating Geometry," Opt. Exp.* (submitted)

All References

- Abraham, F. F. **1974**, *Homogeneous nucleation theory* (Academic Press, NY)
- Alvarenga, A. D.; Grimsditch, M.; Bodnar, R. J. "*Elastic Properties of Water under Negative Pres-sure," J. Chem. Phys.* **1993**, 98, 8392.
- Aminabhavi, T. M.; Patil, V. B.; Aralaguppi, M. I.; Phayde, H. T. S. *"Density, viscosity, and refractive index of the binary mixtures of cyclohexane with hexane, heptane, octane, nonane, and decane at (298.15, 303.15, and 308.15) K," J. Chem. Eng. Data* **1996**, 41, 521.
- Andersen, H. C.; Weeks, J. D.; Chandler, D. *"Relationship between the hard-sphere fluid and fluids with realistic repulsive forces," Phys. Rev. A* **1971***,* 4, 1597.
- Andersen, H. C.; Chandler, D.; Weeks, J. D. *"Roles of repulsive and attractive forces in liquids, The equilibrium theory of classical fluids," Adv. Chem. Phys.* **1976**, 34, 105.
- Assael, M. J.; Dalaouti, N. K.; Dymond, J. H. "Viscosity of toluene plus cyclopentane mixtures: Measurements and prediction,*" Int. J. Thermophys.* **2000**, 21, 621.
- Bartsch, E.; Bertagnolli, H.; Schulz, G.; Chieux, P. *"A neutron and X-ray diffraction study of the binary liquid aromatic system benzene-hexafluorobenzene*. I: The *pure components.," Ber. Bunsen-Ges. Phys. Chem.* **1985**, 89, 147.
- Bedard-Hearn, M. J.; Larsen, R. E.; Schwartz, B. J. *"The role of solvent structure in the absorption spectrum of solvated electrons: Mixed quantum/classical simulations in tetrahydrofuran," J. Chem. Phys.* **2005**, 122, 134506.

- Berne, B. J.; Pecora, R. *Dynamic Light Scattering*; Wiley: New York, **1976**.
- Bertagnolli, H.; Engelhardt, T.; Chieux, P. *" Study of dipolar interaction in liquid pyridine by X-Ray and neutron diffraction," Ber. Bunsen-Ges. Phys. Chem.* **1986**, 90, 512.
- Berthelot, M. *"Sur Quelques Phonomenes de Dilatation Forcee des Liquides," Ann. Chim. Phys.* **1850**, 30, 232.
- Bhadani, S. N. *"Conductance Studies in Hexamethylphosphoramide," Indian J. Chem.* **1972**, 10, 88.
- Bowron, D. T.; Finney, J. L.; Soper, A. K. *"The structure of liquid tetrahydrofuran," J. Am. Chem. Soc.* **2006**, 128, 5119.
- Bradley, E. B.; Mathur, M. S.; Frenzel, C. A. *"New Measurements of the Infrared and the Raman Spectrum of S_2Cl_2," J. Chem. Phys.* **1967,** 47, 4325.
- Brady, G. W.; Fein, D. B. *"Diffraction studies of molecular interaction. Low electron-density fluctuations induced by association," J. Appl. Crystallogr.* **1975**, 8, 261.
- Briggs, J. M.; Matsui, T.; Jorgensen, W. L. "Monte Carlo Simulations of Liquid Alkyl Ethers with the OPLS Potential Functions," J. Comput. Chem. **1990**, 11, 958.
- Butcher, P. N.; Cotter, D. *The Elements of Nonlinear Optics*; Cambridge University Press: Cambridge, U.K., **1990**.
- Cabaco, M. I.; Danten, Y.; Besnard, M.; Guissani, Y.; Guillot, B. *"Evidence of dimer formation in neat liquid 1,3,5-trifluorobenzene" Chem. Phys. Lett.* **1996**, 262, 120.

- Cabaco, M. I.; Danten, Y.; Besnard, M.; Guissani, Y.; Guillot, B. *"Neutron diffraction and molecular dynamics study of liquid benzene and its fluorinated derivatives as a function of temperature," J. Phys. Chem. B* **1997**, 101, 6977.
- Cabaco, M. I.; Tassaing, T.; Danten, Y.; Besnard, M. *"Evolution of the local order in 1,3,5-trifluorobenzene from the liquid state up to supercritical conditions," J. Phys. Chem. A* **2000**, 104, 10986.
- Cabaco, M. I.; Tassaing, T.; Danten, Y.; Besnard, M. *"Structural study of the 1-3-5 trifluorobenzene dimer stability: from liquid to gas densities using supercritical conditions," Chem. Phys. Lett.* **2000**, 325, 163.
- Cabaco, M. I.; Besnard, M.; Tassaing, T.; Danten, Y. *"Local density inhomogeneities detected by Raman scattering in supercritical hexafluorobenzene," Pure Appl. Chem.* **2004**, 76, 141.
- Cang, H.; Li, J.; Fayer, M. D. *"Orientational Dynamics of the Ionic Organic Liquid 1-Ethyl-3-Methylimidazolium Nitrate," J. Chem. Phys.* **2003**, 119, 13017.
- Castner, E. W., Jr.; Chang, Y. J.; Melinger, J. S.; McMorrow, D. *"Femtosecond Fourier-transform spectroscopy of low-frequency intermolecular motions in weakly interacting liquids ," J. Lumin.* **1994**, 60/61, 723.
- Castner, Jr. E. W.; Maroncelli, M. "*Solvent Dynamics Derived from Optical Kerr Effect*, *Dielectric Dispersion, and Time-Resolved Stokes Shift Measurements: An Empirical Comparison," J. Mol. Liq.* **1998**, 77, 1.
- Chang, Y. J.; Castner Jr., E. W. *"Femtosecond dynamics of hydrogen-bonding solvents*. *Formamide and N-methylformamide in acetonitrile*, *DMF, and water," J. Chem. Phys.* **1993**, 99, 113.

- Chang, Y. J.; Castner Jr., E. W. *"Deuterium Isotope Effects on the Ultrafast Solvent. Relaxation of Formamide and N,N-Dimethylformamide," J. Phys. Chem.* **1994**, 98, 9712.
- Chang, Y. J.; Castner, E. W., Jr. *"Intermolecular dynamics of substituted benzene and cyclohexane liquids, studied by femtosecond nonlinear-optical polarization spectroscopy," J. Phys. Chem.* **1996**, 100, 3330.
- Chang, Y. J.; Cong, P. J.; Simon, J. D. *"Isotropic and anisotropic intermolecular dynamics of liquids studied by femtosecond position-sensitive Kerr lens spectroscopy," J. Chem. Phys.* **1997**, 106, 8639.
- *Chem 3D Pro*, version 5.0; CambridgeSoft: Cambridge, MA, **1999**.
- Cheng, J. X.; Volkmer, A.; Book, L. D.; Xie, X. S. *"An epi-detected anti-Stokes Raman scattering (E-CARS) microscope with high spectral resolution and high sensitivity," J. Phys. Chem. B* **2001**, 105, 1277.
- Cheng, J. X.; Book, L. D.; Xie, X. S. *"Polarization coherent anti-Stokes Raman scattering microscopy," Opt. Lett.* **2001,** 26, 1341.
- Cheng, J. X.; Volkmer, A.; Xie, X. S. *"Theoretical and experimental characterization of coherent anti-Stokes Raman scattering microscopy," J. Opt. Soc. Amer. B* **2002,** 19, 1363.
- Comelli, F.; Francesconi, R.; Bigi, A.; Rubini, K. *"Molar heat capacities, densities, viscosities, and refractive indices of dimethyl sulfoxide plus tetrahydropyran and +2-methyltetrahydrofuran at (293.15, 303.15, and 313.15) K," J. Chem. Eng. Data* **2007**, 52, 639.

- Cong, P.; Deuel, H. P.; Simon, J. D. *"Structure and dynamics of molecular liquids investigated by optical-heterodyne detected Raman-induced Kerr effect spectroscopy* (*OHD-RIKES*)*" Chem. Phys. Lett.* **1995**, 240, 72.
- Cong, P. J.; Chang, Y. J.; Simon, J. D. *"Complete determination of intermolecular spectral densities of liquids using position-sensitive Kerr lens spectroscopy," J. Phys. Chem.* **1996**, 100, 8613.
- Constantine, S.; Gardecki, J. A.; Zhou, Y.; Ziegler, L. D.; Ji, X. D.; Space, B. *"A novel technique for the measurement of polarization-specific ultrafast Raman responses," J. Phys. Chem. A* **2001**, 105, 9851.
- Danten, Y.; Cabaco, M. I.; Tassaing, T.; Besnard, M. *"A structural study of the hexafluorobenzene from liquid to supercritical conditions using neutron diffraction and molecular dynamics," J. Chem. Phys.* **2001**, 115, 4239.
- de Boeij, W. P.; Pshenichnikov, M. S.; Wiersma, D. A. *"Ultrafast Solvation Dynamics Explored by Femtosecond Photon Echo Spectroscopies," Annu. Rev. Phys. Chem.* **1998**, 49, 99.
- Debye, P. *Polar Molecules* Dover, New York, **1929**.
- Deeg, F. W.; Fayer, M. D. *"Analysis of complex molecular dynamics in an organic liquid by polarization selective subpicosecond transient grating experiments," J. Chem. Phys.* **1989**, 91, 2269.
- Deeg, F. W.; Fayer, M. D. *"Transient Grating Optical Kerr Effect Measurements of Reorientational Dynamics in Liquids and Liquid Crystalline Samples," J. Mol. Liq.* **1990**, 45, 19.

- DeMore, B. B.; Wilcox, W. S.; Goldstein, J. H. *"Microwave Spectrum and Dipole Moment of Pyridine," J. Chem. Phys.* **1954**, 22, 876.
- Denk, W.; Strickler, J. H.; Webb, W., *"Two-photon laser scanning fluorescence microscopy," Science* **1990**, 248, 73.
- Dhar, L.; Rogers, J. A.; Nelson, K. A. *"Time-Resolved Vibrational Spectroscopy in the Impulsive Limit," Chem. Rev.* **1994**, 94, 157.
- Donoghue, J. J.; Vollrath, R. E.; Gerjuoy E. "*The tensile strength of benzene," J. Chem. Phys.* **1951,** *19*, 55.
- Drake, J. M.; Klafter, J., Eds.; *Molecular Dynamics in Restricted Geometries*; Wiley: New York, **1989**.
- Drake, J. M.; Klafter, J.; Kopelman, R.; Awschalom, D.D., Eds.; *Dynamics in Small Confining Systems*; Materials Research Society: Pittsburgh, **1993**; Vol. 290, pp 377.
- Drake, J. M.; Klafter, J.; Kopelman, R.; Troian, S. M., Eds.;*Dynamics in Small Confining Systems II;* Materials Research Society: Pittsburgh, **1995**; Vol. 366, pp 466.
- Drake, J. M.; Klafter, J.; Kopelman, R., Eds. *Dynamics in Small Confining Systems III*;Materials Research Society: Pittsburgh, **1997**; Vol. 464, pp 388.
- Drake, J. M.; Grest, G. S.; Klafter, J.; Kopelman, R.,Eds.;*Dynamics in Small Confining Systems IV*; Materials Research Society: Warrendale, PA, **1999**; Vol. 543, pp 372.
- Duguay, M. A.; Hansen, J. W. *"An Ultrafast High Gate," Appl. Phys. Lett.* **1969**, 15, 192.

- Durig, J. R.; Drew, B. R.; Koomer, A.; Bell, S. *"Infrared and Raman spectra, conformational stability, ab initio calculations of structure and vibrational assignment of butyronitrile," Phys. Chem. Chem. Phys.* **2001**, 3, 766.
- Eaves, J. D.; Fecko, C. J.; Stevens, A. L.; Peng, P.; Tokmakoff, A. *"Polarization-selective femtosecond Raman spectroscopy of low-frequency motions in hydrated protein films," Chem. Phys. Lett.* **2003,** 376, 20.
- Eichler, H. J.; Günter, P.; Pohl, D.W. *Laser-Induced Dynamic Gratings*. **1986**, New York: Springer-Verlag.
- Elola, M. D.; Ladanyi, B. M. *"Molecular dynamics study of polarizability anisotropy relaxation in aromatic liquids and its connection with local structure," J. Phys. Chem. B* **2006**, 110, 15525.
- Farrer, R. A.; Loughnane, B. J.; Deschenes, L. A.; Fourkas, J. T. *"Level-dependent damping in intermolecular vibrations: Linear spectroscopy," J. Chem. Phys.* **1997**, 106, 6901.
- Farrer, R. A.; Loughnane, B. J.; Fourkas, J. T. *"Dynamics of confined carbon disulfide from 165 to 310 K," J. Phys. Chem. A* **1997**, 101, 4005.
- Farrer, R. A.; Fourkas, J. T. *"Orientational Dynamics of Liquids Confined in Nanoporous Sol-Gel Glasses Studied by Optical Kerr Effect Spectroscopy," Acc. Chem. Res.* **2003**, 36, 605.
- Fecko, C. J.; Eaves, J. D.; Tokmakoff, A. *"Isotropic and anisotropic Raman scattering from molecular liquids measured by spatially masked optical Kerr effect spectroscopy," J. Chem. Phys.* **2002,** 117, 1139.

- Foggi, P.; Bartolini, P.; Bellini, M.; Giorgini, M. G.; Morresi, A.; Sassi, P.; Cataliotti, R. S. *"Intermolecular and diffusive dynamics of pure acetonitrile isotopomers studied by depolarized Rayleigh scattering and femtosecond optical kerr effect," Eur. Phys. J. D* **2002**, 21, 143.
- Fourkas, J. T.; Fayer, M. D. *"The Transient Grating: A Holographic Window to Dynamic Processes," Acc. Chem. Res.*, **1992**, 25, 227.
- Fourkas, J. T., *Nonresonant Intermolecular Spectroscopy of Liquids*, in *Ultrafast Infrared and Raman Spectroscopy*, Fayer, M. D. Editor. **2001**, Marcel Dekker: New York. p. 473-512.
- Frankiss, S. G. "*Vibrational spectra and structures of S_2Cl_2, S_2Br_2, Se_2Cl_2 and Se_2Br_2," J. Mol. Struct.* **1968,** 2, 271.
- Froba, A. P.; Pellegrino, L. P.; Leipertz, A. *"Viscosity and surface tension of saturated n-pentane," Int. J. Thermophys.* **2004**, 25, 1323.
- Giner, B.; Gascon, I.; Villares, A.; Cea, P.; Lafuente, C. *"Densities and viscosities of the binary mixtures of tetrahydrofuran with isomeric chlorobutanes at 298.15 K and 313.15 K," J. Chem. Eng. Data* **2006**, 51, 1321.
- Glorieux, C.; Nelson, K. A.; Hinze, G.; Fayer, M. D. *"Thermal, Structural and Orientational Relaxation of Supercooled Salol Studied by Polarization-dependent Impulsive Stimulated Scattering," J. Chem. Phys.* **2002**, 116, 3384.
- Gottke, S. D.; Cang, H.; Bagchi, B.; Fayer, M. D. *"Comparison of the Ultrafast to Slow Timescale Dynamics of Three Liquid Crystals in the Isotropic Phase," J. Chem. Phys.* **2002**, 116, 6339.

- Gradshteyn, I. S.; Ryzhik, I. M. *Tables of Integrals, Series, and Products*; Academic Press: San Diego, CA, **1980**.
- Green, J. L.; Durben, D. J.; Wokf, G. H.; Angell, C. A. *"Water and Solutions at Negative Pressure: Ra-man Spectroscopic Study to -80 Megapascals," Science* **1990**, 249, 649.
- Heisler, I. A.; Correia, R. R. B.; Buckup, T.; Cunha, S. L. S.; da Silveira, N. P. *"Time-resolved optical Kerr-effect investigation on CS2/polystyrene mixtures," J. Chem. Phys.* **2005**, 123, 6.
- Henderson, S. J.; Speedy, R. J. *"A Berthelot-Bourdon tube method for studying water under tension," J. Phys. E* **1980**, 13, 778.
- Henriksen, N. E.; Engel, V. "*Femtosecond pump-probe spectroscopy: A theoretical analysis of transient signals and their relation to nuclear wave packet motion," Int. Rev. Phys. Chem.*, **2001**, 20, 93.
- Higashigaki, Y.; Wang, C. H. *"Rayleigh-Brillouin Light-Scattering-Studies of $NC(CH_2)_nCN$ Liquids," Mol. Phys.* **1982**, 45, 493.
- Hinze, G.; Brace, D. D.; Gottke, S. D.; Fayer, M. D. *"A Detailed Test of Mode-Coupling Theory on All Times Scales: Time Domain Studies of Structural Relaxation in a Supercooled Liquid," J. Chem. Phys.* **2000**, 113, 3723.
- Holland, R. S.; Smyth, C. P. *"Microwave Adsorption and Molecular Structure in Liquids .10. The Relaxation Times of 9 Heterocyclic Molecules," J. Phys. Chem.* **1955**, 59, 1088.

- Holz, M.; Mao, X. A.; Seiferling, D.; Sacco, A. *"Experimental study of dynamic isotope effects in molecular liquids: Detection of translation-rotation coupling," J. Chem. Phys.* **1996**, 104, 669.
- Hunt, N. T.; Jaye, A. A.; Meech, S. R. *"Ultrafast dynamics in microemulsions: optical Kerr effect study of the dispersed oil phase in a carbon disulfide-dodecyltrimethylammonium bromide-water microemulsion," J. Phys. Chem. B* **2003,** 107, 3405.
- Hunt, N. T.; Jaye, A. A.; Meech, S. R. *"Polarisation-resolved ultrafast Raman responses of carbon disulfide in solution and microemulsion environments," Chem. Phys. Lett.* **2003**, 371, 304.
- Hunt, N. T.; Meech, S. R. *"Ultrafast dynamics of polybutadiene probed by optically heterodyne-detected optical-Kerr-effect spectroscopy ," Chem. Phys. Lett.* **2004**, 400, 368.
- Hunt, N. T.; Meech, S. R. "*Orientational and Interaction Induced Dynamics in the Isotropic Phase of a Liquid Crystal: Polarisation Resolved Ultrafast Optical Kerr Effect Spectroscopy" J. Chem. Phys.* **2004**, 120, 10828.
- Hunt, N. T.; Jaye, A. A.; Hellman, A.; Meech, S. R. *"Ultrafast dynamics of styrene microemulsions, polystyrene nanolatexes, and structural analogues of polystyrene," J. Phys. Chem. B* **2004**, 108, 100.
- Hunt, N. T.; Jaye, A. A.; Meech, S. R. "Ultrafast dynamics in complex fluids observed through the ultrafast optically-heterodyne-detected optical-Kerr-effect (OHD-OKE)," Phys. Chem. Chem. Phys. **2007**, 9, 2167.

- Imre, A.; Van Hook, W. A. *"Liquid-liquid equilibria in polymer solutions at negative pressure," Chem. Soc. Rev.* **1998**, 27,117.
- Ippen, E. P.; Shank, C. V. *"Picosecond Response of a High-Repetition-Rate Cs2 Optical Kerr Gate," Appl. Phys. Lett.* **1975**, 26, 92.
- Ito, N.; Kato, T. *"Orientational pair correlation of pyridine and 2,4-dimethylpyridine in water* by *depolarized Rayleigh scattering and nuclear magnetic resonance spectra," J. Phys. Chem.* **1984**, 88, 801.
- Jatkar, S. K. K.; Deshpande, C. M. *"Dielectric constant and dipole moment; pyridine and 2,4,6-trimethylpyridine," J. Indian Chem. Soc.* **1960**, 37, 11.
- Jaye, A. A.; Hunt, N. T.; Meech, S. R. *"Temperature- and solvation-dependent dynamics of liquid sulfur dioxide studied through the ultrafast optical Kerr effect," J. Chem. Phys.* **2006**, 124, 24506.
- Jou, F. Y.; Freeman, G. R. *"Shapes of optical spectra of solvated electrons. effect of pressure," J. Phys. Chem.* **1977**, 81, 909.
- Kalpouzos, C.; Lotshaw, W. T.; McMorrow, D.; Kenney-Wallace, G. A. *"Femtosecond Laser-induced Kerr responses in liquid CS_2, " J. Phys. Chem.* **1987**, 91, 2028.
- Kalpouzos, C.; McMorrow, D.; Lotshaw, W. T.; Kenney-Wallace, G. A., *"Femtosecond laser-induced optical kerr dynamics in CS_2/alkane binary solutions," Chem. Phys. Lett.* **1988**, 150, 138.
- Kamada, K.; Ueda, M.; Ohta, K.; Wang, Y.; Ushida, K.; Tominaga, Y. *"Molecular dynamics of thiophene homologues investigated by femtosecond*

optical Kerr effect and low frequency Raman scattering spectroscopies," J. Chem. Phys. **1998**, 109, 10948.

- Kaufman, L. J.; Heo, J. Y.; Ziegler, L. D.; Fleming, G. R. "*Heterodyne detected fifth-order nonresonant Raman scattering from room temperature CS2," Phys. Rev. Lett.* **2002**, 88, 207402.
- Khalil, M.; Demirdoven, N.; Golonzka, O.; Fecko, C. J.; Tokmakoff, A. *"A phase-sensitive detection method using diffractive optics for polarization-selective femtosecond Raman spectroscopy," J. Phys. Chem. A* **2000**, 104, 5711.
- Kinoshita, S.; Kai, Y.; Ariyoshi, T.; Shimada, Y. *"Low Frequency Modes Probed by Time-Domain Optical kerr Effect Spectroscopy," Int. J. Mod. Phys. B* **1996**, 10, 1229.
- Kivelson, D.; Madden, P. A. *"Light-Scattering-Studies of Molecular Liquids," Annu. Re*v. *Phys. Chem.* **1980**, 31, 523.
- Kobayashi, M.; Fujita, K.; Kaneko, T.; Takamatsu, T.; Nakamura, O.; Kawata, S. *"Second-harmonic-generation microscope with a microlens array scanner," Opt. Lett.* **2002**, 27, 1324.
- Kurnit, N. A.; Abella, I. D.; Hartmann, S.R., *"Observation of a photon Echo," Phys. Rev. Lett.* **1964**, 13, 567.
- Ladanyi, B. M.; Klein, S. *"Contributions of rotation and translation to polarizability anisotropy and solvation dynamics in acetonitrile," J. Chem. Phys.* **1996**, 105, 1552.
- Lakowicz, J. R. *Principles of Fluorescence Spectroscopy*. 2 ed. **1999**, Berlin: Springer.

- Li, J.; Wang, I.; Fruchey, K.; Fayer, M. D. *"Dynamics in Supercooled Ionic Organic Liquids and Mode Coupling Theory Analysis," J. Phys. Chem. A* **2006**, 110, 10384.
- Liu, G.; Li, Y.; Jonas, J. *"Confined geometry effects on reorientational dynamics of molecular liquids in porous silica glasses," J. Chem. Phys.* **1991**, 95, 6892.
- Lotshaw, W. T.; McMorrow, D.; Thantu, N.; Melinger, J. S.; Kitchenham, R. *"Intermolecular Vibrational Coherence in Molecular Liquids," J. Raman Spectrosc.* **1995**, 26, 571.
- Loughnane, B. J.; Farrer, R. A.; Fourkas, J. T. *"Evidence for the direct observation of molecular exchange of a liquid at the solid/liquid interface," J. Phys. Chem. B* **1998**, 102, 5409.
- Loughnane, B. J.; Fourkas, J. T. *"Geometric effects in the dynamics of a nonwetting liquid in microconfinement: An optical Kerr effect study of methyl iodide in nanporous glasses," J. Phys. Chem. B* **1998**, 102, 10288.
- Loughnane, B. J.; Farrer, R. A.; Fourkas, J. T. Rotational Diffusion of Microconfined Liquids. In Dynamics in Small Confining Systems IV; Materials Research Society: Pittsburgh, **1999**; pp 33.
- Loughnane, B. J.; Scodinu, A.; Farrer, R. A.; Fourkas, J. T.; Mohanty, U. *"Exponential intermolecular dynamics in optical Kerr effect spectroscopy of small-molecule liquids," J. Chem. Phys.* **1999**, 111, 2686.
- Loughnane, B. J.; Farrer, R. A.; Scodinu, A.; Fourkas, J. T. *"Dynamics of a wetting liquid in nanopores: An optical Kerr effect study of the dynamics of acetonitrile confined in sol-gel glasses," J. Chem. Phys.* **1999**, 111, 5116.

- Loughnane, B. J.; Scodinu, A.; Fourkas, J. T. *"Extremely slow dynamics of a weakly wetting liquid at a solid/liquid interface: CS2 confined in nanoporous glasses," J. Phys. Chem. B* **1999**, 103, 6061.
- Loughnane, B. J.; Scodinu, A.; Fourkas, J. T. *"Temperature-dependent optical Kerr effect spectroscopy of chloroform in restricted geometries," Chem. Phys.* **2000**, 253, 323.
- Loughnane, B. J.; Farrer, R. A.; Scodinu, A.; Reilly, T.; Fourkas, J. T. *"Ultrafast Spectroscopic Studies of the Dynamics of Liquids Confined in Nanoporous Glasses," J. Phys. Chem. B* **2000**, 104, 5421.
- Loughnane, B. J.; Scodinu, A.; Fourkas, J. T. *"Temperature-dependent optical Kerr effect spectroscopy of aromatic liquids," J. Phys. Chem. B* **2006**, 110, 5708.
- Majors, R. E.; Hopper, M. J. *"Studies of siloxane phases bonded to silica gel for use in high performance liquid chromatography," J. Chromat. Sci.* **1974,** 12, 767.
- Marcus, Y. *Solvent Mixtures: Properties and Selective Solvation*; Marcel Dekker: New York, **2002**.
- Martini, I. B.; Barthel, E. R.; Schwartz, B. J. *"Optical control of electrons during electron transfer," Science* **2001**, 293, 462.
- Matsubara, I. *"Infrared Spectrum and Molecular Configuration of Glutaronitrile," J. Chem. Phys.* **1961**, 35, 373.
- Mayer, G.; Gires, F. *"Physique Moleculaire - Action Dune Onde Lumineuse Intense Sur Lindice De Refraction Des Liquides," Compt. Rend.* **1964**, 258, 2039.

- McMorrow, D.; Lotshaw, W. T.; Kenney-Wallace, G. A. *"Femtosecond Optical Kerr Studies on the Origin of the Nonlinear Responses in Simple Liquids," IEEE J. Quantum Electron.* **1988**, 24, 443.
- McMorrow, D. *"Separation of Nuclear and Electronic Contributions to Femtosecond Four-Wave Mixing Data," Opt. Comm.*, **1991,** 86, 236.
- McMorrow, D.; Lotshaw, W. T. *"Dephasing and relaxation in coherently excited ensembles of intermolecular oscillators," Chem. Phys. Lett.* **1991**, 178, 69.
- McMorrow, D.; Lotshaw W. T. *"Intermolecular Dynamics in Acetonitrile Probed with Femtosecond Fourier Transform Raman Spectroscopy," J. Phys. Chem.*, **1991**, 95, 10395.
- McMorrow, D.; Lotshaw, W. T. *"Evidence for Low-Frequency (Approximate-to-15 cm^{-1}) Collective Modes in Benzene and Pyridine Liquids," Chem. Phys. Lett.* **1993**, 201, 369.
- Megiel, E.; Kasprzycka-Guttman, T.; Jagielska, A.; Wroblewska, L. "*A theoretical and experimental N-14 NMR study of association of pyridine*," J. Mol. Struct. **2001**, 569, 111.
- Millard, A. C.; Wiseman, P. W.; Fittinghoff, D. N.; Wilson, K. R.; Squier, J. A.; Muller, M. *"Third harmonic generation microscopy using a compact, femtosecond fiber laser source," Appl. Opt.* **1999**, 38, 7393.
- Millard, A. C.; Fittinghoff, D. N.; Wiseman, P. W.; Muller, M.; Brakenhoff, G. J.; Squier, J. A.; Wilson, K. R. *"Three dimensional, third harmonic microscopy of living systems," Biophys. J.* **2000**, 78, 800.

- Mootz, D.; Wussow, H. G. "*Crystal structures of pyridine and pyridine trihydrate*," *J. Chem. Phys.* **1981**, 75, 1517.
- Moran, A. M.; Nome, R. A.; Scherer, N. F. *"Field-resolved measurement of reaction-induced spectral densities by polarizability response spectroscopy," J. Chem. Phys.* **2007**, 127, 184505.
- Moreaux, L.; Sandre, O.; Blanchard-Desce, M.; Mertz, J. *"Membrane imaging by simultaneous second-harmonic generation and two-photon microscopy," Opt. Lett.* **2000**, 25, 320.
- Murry, R. L.; Fourkas, J. T. *"Polarization selectivity of nonresonant spectroscopies in isotropic media," J. Chem. Phys.* **1997**, 107, 9726.
- Murry, R. L.; Fourkas, J. T.; Keyes, T. *"Nonresonant intermolecular spectroscopy beyond the Placzek approximation. I. Third-order spectroscopy," J. Chem. Phys.* **1998**, 109, 2814.
- Murry, R. L.; Fourkas, J. T.; Li, W.-X.; Keyes, T. "Mechanisms of light scattering in supercooled liquids," Phys. Rev. Lett. **1999**, 83, 3550.
- Neelakandan, M.; Pant, D.; Quitevis, E. L. "Reorientational and Intermolecular Dynamics in Binary Liquid Mixtures of Hexafluorobenzene and Benzene: Femtosecond Optical Kerr Effect Measurements," Chem. Phys. Lett. **1997**, 265, 283.
- Neelakandan, M.; Pant, D.; Quitevis, E. L. *"Structure and intermolecular dynamics of liquids: Femtosecond optical Kerr effect measurements in nonpolar fluorinated benzenes," J. Phys. Chem. A* **1997**, 101, 2936.
- Parker, M. E.; Heyes, D. M. *"Molecular Dynamics Simulations of Stretched*

Water: Local Structure and Spectral Signatures," J. Chem. Phys. **1998**, 108, 9039.

- Patrick, C. R.; Prosser, G. S. *"A molecular complex of benzene and hexafluorobenzene," Nature* **1960**, 187, 1021.
- Portuondo-Campa, E.; Tortschanoff, A.; van Mourik, F.; Chergui, M. *"Liquid Dynamics in ZrO_2 Nanoporous Films," Chem. Phys.* **2007**, 341, 11.
- Potma, E. O.; de Boeij, W. P.; Wiersma, D. A. *"Femtosecond dynamics of intracellular water probed with nonlinear optical Kerr effect microspectroscopy," Biophys. J.* **2001,** 80, 3019.
- Quitevis, E. L.; Neelakandan, M. *"Femtosecond optical Kerr effect studies of liquid methyl iodide," J. Phys. Chem.* **1996**, 100, 10005.
- Rajian, J. R.; Li, S. F.; Bartsch, R. A.; Quitevis, E. L. *"Temperature-Dependence of the Low-Frequency Spectrum of 3-Pentyl-1-methylimidazolium Bis(trifluoromethanesulfonyl)imide Studied by Optical Kerr Effect Spectroscopy," Chem. Phys. Lett.* **2004**, 393, 372.
- Ricci, M.; Bartolini, P.; Chelli, R.; Cardini, G.; Califano, S.; Righini, R. *"The fast dynamics of benzene in the liquid phase - Part I. Optical Kerr effect experimental investigation ," Phys. Chem. Chem. Phys.* **2001**, 3, 2795.
- Ricci, M.; Wiebel, S.; Bartolini, P.; Taschin, A.; Torre, R. *"Time-resolved optical Kerr effect experiments on supercooled benzene and test of mode-coupling theory ," Philos. Mag.* **2004**, 84, 1491.

- Rigby, D.; Roe, R. J. *"Molecular-Dynamics Simulation of Polymer Liquid and Glass .2. Short-Range Order and Orientation Correlation," J. Chem. Phys.* **1988**, 89, 5280.
- Righini, R. *"Ultrafast Optical Kerr Effect in Liquids and Solids," Science* **1993**, 262, 1386.
- Rollett, A. D. **2002**, *Microstructure-properties: II Nucleation rate* (lecture notes)
- Ruhman, S.; Kohler, B.; Joly, A. G.; Nelson, K. A. *"Intermolecular Vibrational Motion in Cs2 Liquid at 165-Less-Than-or-Equal-to-T-Less-Than-or-Equal-to-300-K Observed by Femtosecond Time-Resolved Impulsive Stimulated Scattering," Chem. Phys. Lett.* **1987**, 141, 16.
- Ruocco, G.; Sampoli, M.; Torcini, A.; Vallauri, R. "*Molecular Dynamics Results for Stretched Water," J. Chem. Phys.* **1993**, 99, 8095.
- Ryu, S.; Stratt, R. M. *"A case study in the molecular interpretation of optical Kerr effect spectra: Instantaneous-normal-mode analysis of the OKE spectrum of liquid benzene," J. Phys. Chem. B* **2004**, 108, 6782.
- Schmidtke, S. J.; Underwood, D. F.; Blank, D. A. "*Probing excited-state dynamics and intramolecular proton transfer in 1-acylaminoanthraquinones via the intermolecular solvent response," J. Phys. Chem. A* **2005**, 109, 7033.
- Sciortino, F.; Essmann, U.; Stanley, E. H.; Hemmati, M.; Shao, J.; Wolf, G. H.; Angell, C. A. "*Mechanical Stability Limits at Positive and Negative Pressures and Crystal-to-Glass Transitions," Phys. Rev. E* **1995**, 52, 6481.

- Scodinu, A.; Fourkas, J. T. *"Comparison of the orientational dynamics of water confined in hydrophobic and hydrophilic nanopores," J. Phys. Chem. B* **2002,** 106, 10292.
- Scodinu, A.; Farrer, R. A.; Fourkas, J. T. *"Direct observation of different mechanisms for the inhibition of molecular reorientation at a solid/liquid interface," J. Phys. Chem. B* **2002**, 106, 12863.
- Shirota, H.; Castner, Jr. E. W. *"Ultrafast dynamics in aqueous Polyacrylamide solutions," J. Am. Chem. Soc.* **2001,** 123, 12877.
- Shirota, H. *"Ultrafast Dynamics of Lliquid Poly(ethylene glycol)s andCcrown Ethers Studied by Femtosecond Raman-induced Kerr Effect Spectroscopy," J. Phys. Chem. B* **2005**, 109, 7053.
- Shirota, H.; Castner, E. W. *"Physical Properties and Intermolecular Dynamics of an Ionic Liquid Compared with its Isoelectronic Neutral Binary Solution," J. Phys. Chem. A* **2005**, 109, 9388.
- Shirota, H.; Castner, E. W. "Molecular Dynamics and Interactions in Aqueous and Dichloromethane Solutions of Polyvinylpyrrolidone," J. Chem. Phys. **2006**, 125, 034904.
- Shirota, H.; Wishart, J. F.; Castner, E. W. *"Intermolecular Interactions and Dynamics of Room Temperature Ionic Liquids That Have Silyl- and Siloxy-Substituted Imidazolium Cations," J. Phys. Chem. B* **2007**, 111, 4819.
- *SigmaPlot*, version 9.0; Systat: Point Richmond, CA, **2004**.

- Sinha, A.; Roy, M. N. *"Densities, viscosities, and sound speeds of some acetate salts in binary mixtures of tetrahydrofuran and methanol at (303.15, 313.15, and 323.15) K," J. Chem. Eng. Data* **2006**, 51, 1415.
- Small, D. M. *The Physical Chemistry of Lipids*; Plenum: New York, **1986**.
- Smith, N. A.; Meech, S. R. *"Ultrafast dynamics of polar monosubstituted benzene liquids studied by the femtosecond optical Kerr effect," J. Phys. Chem. A* **2000**, 104, 4223.
- Smith, N. A.; Meech, S. R. *"Optically-Heterodyne-Detected Optical Kerr Effect (OHD-OKE): Applications in Condensed Phase Dynamics," Int. Rev. Phys. Chem.* **2002**, 21, 75.
- So, P. T. C.; Dong, C. Y.; Masters, B. R.; Berland, K. M. *"Two-photon excitation fluorescence microscopy," Annu. Rev. Biomed. Eng.* **2000,** 2, 399.
- Squier, J. A.; Muller, M.; Brakenhoff, G. J.; Wilson, K. R. *"Third harmonic generation microscopy," Opt. Expr.* **1998**, 3, 315.
- Steffen, T.; Meinders, N. A. C. M.; Duppen, K. *"Microscopic Origin of the Optical Kerr Effect Response of CS2-Pentane Binary Mixtures," J. Phys. Chem. A* **1998,** 102, 4213.
- Tanimura, Y.; Mukamel, S. *"Two-dimensional femtosecond vibrational spectroscopy of liquids," J. Chem. Phys.* **1993**, 99, 9496.
- Tassaing, T.; Cabaco, M. I.; Danten, Y.; Besnard, M. *"The structure of liquid and supercritical benzene as studied by neutron diffraction and molecular dynamics," J. Chem. Phys.* **2000**, 113, 3757.

- Thorbjor, J.; Ellestad, O. H.; Klaeboe, P.; Torgrims. T. "*Substituted Propanes*. Part VIII. The *Vibrational Spectra* of. *1,3-Dicyanopropane* (*Glutaronitrile*) ," *Acta Chem. Scand.* **1972**, 26, 3799.
- Torre, R.; Bartolini, P.; Pick, R. M. "Time-resolved optical Kerr effect in a fragile glass-forming liquid, salol," *Phys. Rev. E* **1998**, 57, 1912.
- Torre, R.; Bartolini, P.; Ricci, M.; Pick, R. M. "*Time-resolved optical Kerr effect on a fragile glass-forming liquid: Test of different mode coupling theory aspects*," *Europhys. Lett.* **2000**, 52, 324.
- Trebino, R.; Hayden, C. C. "*Antiresonant-ring transient spectroscopy*," *Opt. Lett.* **1991,** 16, 493.
- Trevena, D. H. *"Streching and superheating of liquids," Contemp. Phys.* **1976**, 17, 109.
- Valeur, B. *Molecular Fluorescence: Principles and Applications*. **2001**, Weinheim: Wiley-VCH.
- Van Doren, J. M.; Kerr, D. M.; Miller, T. M.; Viggiano, A. A. *"Electron attachment and detachment, and the electron affinities of C_5F_5N and C_5HF_4N," J. Chem. Phys.* **2005**, 123*,* 114303.
- Vanamerongen, H.; Vangrondelle, R. *Transient Absorption-Spectroscopy in Study of Processes and Dynamics in Biology*, in *Biochemical Spectroscopy*. **1995**, p. 201-226.
- Volkmer, A.; Cheng, J. X.; Xie, X. S. *"Vibrational imaging with high sensitivity via epidetected coherent anti Stokes Raman scattering microscopy," Phys. Rev. Lett.* **2001,** 8702, 023901.

- Volkmer, A.; Book, L. D.; Xie, X. S. *"Time-resolved coherent anti-Stokes Raman scattering: imaging based on Raman free induction decay," Appl. Phys. Lett.* **2002,** 80, 1505.
- Weast, R. C. *CRC Handbook of Chemistry and Physics* 66th edition (CRC Press, Boca Raton, **1985**).
- Weeks, J. D.; Chandler, D.; Andersen, H. C. *"Role of repulsive forces in forming the equilibrium structure of simple liquids," J. Chem. Phys.* **1971**, 54**,** 5237.
- Xiao, D.; Rajian, J. R.; Li, S. F.; Bartsch, R. A.; Quitevis, E. L. *"Additivity of the Optical Kerr Effect Spectra in Binary Ionic Liquid Mixtures: Implications for Nanostructural Organization," J. Phys. Chem. B* **2006**, 110, 16174.
- Zheng, Q.; Durben, D. J.; Wolf, G. H.; Angell, C. A. *"Liquids at Large Negative Pressures: Water at the Homogeneous Nucleation Limit," Science* **1991**, 254, 829.
- Zhong, Q.; Zhu, X.; Fourkas, J. T. *"Antiresonant-ring Kerr spectroscopy," Opt. Expr.* **2007**, 15, 6561
- Zhong, Q.; Zhu, X.; Fourkas, J. T. *"Temperature-dependent orientational dynamics of 1,n-dicyano n-alkanes," J. Phys. Chem. B* **2008**, 112, 3115.
- Zhong, Q.; Fourkas, J. T. *"Searching for voids in liquids with optical Kerr effect spectroscopy,"* J. Phys. Chem. B **2008**，112，8656.
- Zhong, Q.; Fourkas, J. T. *"Shape and Electrostatic Effects in Optical Kerr Effect Spectroscopy of Aromatic Liquids," J. Phys. Chem. B* **2008**, 112, 15342.
- Zhu, X.; Farrer, R. A.; Gershgoren,E.; Kapteyn, H. C.; Fourkas, J. T. "*Mode-selective optical Kerr effect spectroscopy," J. Phys. Chem. B* **2004,** 108, 3384.

- Zhu, X.; Farrer, R. A.; Fourkas, J. T. "*Optical Kerr effect spectroscopy using time-delayed pairs of pump pulses with orthogonal polarizations," J. Phys. Chem. B* **2005,** 109, 8481.
- Zhu, X.; Farrer, R. A.; Fourkas, J. T. *"Ultrafast orientational dynamics of nanoconfined benzene," J. Phys. Chem. B* **2005** 109, 12724.
- Zhu, X.; Farrer, R. A.; Zhong, Q.; Fourkas, J. T. *"Orientational diffusion of n-alkyl cyanides," J. Phys. Cond. Matt.* **2005**, 17, 4105.